Eur. Phys. J. C (2025) 85:416
https://doi.org/10.1140/epjc/s10052-025-13924-5

THE EUROPEAN PHYSICAL JOURNAL C

Regular Article - Experimental Physics

Measurement of the Lund jet plane in hadronic decays of top quarks and W bosons with the ATLAS detector

ATLAS Collaboration[⋆]

CERN, 1211 Geneva 23, Switzerland

Received: 16 July 2024 / Accepted: 13 February 2025

Abstract The Lund jet plane (LJP) is measured for the first time in $t\bar{t}$ events, using 140 fb^{-1} of $\sqrt{s} = 13$ TeV pp collision data collected with the ATLAS detector at the LHC. The LJP is a two-dimensional observable of the sub-structure of hadronic jets that acts as a proxy for the kinematics of parton showers and hadron formation. The observable is constructed from charged particles and is measured for $R = 1.0$ anti-k_t jets with transverse momentum above 350 GeV containing the full decay products of either a top quark or a daughter W boson. The other top quark in the event is identified from its decay into a b-quark, an electron or a muon and a neutrino. The measurement is corrected for detector effects and compared with a range of Monte Carlo predictions sensitive to different aspects of the hadronic decays of the heavy particles. In the W-boson-initiated jets, all the predictions are incompatible with the measurement. In the top quark initiated jets, disagreement with all predictions is observed in smaller subregions of the plane, and with a subset of the predictions across the fiducial plane. The measurement could be used to improve the tuning of Monte Carlo generators, for better modelling of hadronic decays of heavy quarks and bosons, or to improve the performance of jet taggers.

1 Introduction

Jets, the sprays of hadrons resulting from the fragmentation of highly energetic quarks and gluons, are among the most commonly observed radiation patterns in the detector experiments at the Large Hadron Collider (LHC) [1]. They are frequently produced in the decays of heavy particles such as the top quark or the Higgs, W or Z bosons, whose properties are studied in detail at the LHC experiments to test the predictions of the Standard Model. The quantum chromodynamic (QCD) radiation that gives rise to jets, the showers of quarks and gluons and their subsequent recombination into hadrons, cannot be described by perturbative QCD and must be modelled using phenomenological models in Monte Carlo (MC) simulations. The Lund jet plane (LJP) [2] is an observable that reconstructs the hierarchy of QCD emissions within jets, thus providing insights into the process of jet formation. The LJP belongs to a category of jet substructure (JSS) observables that make use of the jet algorithms that are used to reconstruct the four-momentum of the particle that initiated the parton shower. This paper presents the first measurement of the LJP for jets initiated by top quarks and W bosons, using a dataset comprising 140 fb^{-1} of pp collision data collected by the ATLAS detector at the LHC at a centre-of-mass energy of 13 TeV. The kinematics of parton showers and hadronisation in these jet topologies are of particular interest due to the large masses of the top and bottom quarks as well as the colour-singlet nature of the W boson.

At the very large centre-of-mass energies achieved by the LHC, unprecedented quantities of heavy particles, including top quarks, have been produced. While the hadronic production of top quarks has been measured with great precision and is well described by perturbative QCD [3,4], hadronic top quark decays are more challenging to measure and model due to the presence of highly boosted decay products. Insights into this process can be gained through measurements of JSS observables, including the LJP, that are sensitive to the different kinematic regimes of parton showers and hadronisation. Recent analyses by ATLAS [5,6] and CMS [7] have measured jet production cross-sections differentially in a wide range of JSS observables, using jets initiated by top quarks or by W bosons from top decays. This measurement complements those published results with a detailed study of the LJP, a JSS observable that has found many new applications in recent years, as described below.

In LHC experiments, jets are typically reconstructed using sequential recombination algorithms. These algorithms perform a recursive sequence of pairwise recombinations of the four-momenta of final-state particles to construct the jet momentum. The most common jet algorithms of this type belong to the k_t-family [8], including the anti-k_t [9] and the Cambridge-Aachen (CA) [10] algorithms. Jet algorithms of

⋆ e-mail: atlas.publications@cern.ch

Published online: 14 April 2025

this kind are particularly suited to hadron collider physics due to their insensitivity to soft and collinear QCD emissions (infrared and collinear safety) [11]. To define the size of the reconstructed jets, the jet algorithms require a choice of the radius parameter R.

The theoretical basis for the LJP observable is the Lund plane [12]. In the development of parton-shower models, where quarks evolve down to the hadronisation energy scale through a succession of soft-gluon emissions, it is useful to plot the range of transverse momenta and angles available to each emission. This two-dimensional (2D) plane spanned by the range of momenta (or alternatively momentum fractions) and angles is called the Lund plane. The tree-like structure of k_t-type jet algorithms is motivated by the branching nature of QCD and can loosely be thought of as mimicking the evolution of the parton shower in reverse, with the finished jet representing the highly energetic particle that initiated the shower and the jet inputs representing the outgoing hadrons. Following this analogy, the LJP is constructed from the transverse momenta and angles of proto-jets, the intermediate steps of the algorithm. By following the higher-p_{T} proto-jet at each step in the clustering tree, one obtains the entries of the primary LJP, which for brevity is simply called the LJP in this paper.

The first measurement of the LJP was performed by ATLAS using fairly narrow jets with a radius parameter $R = 0.4$ in 139 fb^{-1} of dijet events at 13 TeV [13]. This result has been used to test analytic predictions [14] using all-order resummations of logarithmic terms in perturbative QCD. A similar measurement for $R = 0.4$ and $R = 0.8$ jets has also been published by CMS [15]. The Lund subjet multiplicity, an observable derived from the LJP but with greater sensitivity to higher-order parton-shower effects, was also measured recently by ATLAS [16]. At the ALICE experiment, which is able to probe jets at lower p_{T} than ATLAS and CMS, LJPs have been used to measure the properties of parton showers without contamination from hadronisation effects [17,18]. JSS observables have long played an important part in the development of jet-tagging algorithms, particularly for the identification of top-quark- and W-boson-initiated jets because these usually exhibit a distinctive multi-pronged internal structure. The taggers often combine innovative machine-learning methods with jet substructure concepts [19–21] including the LJP [22,23]. The LJP was also exploited recently in CMS to improve the calibration of multi-pronged jets produced by highly boosted objects [24].

The jets studied in this analysis are $R = 1.0$ (large-R) jets with transverse momentum (p_{T}) larger than 350 GeV. A single jet is studied in each event. The targeted events contain top quarks from $t\bar{t}$ pairs that decay into a W boson and a b quark, with one of the W bosons decaying hadronically into jets, and the other into an electron or muon and a neutrino. The selected events are separated in two categories, targeting different decay topologies in the large-R jet used to measure the LJP. Events are assigned to either the 'top jet' or 'W jet' category depending on the mass of the large-R jet and its distance from the nearest $R = 0.4$ (small-R) jet that is identified as coming from a b-quark decay (b-tagged jet).

Following the introduction to the measurement in this section, the definition of the LJP is given in Sect. 2. A description of the ATLAS detector is presented in Sect. 3. In Sect. 4 the dataset and MC simulated samples are described in detail, as are the reconstructed objects and applied selections in Sect. 5. The procedure for estimating contributions from background processes is described in Sect. 6, while the details of the LJP measurement are given in Sect. 7. Uncertainties associated with the measurement are discussed and presented in Sect. 8. The results are presented in Sect. 9, followed by the conclusion in Sect. 10.

2 The Lund jet plane

The LJP is a rich representation of the kinematic structure of the radiation that constitutes a jet. The original definition of the Lund plane was based on the theoretical kinematics of quark and gluon emissions inside a parton shower. Colour confinement prevents us from observing these emissions directly; however, a proxy for their kinematics can be constructed from jets, allowing the radiation patterns inside the jet to be interpreted similarly to a parton shower. The jet algorithms used at the LHC are informed by the physics of parton showers, in order to be insensitive to soft and collinear emissions, that do not modify the kinematics of the outgoing hard partons. One jet algorithm that is of particular interest for studying jet substructure is the CA algorithm, which imposes an angle-ordered hierarchy on the sequence of recombinations. This structure is analogous to the angular ordering that emerges when considering a series of gluon emissions in a parton shower, a well-known effect and fundamental property of all quantum field theories. The CA algorithm begins by combining pairs of four-momenta of the final-state particles, or their equivalent objects in the detector, into *proto-jets*, based on the following metric:

$$d_{ij} = \frac{\Delta R_{ij}^2}{R^2},$$

where ΔR_{ij} is the distance in the (y, ϕ) plane, defined below, between particles i and j, and R is a parameter of the algorithm. For each particle i the algorithm evaluates the minimum of all d_{ij}. If this is smaller than one, the four-momenta of particles i and j are combined into a *proto-jet*, otherwise particle i is removed from the list. The procedure is applied recursively to each pair of proto-jets i, j until there are none left with $\Delta R_{ij} < R$.

The procedure for reconstructing the Lund jet plane is illustrated in Fig. 1. The steps of the clustering sequence are followed in reverse, starting with the finished jet, and then considering the pairs of proto-jets in the previous steps. Each pair of proto-jets is used to fill a point in the LJP with the following coordinates:

$$\Delta R^2 = (y_i - y_j)^2 + (\phi_i - \phi_j)^2, \quad z = \frac{p_{\mathrm{T}}^j}{p_{\mathrm{T}}^i + p_{\mathrm{T}}^j},$$

where y is the rapidity, ϕ is the azimuthal angle in the reference frame of the jet, and p_{T} is the transverse momentum.[1] The indices i, j denote the two 'proto-jets', such that $p_{\mathrm{T}}^j < p_{\mathrm{T}}^i$. In analogy with a parton shower, the lower-p_{T} proto-jet is commonly referred to as the *emission*, while the higher-p_{T} one is called the *core*. The CA-clustering sequence is traversed by repeatedly unclustering the core branch until it is represented by a single jet constituent, adding a point to the LJP at each step. This definition of the plane is often referred to as the primary LJP, since child branches of the emissions are not considered. These emissions would be included in what is called the secondary LJP or even higher-order planes. These higher-order LJPs are not considered in this measurement because they are made up of very soft emissions and are much less densely populated than the primary LJP.

The LJP coordinates ΔR and z are dimensionless quantities invariant under Lorentz boosts along the z-axis and represent the emission angle and transverse momentum fraction. Since the emissions evolve through a wide range of angles and energy fractions, it is convenient to parameterise the LJP using the logarithms $\ln(R/\Delta R)$ and $\ln(1/z)$. In the final measurement, the histograms of the LJP coordinates for all emissions are normalised using the total number of jets N_{jets} and the bin widths to give the density of emissions

$$\frac{1}{N_{\mathrm{jets}}} \frac{\mathrm{d}^2 N_{\mathrm{emissions}}}{\mathrm{d}\ln(R/\Delta R)\,\mathrm{d}\ln(1/z)}. \tag{1}$$

The jets studied in this analysis originate from the decays of top quarks and W bosons, and consequently contain the particle spray produced by the showering of the heavy particles and the subsequent hadronisation of the decay products. This implies that one of the proto-jet pairs encountered in the LJP declustering will approximately coincide with the outgoing quarks from the heavy-particle decay. That proto-jet pair will have a different momentum-sharing fraction and angular separation than those where the core and the emission correspond approximately to a gluon splitting or the radiation of a gluon from a quark. This produces a structure in the LJP for hadronic decays of top quarks and W bosons that is distinctive from that encountered in studies of jets originating from gluons or light quarks [13,15]. This measurement, similarly to all previous LJP measurements, employs only charged particles to reconstruct the plane. The measured LJP differs only slightly from the observable for all final-state particles, as QCD is approximately symmetric under isospin transformations.

3 ATLAS detector

The ATLAS experiment [25] at the LHC is a multipurpose particle detector with a forward–backward symmetric cylindrical geometry and nearly 4π coverage in solid angle. It consists of an inner tracking detector surrounded by a thin superconducting solenoid providing a 2T axial magnetic field, electromagnetic and hadron calorimeters, and a muon spectrometer. The inner tracking detector covers the pseudorapidity range $|\eta| < 2.5$. It consists of silicon pixel, silicon microstrip, and transition radiation tracking detectors. Lead/liquid-argon (LAr) sampling calorimeters provide electromagnetic (EM) energy measurements with high granularity. A steel/scintillator-tile hadron calorimeter covers the central pseudorapidity range ($|\eta| < 1.7$). The endcap and forward regions are instrumented with LAr calorimeters for both the EM and hadronic energy measurements up to $|\eta| = 4.9$. The muon spectrometer surrounds the calorimeters and is based on three large superconducting air-core toroidal magnets with eight coils each. The field integral of the toroids ranges between 2.0 and 6.0T m across most of the detector. The muon spectrometer includes a system of precision chambers for tracking and fast detectors for triggering. A two-level trigger system is used to select events. The first-level trigger is implemented in hardware and uses a subset of the detector information to accept events at a rate below 100kHz. This is followed by a software-based trigger that reduces the accepted event rate to 1kHz on average depending on the data-taking conditions. An extensive software suite [26] is used in data simulation, in the reconstruction and analysis of real and simulated data, in detector operations, and in the trigger and data acquisition systems of the experiment.

[1] The coordinate system used at ATLAS is right-handed, with the origin located at the expected *interaction point* (IP) in the centre of the detector. The x-axis points from the IP to the centre of the LHC ring, the y-axis points upward and the z-axis points along the direction of the beam pipe. Cylindrical coordinates (r, ϕ) are used in the $x-y$ plane, where ϕ is the azimuthal angle around the beam pipe. The *pseudorapidity* is defined in terms of the polar angle θ from the z-axis as $\eta = -\ln[\tan(\theta/2)]$. The pseudorapidity is equivalent to the rapidity $y = (1/2)\ln[(E + p_z)/(E - p_z)]$ in the limit of massless particles. Differences in rapidity are invariant under a Lorentz boost along the z-axis.

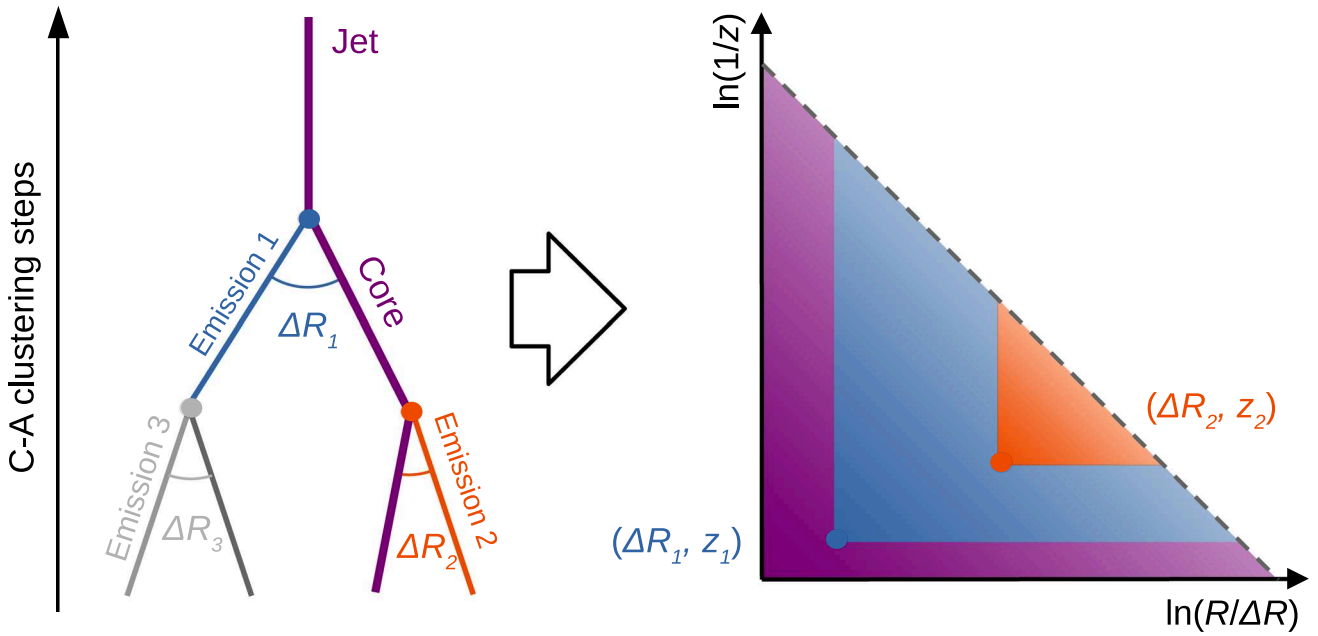

Fig. 1 Illustration showing the process by which the LJP is constructed. The CA algorithm clusters pairs of proto-jets according to angular separation ΔR. At each step, the higher-p_{T} proto-jet is considered to be the core and the lower-p_{T} one the emission. The variables $\ln(R/\Delta R)$ and $\ln(1/z)$ are plotted on the LJP for each emission originating from the core branch at each step. Of the three emissions shown, only emissions 1 and 2 are part of the (primary) LJP. The size of the phase space in which subsequent emissions may appear is indicated by the coloured areas. The dashed line indicates the boundary of the low-k_t regime beyond which the number of emissions is strongly suppressed

4 Data and simulated event samples

4.1 Data sample

The measurement is performed on data collected by the ATLAS detector at the LHC from 2015 to 2018 in pp collisions at $\sqrt{s} = 13$ TeV. The data must satisfy quality requirements, ensuring that all detector subsystems were fully operational during data taking [27]. The data sample corresponds to an integrated luminosity of 140.1 ± 1.2 fb^{-1} [28]. The combined integrated luminosity and associated uncertainty is determined primarily by the LUCID-2 detector [29], complemented by measurements using the inner detector and calorimeters.

The events were preselected using a combination of single-lepton triggers [30–32] that require an event to have at least one electron or muon candidate with $p_{\mathrm{T}} > 26$ GeV (or $p_{\mathrm{T}} > 24$ GeV and $p_{\mathrm{T}} > 20$ GeV, respectively, for electrons and muons in 2015 data). Leptons passing the lowest-p_{T} electron trigger or muon trigger are required to be isolated from other detector signals. These triggers are complemented by higher-p_{T} triggers without such isolation requirements.

4.2 Monte Carlo simulations

Monte Carlo simulations are employed in different stages of the analysis: to quantify the acceptance, efficiency and resolution of the detector and the reconstruction and selection applied, and to estimate the uncertainties due to the object calibrations and the modelling of signal and background processes. Detector effects were incorporated using a simulation of the ATLAS detector [33] based on GEANT4 [34].

In all generator configurations excluding SHERPA, the decays of bottom and charm hadrons from top quarks were simulated using the EVTGEN program [35].

In all simulated event samples, the effect of other interactions in the same, previous and next bunch crossings (pile-up) was incorporated by overlaying the hard-scatter event with a number of simulated inelastic pp events from the PYTHIA 8.186 [36] MC generator using a set of tuned parameters called the A3 tune [37].

4.2.1 Monte Carlo signal samples

These samples are used at different stages of the analysis, as illustrated in Sects. 7 and 8, and also for comparisons with the measured LJP in Sect. 9.

The signal is defined as events containing prompt $t\bar{t}$ pairs. Both single top and $t\bar{t}$ production in association with a vector boson or Higgs boson are treated as irreducible backgrounds (see Sect. 4.2.2). Only samples containing events with at least one lepton from a top or anti-top quark decay are used to model the $t\bar{t}$ signal.

POWHEG+PYTHIA 8 The nominal sample, which is used to model the signal and derive corrections for detector effects, was simulated at next-to-leading-order (NLO) precision in QCD using the POWHEG BOX v2 [38–41] matrix-element generator. The NNPDF 3.0nlo [42] set of parton distribution functions (PDFs) was employed, the h_{damp} parameter was set to $1.5\,m_t$ [43], where a top quark mass m_t of 172.5 GeV is assumed and the $p_{\text{T}}^{\text{hard}}$ parameter is set to = 0 [44]. The functional form of the renormalisation and factorisation scales (μ_{r} and μ_{f}) was set to that of the default scale $\sqrt{m_t^2 + p_{\text{T}}^2}$. Parton showering (PS) and hadronisation were modelled with the PYTHIA 8.230 generator [45] using the A14 tune [46] and the NNPDF 2.3lo set of PDFs [47]. The same PYTHIA 8 tune and PDF set was used for all processes simulated using this generator, unless otherwise specified.

Several alternative POWHEG+PYTHIA 8 samples are generated modifying specific settings compared to the nominal.

POWHEG+PYTHIA 8 h_{damp} var. The h_{damp} parameter in POWHEG regulates the amount of radiation against which the $t\bar{t}$ system recoils. To assess the associated uncertainty, an additional $t\bar{t}$ sample with $h_{\text{damp}} = 3.0\,m_t$ is used [48].

POWHEG+PYTHIA 8 (ISR Up/Down, FSR Up/Down) To estimate the uncertainty associated with the modelling of initial-state radiation (ISR) in $t\bar{t}$ production, the scale parameters μ_{r} and μ_{f} in the signal POWHEG+PYTHIA 8 sample are simultaneously varied by a factor of two or a half, while also changing the Var3c eigentune of the A14 PYTHIA 8 tune [46]. Similarly, to estimate the effect of the final-state radiation (FSR) uncertainty, variations of the scale parameter $\mu_{\text{r}}^{\text{FSR}}$ by a factor of two or a half are included. The A14 tune includes a nominal $\alpha_{\text{s}}^{\text{FSR}}(m_Z)$ value of 0.127. Changing the $\mu_{\text{r}}^{\text{FSR}}$ scale results in $\alpha_{\text{s}}^{\text{FSR}}(m_Z)$ values of 0.114 and 0.142 for the *FSR Up* and *FSR Down* samples, respectively. All components of this uncertainty are obtained by applying the PYTHIA 8 internal reweighting feature.

POWHEG+PYTHIA 8 (MEC Off) The nominal POWHEG+PYTHIA 8 sample includes matrix-element corrections (MEC) to the parton showers in both production and decay. These corrections exploit tree-level matrix elements that describe the emission(s) of interest to improve the accuracy of the prediction and approximate the emission at NLO precision [49]. An additional sample with the MECs turned off was produced to quantify the effect of these corrections in comparison with the measured LJP.

POWHEG+PYTHIA 8 (RTT) Another POWHEG+PYTHIA 8 sample, called recoil-to-top (RTT), was generated to estimate an associated uncertainty. This sample employs a different strategy for the treatment of recoil against gluon emissions from b-quarks originating in top quark decays. In the nominal setting, only the b-quark makes up the recoil system, while the RTT configuration uses the on-shell W boson and the top quark itself [50].

POWHEG+PYTHIA 8 ($p_{\text{T}}^{\text{hard}}$) To evaluate the uncertainty from the procedure for matching the hard-scatter process with the parton shower, an alternative sample was produced with the $p_{\text{T}}^{\text{hard}}$ parameter [51] in PYTHIA 8.230 set to 1. This parameter changes the scale used to veto emissions in the PS to avoid overlaps between the phase spaces of the outgoing partons and the initial emissions of the PYTHIA shower, and as a consequence it influences both the phase space available for emissions and the related kinematic observables, such as the number of jets or the momentum of the $t\bar{t}$ system.

POWHEG+HERWIG (7.0, 7.1, 7.2) A sample produced with the POWHEG matrix-element generator and the alternative HERWIG 7.2 [52] parton-shower and hadronisation model is used to estimate the associated modelling uncertainty. In this alternative sample, the HERWIG 7.2 default set of tuned parameters and the MMHT2014 lo PDF set [53] are used. Additional MC samples are used to perform comparisons with the measured LJP; these employ HERWIG 7.0.4 and HERWIG 7.1.3 with the MMHT2014 lo PDF set and the default tunes for HERWIG 7.0 [54] and HERWIG 7.1 [55] respectively. The various HERWIG 7 generator versions differ in terms of tunes of the hadronisation parameters, simulation of multiple-parton interactions and choice of evolution variable in the parton shower.

MADGRAPH5_AMC@NLO+PYTHIA 8 Samples from additional $t\bar{t}$ matrix-element generator set-ups are compared with the measurement. One such sample was obtained using the MADGRAPH5_AMC@NLO 2.6.0 generator [56] (later referred to as AMC@NLO) with the NNPDF 3.0nlo PDF set for the hard-scatter simulation, the same functional form of μ_{r} and μ_{f} as used in POWHEG, and the shower starting scale set to $\mu_q = H_{\text{T}}/2$, where H_{T} is defined as the scalar sum of the p_{T} of all outgoing partons. This hard-scatter generator was interfaced to PYTHIA 8. The MEC corrections are disabled in this sample.

SHERPA 2.2.10 A sample from a generator chain completely different from those above was obtained using SHERPA 2.2.10 [57]. The sample uses NLO-accurate matrix elements for processes with up to one additional parton, and

LO-accurate matrix elements for up to four additional partons. These were calculated using the Comix [58] and OpenLoops [59–61] libraries. The central energy scale in this sample has the functional form $\mu^2 = m_t^2 + 0.5 \times (p_{\mathrm{T},t}^2 + p_{\mathrm{T},\bar{t}}^2)$. These were matched with the Sherpa parton-shower simulations [62]. The CKKW matching scale for additional emissions was set to 30 GeV.

In the Powheg and MadGraph generators, top quarks are decayed at leading order with the narrow-width approximation and dedicated corrections to preserve spin correlations and include off-shell effects [63]. All $t\bar{t}$ samples are normalised to the cross-section $\sigma(t\bar{t})_{\mathrm{NNLO+NNLL}} = 832 \pm 51$ pb calculated at next-to-next-to-leading order (NNLO) in QCD including the resummation of next-to-next-to-leading logarithmic (NNLL) soft-gluon terms, calculated using the Top++ 2.0 program [64–70].

4.2.2 Monte Carlo background samples

The production of a top quark in association with a W boson (tW) was modelled using the Powheg Box v2 generator at NLO in QCD, using the five-flavour scheme and the NNPDF 3.0nlo set of PDFs. The diagram-removal (DR) scheme [71] was used to remove interference and overlap with $t\bar{t}$ production, while the diagram-subtraction (DS) scheme [43,71] was employed to estimate the uncertainty in the interference treatment. Single top quark t-channel and s-channel production was modelled using the Powheg Box v2 generator at NLO in QCD, with the NNPDF 3.0nlo set of PDFs. The four-flavour scheme was used for the t-channel, while the five-flavour scheme was employed in the s-channel modelling. Parton showering and hadronisation in the single top-quark processes was modelled with Pythia 8.230 using the A14 tune.

Production of a W or Z boson in association with jets was simulated using the Sherpa 2.2.1 [57] generator, using NLO matrix elements for up to two partons, and LO matrix elements for up to four partons, calculated with the Comix [58] and OpenLoops [59–61] libraries. These were matched with the Sherpa parton-shower simulations. The samples are normalised to the NNLO predicted total cross-section [72].

The production of $t\bar{t}Z$ and $t\bar{t}W$ events was modelled at NLO in QCD using the aMC@NLO 2.3.3 generator, while the $t\bar{t}H$ process was modelled using Powheg Box v2. Parton showering and hadronisation in these processes was performed using Pythia 8.210 ($t\bar{t}Z$ and $t\bar{t}W$) or Pythia 8.230 ($t\bar{t}H$). The diboson final states ($VV, V = Z/W$) were modelled using the Sherpa 2.2.2 generator, including off-shell effects and virtual Higgs boson contributions where appropriate.

5 Object definitions and event selection

Tracks are reconstructed by applying an iterative algorithm to hits in the inner detector [73]. They are required to have $p_{\mathrm{T}} > 500$ MeV and $|\eta| < 2.5$, and must pass quality requirements based on the number of layers crossed in the silicon tracking detectors. Additionally, to reduce pile-up contamination, the tracks are required to be matched to the primary vertex by having a transverse impact parameter $|d_0|$, relative to the beam line, of less than 2 mm and a longitudinal impact parameter z_0, relative to the primary vertex, satisfying $|z_0 \sin(\theta)| < 3$ mm, where θ represents the track's polar angle. The primary vertex is defined as the vertex with the largest $\sum p_{\mathrm{T}}^2$ of the associated tracks among all the vertices with at least two associated tracks with $p_{\mathrm{T}} > 500$ MeV.

Large-R jets are reconstructed using the anti-k_t algorithm [9] with radius parameter $R = 1.0$, as implemented in FastJet [74]. The jets are built from topological clusters of energy deposits in the calorimeter (*topoclusters*) which are calibrated using the local hadronic cell weighting scheme [75]. The *trimming* algorithm [76], with parameters $R_{\mathrm{trim}} = 0.2$ and $f_{\mathrm{trim}} < 0.05$, is applied to the jet inputs to mitigate the effects of pile-up and underlying event on the reconstructed jet. All large-R jets are required to have $|\eta| < 1.1$ and $p_{\mathrm{T}} > 200$ GeV. The Large-R jets are defined in the manner above for this measurement because they have been widely studied in ATLAS analyses and the calibration of their energy scale and resolution, with associated systematic uncertainties, is well understood [77].

Small-R jets are reconstructed by applying the anti-k_t algorithm with radius parameter $R = 0.4$ to tracking and calorimetry information, combined using the particle-flow algorithm [78]. In order to suppress jets originating from pile-up, small-R jets with $p_{\mathrm{T}} < 60$ GeV are required to be associated with the primary vertex according to the jet-vertex-tagger algorithm (JVT) [79]. All small-R jets used in the analysis are required to have $p_{\mathrm{T}} > 30$ GeV and $|\eta| < 2.4$. The small-R jets are identified as originating from a b-hadron by using a multivariate algorithm [80] that combines information about large-impact-parameter tracks, the topological decay chain, and displaced decay vertices. The working point used has an efficiency of 77% in simulated $t\bar{t}$ events and a corresponding rejection factor of 5 or 200 for jets initiated by c-quarks or light quarks and gluons, respectively. The energies of small-R and large-R jets are corrected by using energy- and η-dependent calibration factors derived from simulation and in situ measurements [77,81].

Electrons are reconstructed from a combination of inner detector and electromagnetic calorimeter (ECAL) information [82]. The reconstruction quality of the electron candidates is classified using a statistical likelihood-function. The electrons must satisfy a stringent reconstruction quality requirement (defined as the 'TightLH' working point

in Ref. [83]) to be considered in the event. Electron candidates must also be isolated from surrounding tracks and topoclusters (defined as the 'FCTight' working point in Ref. [83]). Electron tracks are matched to the primary vertex by requiring a transverse impact parameter significance $|d_0/\sigma(d_0)| < 5$ and $|z_0 \sin(\theta)| < 0.5$ mm. Topoclusters associated with electron candidates are required to lie within the region $|\eta| < 2.5$, excluding the barrel–endcap transition region $1.37 < |\eta| < 1.52$ in the ECAL. To match the p_{T} requirement of the trigger and ensure a high trigger efficiency, reconstructed electrons are required to have $p_{\mathrm{T}} > 27$ GeV.

Muons are reconstructed by combining inner-detector tracks with tracks reconstructed in the muon spectrometer [84]. Their inner-detector tracks are matched to the primary vertex by requiring $|d_0/\sigma(d_0)| < 3$ and $|z_0 \sin(\theta)| < 0.5$ mm. The muons must be well reconstructed (at the 'Medium' working point, as defined in Ref. [84]) and must satisfy the same stringent isolation requirements as the electrons. Like the electrons, the muons are required to have $|\eta| < 2.5$ and $p_{\mathrm{T}} > 27$ GeV.

The missing transverse momentum $\mathbf{p}_{\mathrm{T}}^{\mathrm{miss}}$, with magnitude $E_{\mathrm{T}}^{\mathrm{miss}}$, is defined as the negative sum of the transverse momenta of the reconstructed and calibrated physical objects, as well as a 'soft term' built from all other tracks that are associated with the primary vertex [85].

To avoid double-counting of energy, an overlap removal procedure is applied to the reconstructed objects. Overlapping objects are removed from the event in the following order: electrons sharing a track with a muon; the closest small-R jet within $\Delta R = 0.2$ of an electron; electrons within $\Delta R = 0.4$ of a small-R jet; small-R jets within $\Delta R = 0.4$ of a muon if they have at most two associated tracks; and muons within $\Delta R = 0.4$ of a small-R jet.

All events employed in the analysis must satisfy a preselection requiring a primary vertex, exactly one muon or one electron, $E_{\mathrm{T}}^{\mathrm{miss}} > 20$ GeV and $E_{\mathrm{T}}^{\mathrm{miss}} + m_{\mathrm{T}}^{W} > 60$ GeV.[2] Events must also contain at least one b-tagged small-R jet j_{b1} close to the lepton ℓ, satisfying $\Delta R(\ell, j_{b1}) < 1.5$. All events are required to have one large-R jet J with $p_{\mathrm{T}} > 350$ GeV separated from the lepton by $\Delta R(\ell, J) > 2.3$. In each event, only the leading (i.e. highest-p_{T}) large-R jet is used to reconstruct the LJP.

Lastly, the large-R jet is classified as belonging to one of two exclusive categories based on its compatibility with the kinematics and topology of a hadronically decaying top quark or W boson. The 'top jet' selection requires the leading large-R jet to have a mass $m_J > 140$ GeV and requires a second b-tagged small-R jet j_{b2} to be contained within the large-R jet, with a distance requirement $\Delta R(J, j_{b2}) < 1.0$. The '$W$ jet' selection only requires the large-R jet to have $60 < m_J < 100$ GeV, with no requirement placed on the presence of additional b-tagged small-R jets in the event.

6 Background estimation

Most of the background processes are estimated using MC simulations, as has been described in Sect. 4. The only exception is the contribution from misreconstructed events in which no real leptons are produced promptly in the hard-scatter process. This category contains 'fake-lepton' events where a lepton is radiated in a hadron decay chain or where a jet is misreconstructed as a lepton. The estimation is performed using a data-driven approach called the matrix method [86]. This technique has been applied in other analyses sharing similar final states [3,6]. The method is based on the definition of *loose* and *tight* criteria for lepton reconstruction quality and isolation. The tight requirements are reported in Sect. 5. Loose leptons do not have any isolation requirement and use the *MediumLH* working point for electron identification. The fake-lepton background is estimated by weighting the data events containing loose leptons by factors based on the known efficiencies for a real or fake lepton to meet the tight criteria. These efficiencies are evaluated using event topologies enriched in real or fake leptons respectively. The fake-lepton background, which is mainly due to multijet events, comprises less than 1% of the predicted sample for both the W and top jets.

The number of events passing the selections in data, and the predictions from the MC samples, is reported in Table 1. From these numbers it follows that the data sample has a purity[3] of 96% in the top jet selection and 82% in the W jet selection. The main source of background is the single-top process, which contributes 48% and 60% of the background in the top jet and W jet selections, respectively.

Table 1 shows there is tension between the measured data and the predicted yield, with their ratio being about 84% in each of the two selections. The same difference is visible in Fig. 2, where kinematic distributions of the large-R jets in the data and MC samples are compared. This mismodelling increases with large-R jet p_{T}, as is visible in Fig. 2a and b. Here, the following trend can be observed: predictions overestimate the data by around 30% in the tail of the distribution and by $15-20$% in the head of the distribution. This mismodelling has been observed in many ATLAS and CMS measurements of the $t\bar{t}$ production cross-section performed in the high (> 350 GeV) top quark p_{T} region and mostly derives from missing higher-order corrections to the normalised NLO matrix-element predictions with parton-shower matching (NLO+PS) [3,87,88]. In addition to the number of events passing each selection, Table 1 also dis-

[2] $m_{\mathrm{T}}^{W} = \sqrt{2 p_{\mathrm{T}}^{\ell} E_{\mathrm{T}}^{\mathrm{miss}} \left(1 - \cos\Delta\phi(\vec{p}_{\mathrm{T}}^{\ell}, \vec{p}_{\mathrm{T}}^{\mathrm{miss}})\right)}$.

[3] Defined as (Data − Background)/Data.

plays the total number of reconstructed LJP emissions (as defined in Sect. 2). The MC emission counts have not been corrected using unfolding or matching between the detector- and particle-level emissions.

Figure 2c and d show the measured distributions of the large-R jet mass in the top jet and W jet selections. The jet mass distributions peak close to the top quark and W boson masses, as would be expected for jets containing the decay products of on-shell top quarks or W bosons.

7 Measurement of the Lund jet plane

7.1 Particle-level object definitions

The LJP observable is reconstructed using stable particles.[4] These are identified in the MC generator record without considering simulations of their interactions with the detector material.

Each particle-level charged lepton is *dressed*, meaning its four-momentum is summed with that of any prompt photon within a cone of size $\Delta R = 0.1$. The $E_{\mathrm{T}}^{\mathrm{miss}}$ is calculated from the *prompt* neutrinos originating from the decays of the on-shell W bosons. Non-prompt charged leptons and neutrinos, which are typically produced in the decays of hadrons, or τ-leptons produced in their decay chains, are not considered. Events where the leptons originate from the decay of a τ-lepton originating from a W boson decay are accepted provided they pass the kinematic selections outlined below.

Particle-level small-R and large-R jets are built from all stable particles in the event except the prompt neutrinos and the dressed charged leptons. Jets are constructed using the anti-k_t algorithm with a radius parameter value of $R = 0.4$ or 1.0. The overlap removal strategy for the particle-level jets and leptons is simpler than at the detector level: dressed muons and electrons are removed from the event if they are separated from a jet by $\Delta R < 0.4$.

Particle-level b-tagging is performed by ghost-matching [89] b-hadrons with $p_{\mathrm{T}} > 5$ GeV to the small-R jets. In the ghost-matching method, the jet algorithm is used to cluster the b-hadrons together with the stable particles making up the jet's constituents while treating the momenta of the former as negligible.

With the particle-level objects passing all the selections above, particle-level signal events must contain exactly one charged lepton with $p_{\mathrm{T}} > 27$ GeV and $|\eta| < 2.5$ originating from the top quark decays, as well as $E_{\mathrm{T}}^{\mathrm{miss}}$, one large-$R$ jet and at least one small-R jet with a ghost-associated b-hadron. The kinematic cuts on the $E_{\mathrm{T}}^{\mathrm{miss}}$ and jets are the same as for the corresponding detector-level objects. The cuts that define the top jet and W jet selections, as described for the detector-level objects in Sect. 5, are also applied at the particle level.

7.2 Reconstruction of the LJP observable

At the detector level, this analysis uses charged-particle tracks as inputs for the CA algorithm to reconstruct the LJP. This approach takes advantage of the high angular resolution of the tracker to reduce the uncertainty of the ΔR coordinate in the LJP. This charged-particle LJP is what was studied in previous measurements [13,15] and is very similar to the all-particle LJP because of the approximate isospin symmetry of QCD. Only tracks ghost-matched [89] to the leading trimmed large-R jet are used to reconstruct the LJP. The topoclusters that make up the jet are clustered together with the tracks using the same jet definition. To leave the jet momentum unaffected, the magnitude of the momentum of each track is set to a value very close to zero. The tracks that are clustered with the constituent topoclusters are called *ghost-tracks* and are subjected to the same trimming algorithms as the jet's constituents.

The particle-level LJP is built from the charged constituents of the particle-level large-R jets. Like the detector-level tracks, these must fulfil the requirements $p_{\mathrm{T}} > 500$ MeV and $|\eta| < 2.5$. Trimming is applied to the particle-level jet constituents with the same parameter values used at the detector level. Also, at particle level, only the leading trimmed large-R is employed to reconstruct the LJP.

The LJP is built using the appropriate detector- or particle-level inputs by following the procedure described in Sect. 2. It should be noted that the CA algorithm is used in the LJP reconstruction even though the large-R jets were built from their constituents using the anti-k_t algorithm. The anti-k_t algorithm is preferred in the reconstruction of the jet four-momentum because it is more resilient to soft radiation and produces regularly shaped jets that are easily calibrated. On the other hand, the CA algorithm is more suited to investigating the jet substructure because it imposes an angular ordering on the emissions in analogy with a parton shower. Reclustering the constituents using different jet definitions affects the observable. This was investigated in Ref. [14] and the effect was found to be small except in the region of large ΔR at the edge of the jet.

7.3 Structure of the Lund jet plane

Various regions of the LJP are sensitive to the kinematics of the top quark and W boson decay as well as the subsequent parton showering and hadronisation of the decay products. At small angles and small p_{T} fractions (upper right-hand corner), the structure of the plane resembles that of light jets while the hard and wide-angle emissions (lower left-hand corner) are sensitive to the top quark and W boson

[4] Particles with $c\tau > 10$ mm, where τ represents the mean proper lifetime of the particle.

Table 1 Predicted and actual yields for the top jets and W jets. The $t\bar{t}$ prediction is from the nominal POWHEG+PYTHIA 8 sample. The second and fourth columns report the actual number of emissions that enter the LJP. The uncertainties are the total uncertainties estimated as described in Sect. 8

	Top jets		W jets	
Sample	Events	Emissions	Events	Emissions
$t\bar{t}$	33800 ± 3400	216000 ± 22000	28000 ± 2900	164000 ± 17000
Single top	650 ± 170	4200 ± 1100	900 ± 1000	22000 ± 6000
$t\bar{t} + V$	330 ± 50	2200 ± 300	330 ± 40	1850 ± 250
Fake leptons	230 ± 120	1400 ± 700	900 ± 400	5400 ± 2800
W + jets	110 ± 40	760 ± 290	1500 ± 600	9100 ± 3400
VV	12 ± 6	80 ± 40	170 ± 90	1000 ± 500
Z + jets	8 ± 4	47 ± 24	100 ± 50	800 ± 400
Total pred.	35100 ± 3400	224533 ± 22000	35000 ± 3100	204000 ± 18000
Data	29328	189902	28686	166533

decays. In the light-jet-like regime, the density of emissions is influenced by the running of $\alpha_S(k_T)$, rising with increasing $z \times \Delta R$ before falling sharply at the hadronisation scale. The quarks decay products of the top quark and W boson have an opening angle proportional to m/p_T, where m is the mass of the top quark or W boson. This gives rise to a second region of high emission densities at corresponding values of ΔR.

The LJPs sensitivity to parton shower effects can be demonstrated by evaluating the ratios of the LJP densities predicted by different MC generators, as shown in Fig. 3. MC generators using different parton-shower algorithms, such as HERWIG 7.2 and PYTHIA 8 in Fig. 3a, produce variations in the density of emissions along diagonals from the top left to the bottom right of the plane. Altering the amount of final-state radiation has a similar effect, as can be seen in Fig. 3b. A comparison of different treatments of the hard-scatter process and the matching to the parton shower, as with the POWHEG and AMC@NLO generators in Fig. 3c, shows smaller differences in the density of soft and collinear emissions. A detailed definition of the different generators is given in Sect. 4.

The detector-level LJP is shown in Fig. 4 for the top jets and the W jets. The quantity plotted is the number of emissions, including background processes. The 2D histogram that makes up the LJP for the top jets (W jets) has equally spaced bins in 11 (12) rows along the $\ln(R/\Delta R)$ direction from 0 (0.4) to 4.8 and 11 columns along the $\ln(1/z)$ direction from 0.69 to 4.9. The fiducial LJP contains only bins with > 0 entries. In both selections, one can distinguish two regions of the plane that are densely populated, one in the bottom left and one along the diagonal of the plane. On the other hand, the top left and top right regions of the plane are very sparsely populated. The separation between the densely populated regions is somewhat greater in the W jet selection.

7.4 Unfolding

The measured LJP is corrected for detector-level effects using the iterative Bayesian unfolding (IBU) procedure [90]. The whole 2D plane is unfolded at once, using corrections derived from the nominal POWHEG+PYTHIA 8 simulated events. The unfolding can be represented by the following equation:

$$\frac{\mathrm{d}^2 N_{\text{emissions}}}{\mathrm{d}\ln(1/z)\,\mathrm{d}\ln(R/\Delta R)} = \frac{1}{\Delta X \Delta Y \epsilon^I_{\text{eff}}} \sum_J M^{-1}{}^I_J \cdot \epsilon^J_{\text{acc}} \cdot (N^J_{\text{obs}} - N^J_{\text{bkg}})$$

where I is the index of the bin in the particle-level LJP,[5] J is the bin index at detector level, ΔX and ΔY are the widths of the bins corresponding to I across the two axes, M is the response matrix (with its inversion representing the unfolding technique), and N_{obs} and N_{bkg} correspond to the number of observed emissions and the predicted background, respectively. The factor ϵ_{eff} corrects for emissions passing the particle-level selection but not the detector-level requirements, while ϵ_{acc} removes the emissions passing the detector-level requirements and not matched to the particle-level ones. The latter factor corrects the LJPs for events that do not pass the particle-level selection, and also for individual detector-level emissions that do not have a corresponding particle-level emission. The matching between detector- and particle-level emissions is performed in the $\eta-\phi$ space after transforming the coordinates into the rest frame of the large-R jet. Detector- and particle-level emissions with a closest match at a distance $\Delta R_{\text{match}} < 0.1$ are used to populate

[5] Here, $I = i_{\Delta R} + j_z \times N_{\Delta R}$, where $N_{\Delta R}$ is the total number of bins along the $\ln(R/\Delta R)$ direction of the plane, $i_{\Delta R}$ is the bin number in the $\ln(R/\Delta R)$ direction of the plane and j_z is the bin number in the $\ln(1/z)$ direction of the plane.

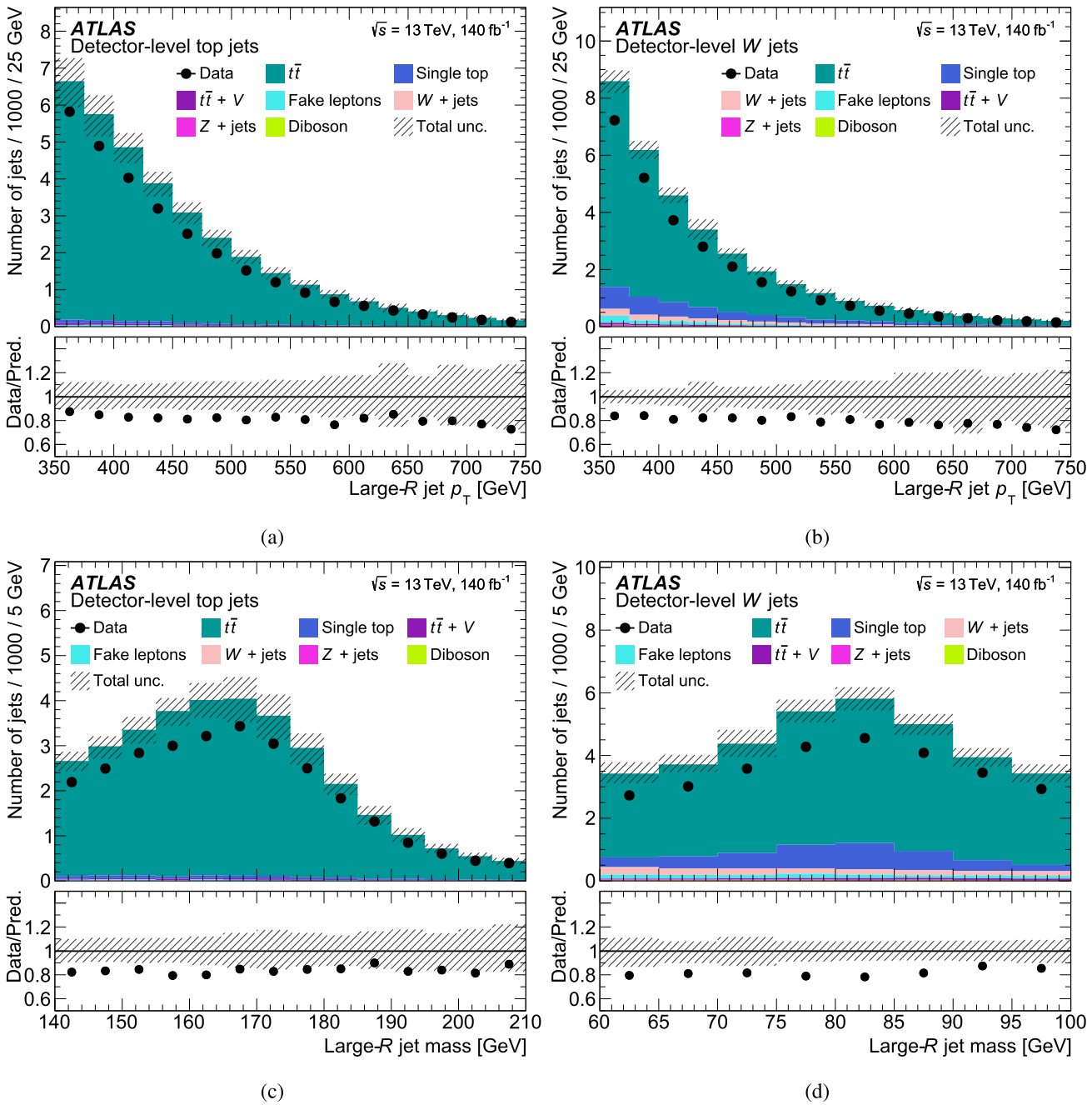

Fig. 2 Detector-level number of events as a function of the large-R jet p_{T} for **a** top jets and **b** W jets and as a function of the large-R jet mass for **c** top jets and **d** W jets. The uncertainty band includes detector and background modelling uncertainty components. In the bottom pad, the ratio of the data to the prediction is shown. The discrepancy between MC predictions and the data is described in the text

the response matrix. A dedicated uncertainty, described in Sect. 8, is estimated to capture the effect of the choice of $\Delta R_{\mathrm{match}}$. The resulting uncertainty is $< 1\%$ across all of the densely populated regions of the plane; hence the closeness of the matching has little effect on the unfolded distribution.

A response matrix is built for each selection. Bin-to-bin migrations between the detector level and the particle level occur mostly between adjacent bins. For $\ln(R/\Delta R)$ bins at identical $\ln(1/z)$ values, the response matrix is on average approximately 90% diagonal. For the $\ln(1/z)$ bins, this value is around 65%. The unfolding corrections for the top jet and W jet selections are shown in Fig. 5. Here, it can be observed that the ϵ_{acc} distribution, excluding some regions of low acceptance in the wide-angle emis-

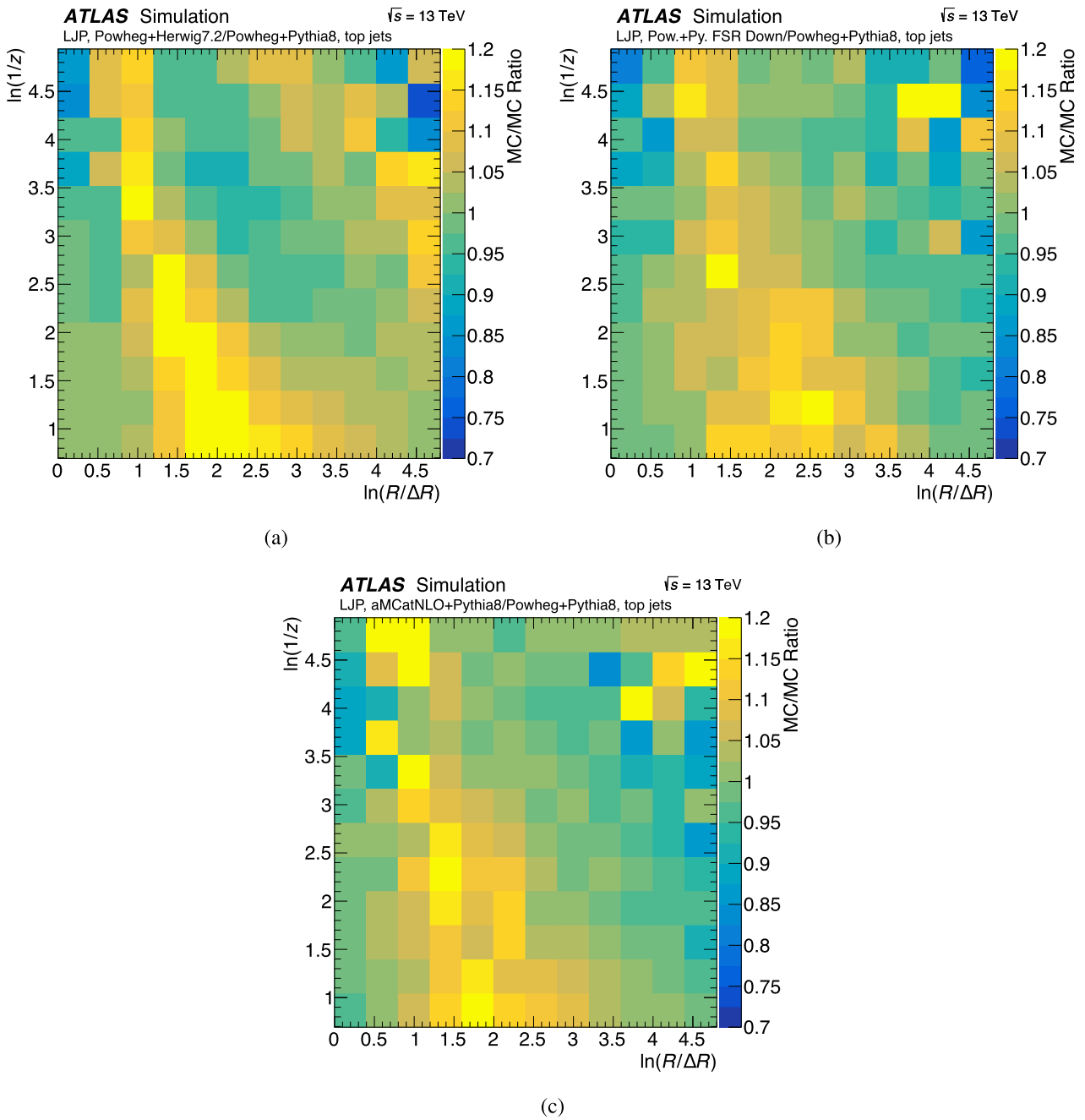

Fig. 3 Ratio of the Lund jet plane density predicted by alternative MC generators to that predicted by POWHEG+PYTHIA 8, for jets including all the top quark decay products. The alternative predictions employed are: **a** POWHEG+HERWIG 7.2, **b** POWHEG+PYTHIA 8 (FSR down) and **c** AMC@NLO+PYTHIA 8. Large deviations from 1 in the top left and top right corners of the plane are mostly due to statistical fluctuations. Definitions of the generator configurations are given in Sect. 4

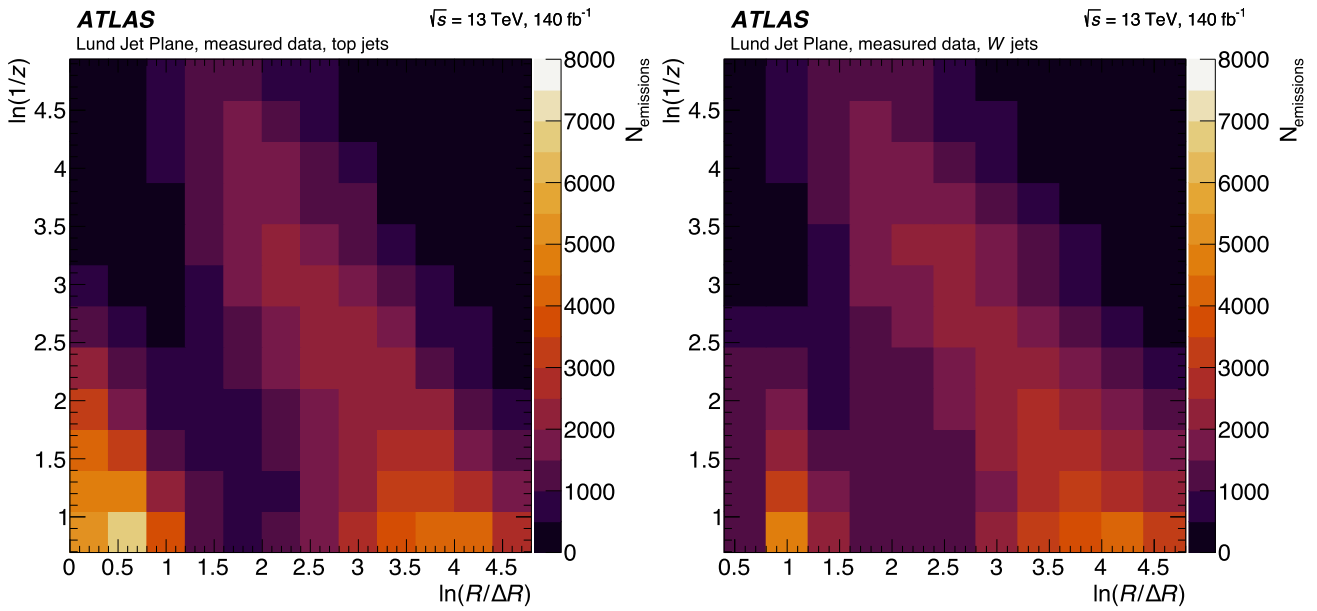

(a) (b)

Fig. 4 Reconstructed LJPs obtained by applying the **a** top jet and **b** W jet selections to the data

sions regions ($\ln(R/\Delta R) < 0.4$), is relatively flat and around 45% (35%) for the top jet (W jet) selection. The difference in acceptance between the two selections is driven by the difference in the mass cut applied. The ϵ_{eff} correction factor is affected by the inefficiencies induced by the b-tagging requirements, and is indeed lower than the acceptance correction. Moreover, one can observe a higher efficiency in the W jet selection, where only one b-tagged jet is required.

Figure 6 shows the ratio of the detector-level LJP to the particle-level LJP in the two selections, with the planes normalised to unity before taking their ratio. The effect of the unfolding procedure on the shape of the distributions can be observed in these ratios. These figures reveal that the main effect of the unfolding, in both selections, is to increase the separation between the hard and soft regimes in the LJP. The peak of the LJP, previously seen at detector level in the lower-left corner of the plane in Fig. 4, is shifted towards softer (i.e. smaller $k_{\text{T}} = z\,\Delta R(p_{\text{T}}^{i} + p_{\text{T}}^{j})$) values at particle level.

The parameter that governs the regularisation in IBU is the number of iterations. Here, four iterations are chosen. This is a compromise that limits statistical fluctuations that grow due to repeated applications of the unfolding procedure, while controlling the statistical bias toward the particle-level MC predictions induced by the regularisation. The effect of this bias on the measurement is quantified by a dedicated uncertainty, introduced in Sect. 8. With the chosen number of iterations, this uncertainty is mostly negligible ($< 1\%$).

After the histograms of emissions in the LJP are unfolded, they are scaled by the total number of large-R jets N_{jets} to obtain the per-jet density of emissions from Eq. (1). Just like the LJP emissions, the measured number of large-R jets is corrected for acceptance and inefficiency effects to obtain a particle-level result.

8 Uncertainties

The measured LJP is affected by several systematic uncertainties related to the objects calibration, background and signal modelling, and analysis method. All uncertainties are propagated through the unfolding procedure by creating pseudo-data that are then unfolded using the nominal corrections (background estimate, acceptance correction, migration matrix and efficiency correction). The signal modelling uncertainties are estimated as non-closure between the unfolded LJP and the particle-level prediction for the corresponding generator set-up. Detector systematic uncertainties are estimated by varying the relevant parameters in the nominal signal and background predictions, using these as pseudo-data. Background modelling uncertainties are estimated in the same way, using alternative background MC samples to produce the pseudo-data.

Correlations between the number of emissions in the LJP and the number of jets are taken into account in the evaluation of the uncertainties by generating pseudo-experiments for each systematic in which both quantities are varied simultaneously according to the size of the uncertainty. The stan-

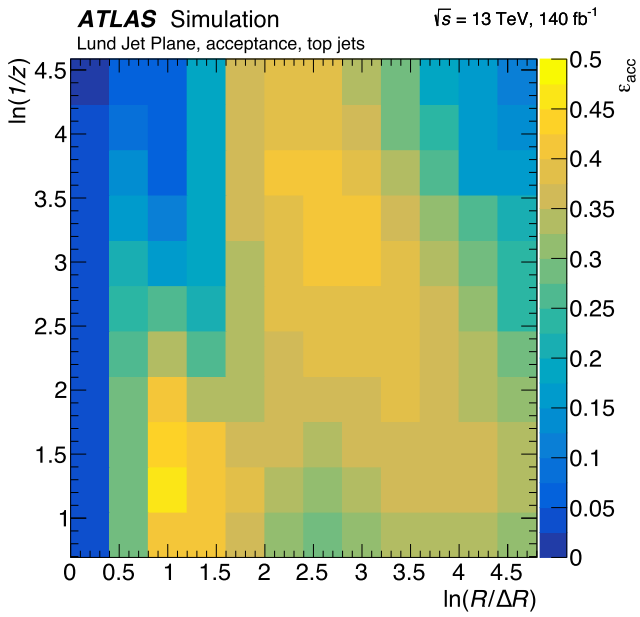

(a)

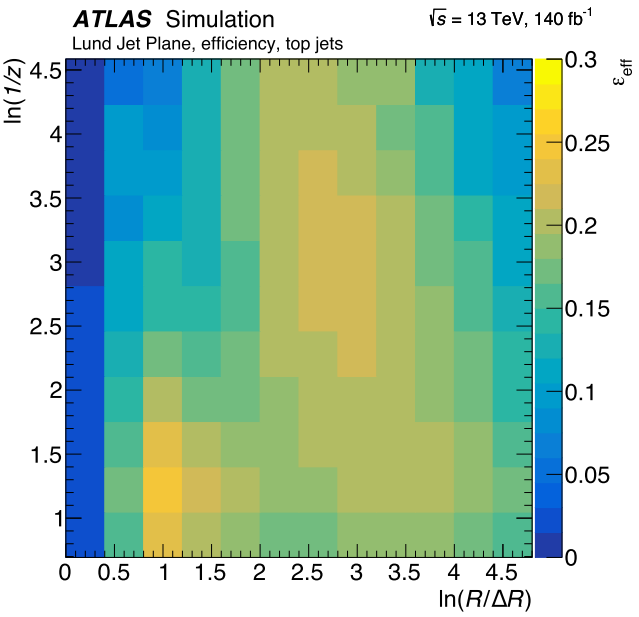

(b)

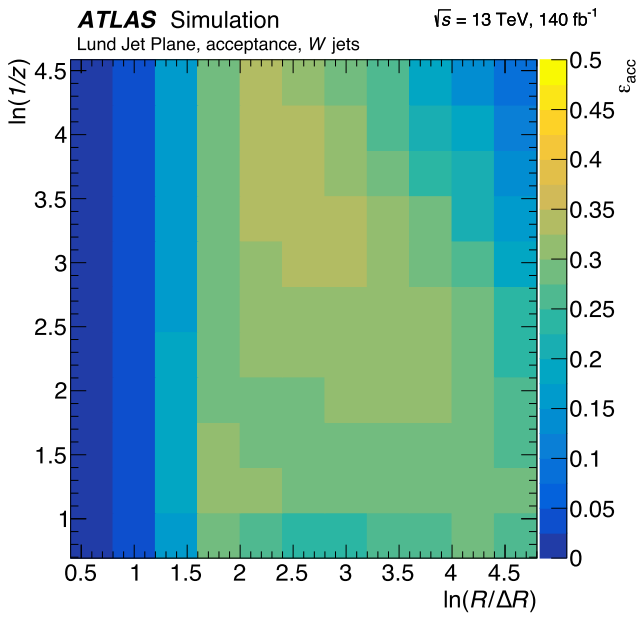

(c)

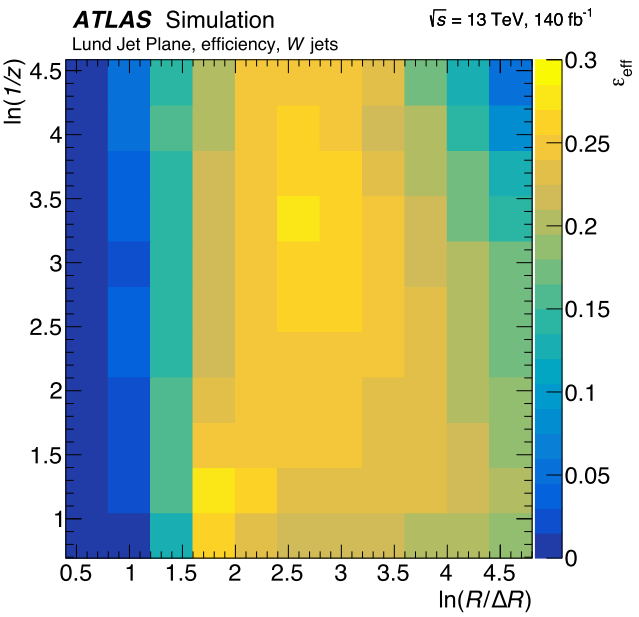

(d)

Fig. 5 Unfolding corrections for the LJP in the **a**, **b** top jet and **c**, **d** W jet selections. The first column reports the ϵ_{acc} factor, sensitive to the selection acceptance and matching between the detector- and particle-level emissions, while the second one shows the ϵ_{eff} corrections. The corrections are evaluated using events simulated with the nominal POWHEG+PYTHIA 8 MC generator

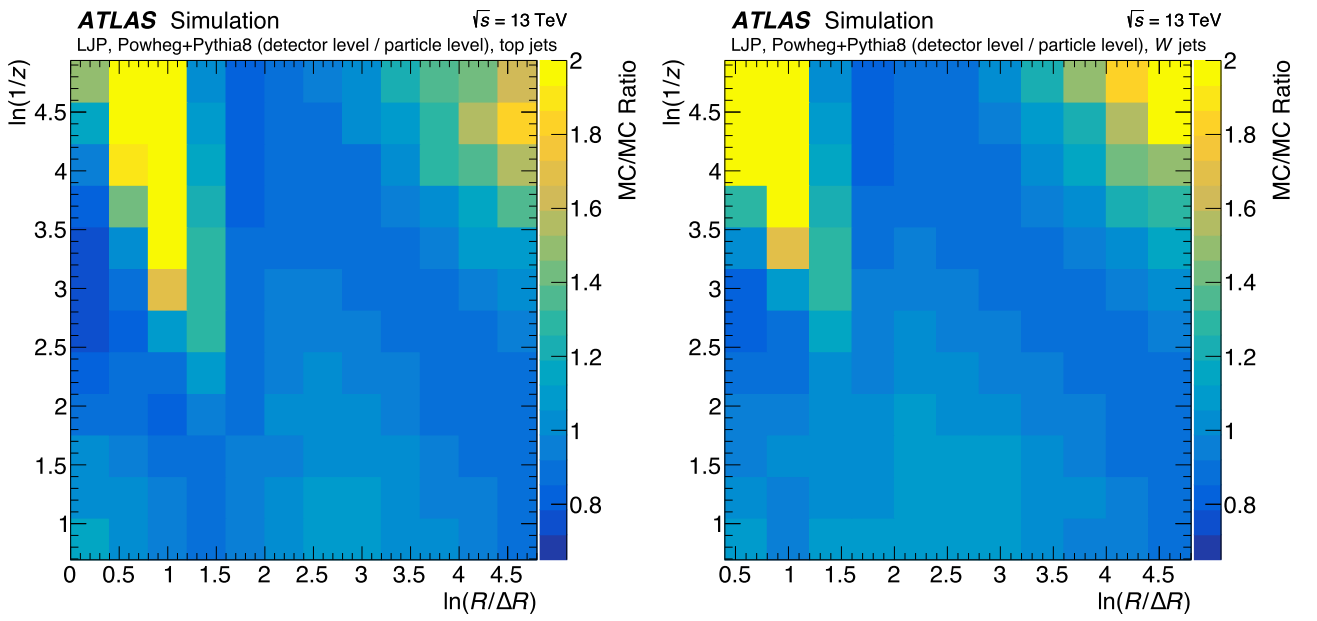

(a) (b)

Fig. 6 Ratios of the detector-level LJP to the particle-level LJP for **a** top jets and **b** W jets. The LJPs are normalised to unity before evaluating the ratio. The LJPs are evaluated using events simulated with the nominal POWHEG+PYTHIA 8 MC generator

dard deviation of the combined variations over the pseudo-experiments gives the total systematic uncertainty.

Uncertainties in the small-R and large-R jet energy scale and resolution [77,81] and large-R jet mass scale and resolution [91], as well as in the b-tagging efficiency [92–94], JVT cut efficiency [79] and $E_{\mathrm{T}}^{\mathrm{miss}}$ reconstruction [95], are included. Uncertainties associated with electrons and muons are estimated for the trigger, reconstruction, identification and isolation efficiencies [82,84], as well as the energy and momentum scales and resolutions [82,96]. The measured LJPs are also affected by uncertainties associated with inner-detector tracks, related to mismodelling of the impact parameters, alignment, tracking efficiency, fake-track rate and reconstruction of tracks in a dense environment [73,97]. The detector-related uncertainties have a considerable impact on the total uncertainty, their size in the centre of the LJP being of the same order as the statistical uncertainty: 5–10% for the top jets and 10–15% for the W jets.

The systematic uncertainty related to the modelling of the $t\bar{t}$ signal process is estimated using alternative Monte Carlo samples. Descriptions of these samples and the meaning of their configurations are presented in Sect. 4. The components of the modelling systematic uncertainty relate to the matrix-element and matching (ME-matching), the parton shower and hadronisation modelling (PS+Had), the assumed recoil system for the decay products of the top quark (RTT), variation of the h_{damp} parameter, FSR and ISR. Lastly, the uncertainty arising from the choice of PDF is estimated using the 30 eigenvectors of the Hessian matrix derived in the PDF4LHC15 uncertainty prescriptions [98]. The $t\bar{t}$ signal modelling uncertainties are the dominant uncertainties of the measurement except in a few very sparsely populated bins at the edges of the plane. The dominant component depends on the region under consideration, as shown in Figs. 8 and 9.

Several uncertainties are evaluated for the contributions from single top quark production, the dominant background process. These include the same ISR and FSR uncertainties considered for $t\bar{t}$, as well as a variation using an alternative treatment of the interference with $t\bar{t}$ in the matrix element (DR/DS). The ISR and FSR uncertainties are treated as uncorrelated with the corresponding variations of the $t\bar{t}$ signal. The inclusive cross-section used to normalise the samples also has an associated uncertainty: 4.2% for the t-channel, 5.4% for the tW-channel and 3.9% for the s-channel process [99,100]. The uncertainties in modelling the single-top process are treated as uncorrelated with the modelling of the $t\bar{t}$ signal. The uncertainty in the W+jets background is estimated by varying the μ_{r} and μ_{f} scales simultaneously by a factor of 2 or 0.5. A 13.3% uncertainty is associated with the normalisation of the $t\bar{t}V$ background [101]. A conservative 50% uncertainty in the normalisation of the diboson, Z+jets and multijet background is considered, given the very small contribution of these backgrounds to the total number of events (1% and 3% in the top jet and W jet selections, respectively). The total uncertainty associated with the background modelling is below 5% across the whole plane.

An unfolding bias uncertainty is estimated using a data-driven method [102]. A set of pseudo-data is obtained by reweighting the predicted particle-level LJP by a smooth function following the ratio of the observed detector-level LJP to the predicted LJP and folding the result using the response matrix. The uncertainty is then evaluated as the non-closure between the unfolded data and the reweighted particle-level distribution. The impact of the uncertainty in the matching procedure between detector- and particle-level emissions on the unfolding procedure, as described in Sect. 7.4, is evaluated by tightening the ΔR matching cut to 0.05. Both uncertainties associated with the unfolding have a small effect (1–3%) on the total uncertainty across the LJP fiducial region.

The uncertainty due to the limited numbers of observed and simulated events is estimated using the bootstrap procedure [103], where weights distributed according to a Poisson distribution with mean 1 are associated with all events to create replicas of the measurement. Each replica is propagated through the unfolding procedure and then divided by the corresponding number of jets, which is also 'bootstrapped' such that statistical correlations with the LJP emissions are preserved. The standard deviation of the unfolded distributions in each bin of the LJP represents the statistical uncertainty. As with the systematic uncertainties, the number of emissions in the LJP and the number of jets are varied simultaneously to account for the correlations induced in the calculation of the emission density.

The uncertainty in the combined 2015–2018 integrated luminosity is 0.83% [28], obtained using the LUCID-2 detector [29] for the primary luminosity measurements, complemented by measurements using the inner detector and calorimeters. The pile-up activity in each MC sample is reweighted to match the conditions in data, and a corresponding uncertainty is evaluated according to the uncertainty in the average number of interactions per bunch crossing.

The total statistical uncertainty and total systematic uncertainty across the LJP are shown in Fig. 7. The statistical uncertainty for the top (W) jets is in the range 5–10% (10–20%) in the bulk of the plane, rising to 50% in the very soft (upper-right) and trimmed (upper-left) edges of the plane. Systematic uncertainties dominate across the whole plane. The total systematic uncertainty outside of the very sparsely populated areas is mostly around 10–30% (10–40%). Peaks of up to 45% (50%) are observed where differences in modelling of the parton shower, hadronisation and ME matching are most pronounced, in the densely populated diagonal and lower-left corner of the plane (cf. the plots shown in Fig. 3). Large peaks of up to 70% are also observed along the less densely populated left edge of the plane, at wide angles, where the W decay products are less likely to be found due to their large boost along the jet's axis.

A summary of the effect of the various sources of uncertainty on a slice through the LJP in the top and W jets is shown in Figs. 8 and 9. Here all the detector uncertainties are grouped together (Total detector), as are the background-related uncertainties (Total background model), signal modelling uncertainties (Total $t\bar{t}$ model) and unfolding bias and matching uncertainties (Total unfolding). The average size of the uncertainty in these slices is 15% and 25% for the top and W jets, respectively, with peaks of up to 40% in both selections. The largest components of the signal modelling uncertainty are shown separately. The modelling of the $t\bar{t}$ signal is the largest source of uncertainty in both selections. The leading component depends on the region of the plane considered and is generally either the FSR, ME-matching or PS+Hadronisation uncertainty. The detector uncertainty components, and especially the tracking uncertainties, become relevant only at very small ΔR where LJP emissions are affected by the detector's spatial resolution. The background and unfolding uncertainties have a negligible impact across the whole plane.

9 Results

The measured density of emissions in the Lund jet plane is shown in Fig. 10a and b for the top and W jet selections respectively. As outlined in Sect. 7.3, the decays of the high-p_{T} top quarks and W bosons can be distinguished in the LJP in the region of $\ln(1/z) < 1.5$, $\ln(R/\Delta R) < 1.5$. In $\eta-\phi$ space, these same hard and wide-angle emissions are what give rise to the three- or two-pronged energy distribution inside the jets. Because the top quark has a larger mass than the W boson, the peak in the lower-left corner of the LJP is shifted towards wider angles for the top jets. The average number of emissions per jet, equivalent to the total integrated density across the LJP shown in Fig. 10, is $6.74 \pm 0.02\,(\mathrm{stat.}) \pm 0.13\,(\mathrm{syst.})$ for the top jets and $6.02 \pm 0.04\,(\mathrm{stat.}) \pm 0.22\,(\mathrm{syst.})$ for the W jets. This implies that, on average, almost one more emission is reconstructed for the top jets, which contain all the decay products of the top quark, than for the W jets. The estimated total uncertainty is greater for the W jets, mainly due to two effects. The first effect is the background modelling uncertainty, which is about 4–5 times greater in these jets. The second and more important effect, is the increased number of events migrating out of the fiducial region due to narrow mass-window cut, which increases the size of the non-closure uncertainties after unfolding corrections.

In the region where ΔR and z are both small, the LJP for the top jets and the W jets resembles that of the light-quark-initiated jets measured in Ref. [13]. Here, a high density of emissions is observed in the transition region between the perturbative and non-perturbative regimes where

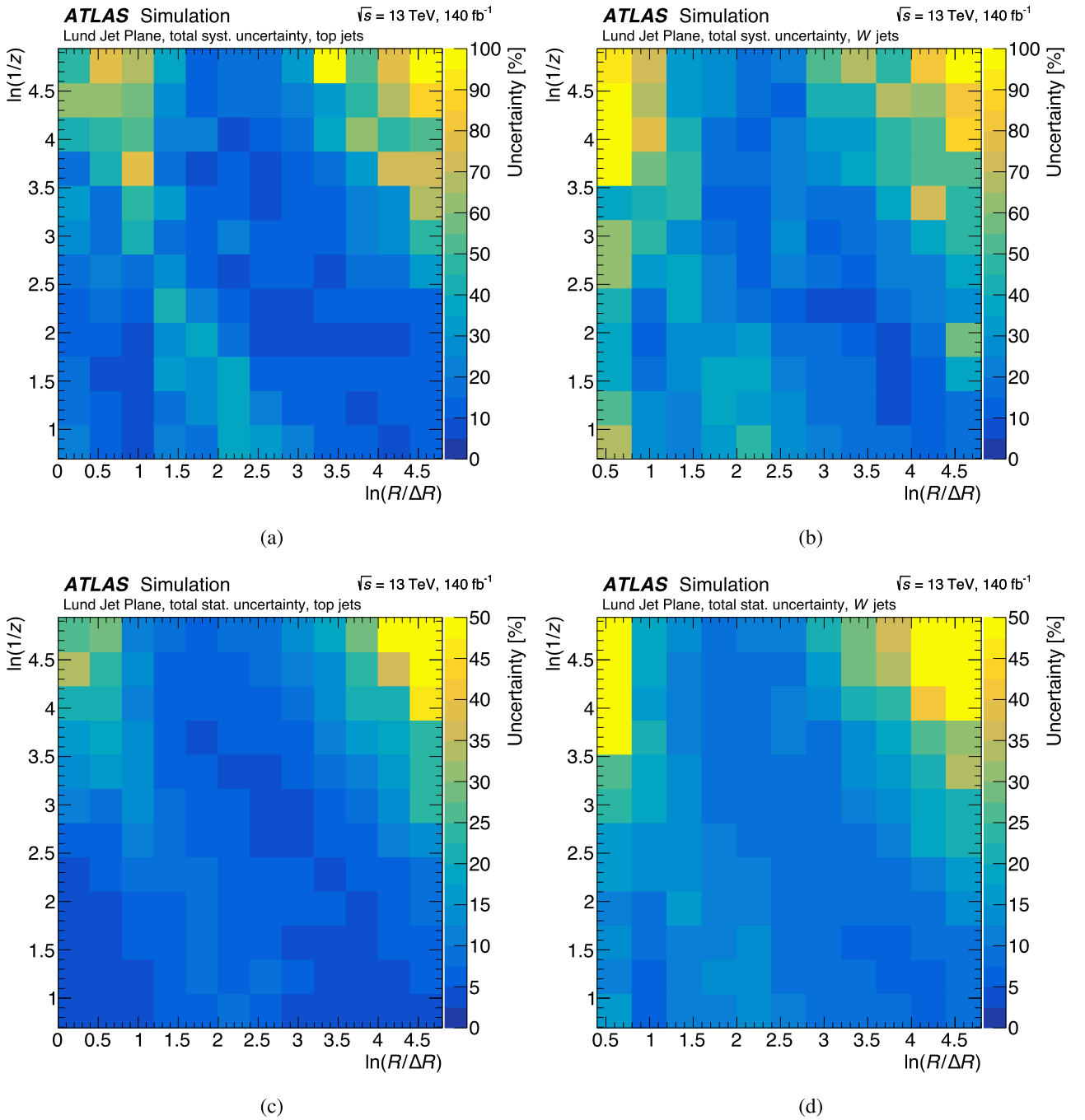

Fig. 7 Total systematic (**a**, **b**) and statistical (**c**, **d**) uncertainty across the LJP. Top jets are shown in **a**, **c**, W jets in **b**, **d**

$k_{\mathrm{T}}(\approx z\,\Delta R p_{\mathrm{T}}^{\mathrm{Jet}}) = \Lambda_{\mathrm{QCD}}$. In the upper-right corner, the number of emissions is suppressed. Here $k_{\mathrm{T}} < \Lambda_{\mathrm{QCD}}$, so the density of emissions receives large corrections from non-perturbative terms proportional to powers of $(k_{\mathrm{T}}/\Lambda_{\mathrm{QCD}})$ [2].

In the upper-left corner of the LJP, there is a low density of emissions due to the trimming procedure that was applied to the jets' constituents. Since the trimming algorithm proceeds by reclustering the jet constituents with a radius parameter $R_{\mathrm{trim}} = 0.2$ and subsequently discarding subjets with a p_{T}-fraction smaller than $f_{\mathrm{trim}} = 0.05$, one can expect this region to be bounded by $\ln(R/\Delta R) \lesssim \ln(R/R_{\mathrm{trim}}) \approx 1.6$ and $\ln(1/z) \gtrsim \ln(1/f_{\mathrm{trim}}) \approx 2.2$.

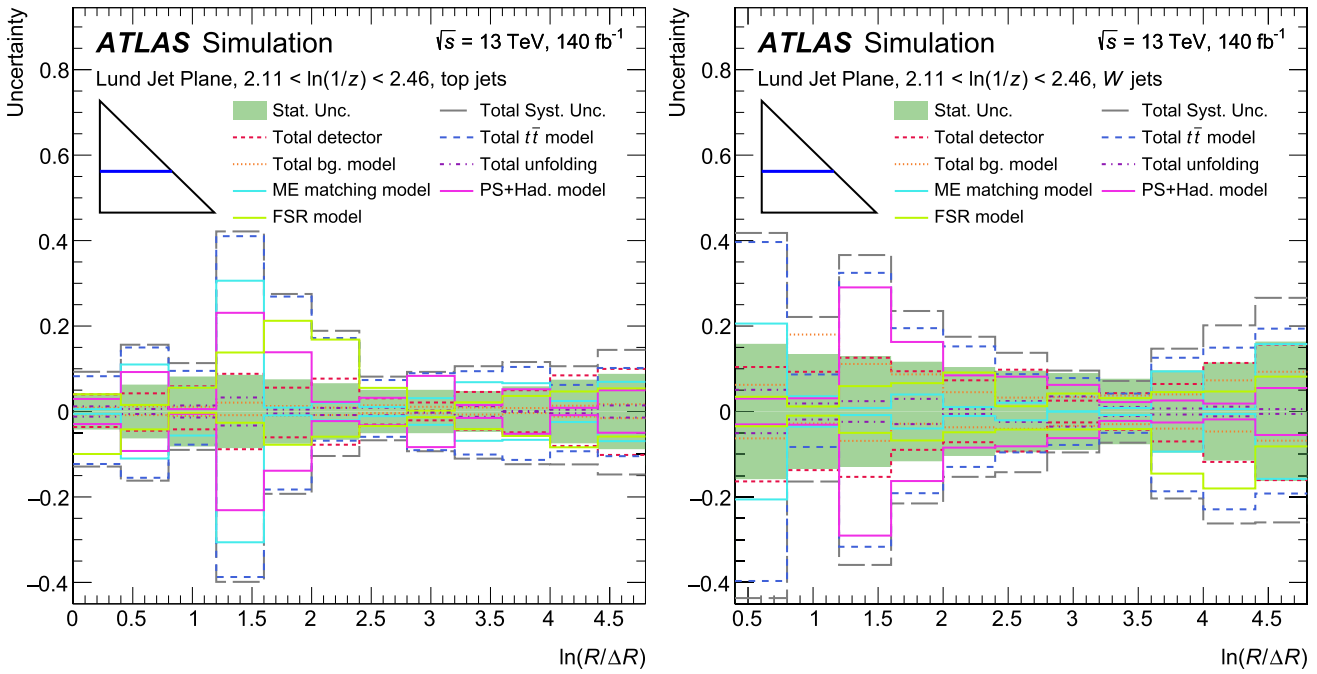

(a) (b)

Fig. 8 Breakdown of the systematic uncertainties on the unfolded density of emissions in a slice through the LJP along $\ln(R/\Delta R)$ for the **a** top jet and **b** W jet selections. The total systematic uncertainty is reported, as well as the total contributions from signal modelling, detector effects, background modelling and unfolding. The major sources of signal modelling uncertainties are also presented in the plot as separate contributions. Not shown are the RTT, PDF and ISR uncertainties, of which the RTT uncertainty contributes the most toward the total $t\bar{t}$ modelling uncertainty. The coloured band represents the total statistical uncertainty

9.1 Comparison with MC predictions

The measured LJP is compared with several Monte Carlo simulations of top-pair production, generated at NLO in QCD and subsequently matched to the PS and hadronisation models, as described in Sect. 4. A quantitative comparison between the measurement and the MC set-ups is obtained by performing χ^2 tests:

$$\chi^2 = V_j^{\mathrm{T}}(C_{\mathrm{syst}} + C_{\mathrm{stat}} + C_j)^{-1}V_j \tag{2}$$

where V is a vector containing the difference between the measurement and the prediction for each generator set-up j, and C^{-1} is the inverse of the covariance matrix, which is calculated from the sum of the following: the statistical covariance (C_{stat}) and systematic covariance (C_{syst}) for the measurement, and the statistical covariance for the simulated sample, C_j. Starting from the systematic uncertainties of the measurement, the matrix C_{syst} is derived with the following assumptions: each component is considered uncorrelated with respect to the other systematic uncertainties and, for each component, the bins of the distribution are considered either fully correlated or uncorrelated, depending on the relative sign of the uncertainties in each bin. The statistical covariance C_{stat} is derived using the 'bootstrap' technique, described for the statistical uncertainty in Sect. 8, where bin-to-bin correlations are calculated from an ensemble of simulated LJP histograms whose statistical variance matches that of the measurement. The statistical uncertainty of the predictions, contained in the matrix C_j, is only due to the number of simulated entries in each bin. Double-sided uncertainties are not symmetrised prior to creating the covariance matrix and enter just once in the calculation. Correlations between bins are evaluated from the sign of the up/down components of the uncertainties. Two bins are considered correlated if the signs of the components in each bin are the same and anti-correlated if they are opposite.

The χ^2 formula in Eq. (2) is used to evaluate how well the measurement agrees with the predictions across the whole regions shown in Fig. 10, as well as in smaller regions and slices thereof. In order to compare χ^2 values for regions of different size, the number of degrees of freedom (NDF), which is equal to the number of bins in the region investigated, must also be considered. The p value for a given χ^2 and NDF is given by the formula $1 - \Gamma(\mathrm{NDF}/2, \chi^2/2)$, where Γ denotes the cumulative distribution function of the gamma distribution.

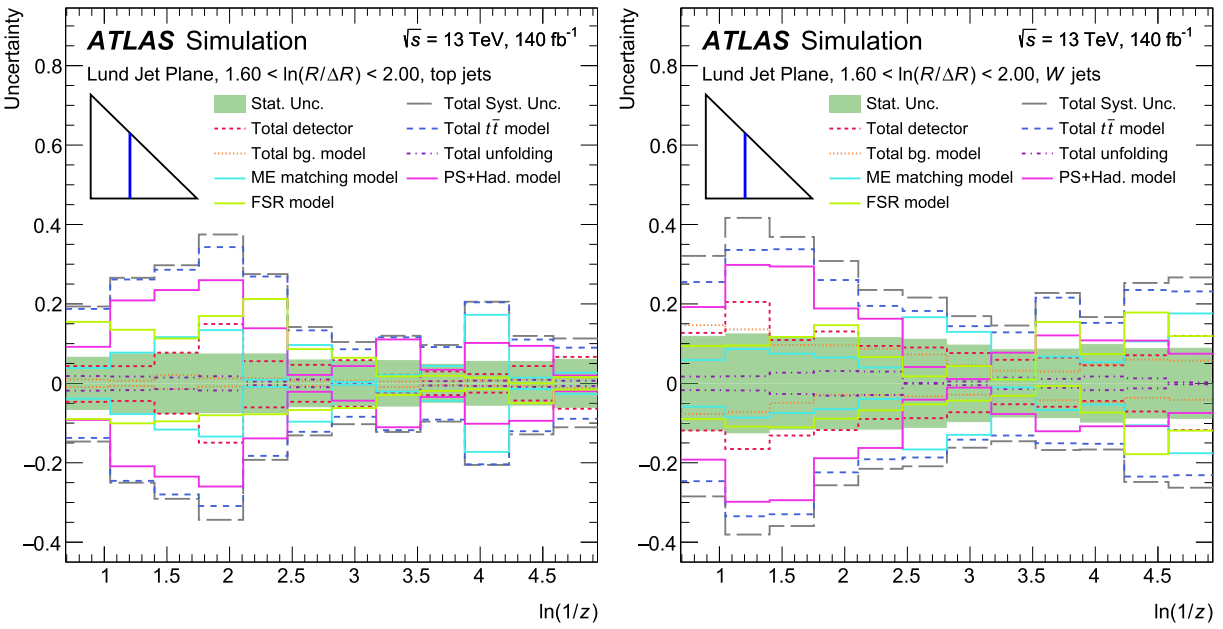

(a) (b)

Fig. 9 Breakdown of the systematic uncertainties in the unfolded density of emissions in a slice through the LJP along $\ln(1/z)$ for the **a** top jet and **b** W jet selections. The total systematic uncertainty is reported, as well as the total contributions from signal modelling, detector effects, background modelling and unfolding. The major sources of signal modelling uncertainties are also presented in the plot as separate contributions. Not shown are the RTT, PDF and ISR uncertainties, of which the RTT uncertainty contributes the most toward the total $t\bar{t}$ modelling uncertainty. The coloured band represents the total statistical uncertainty

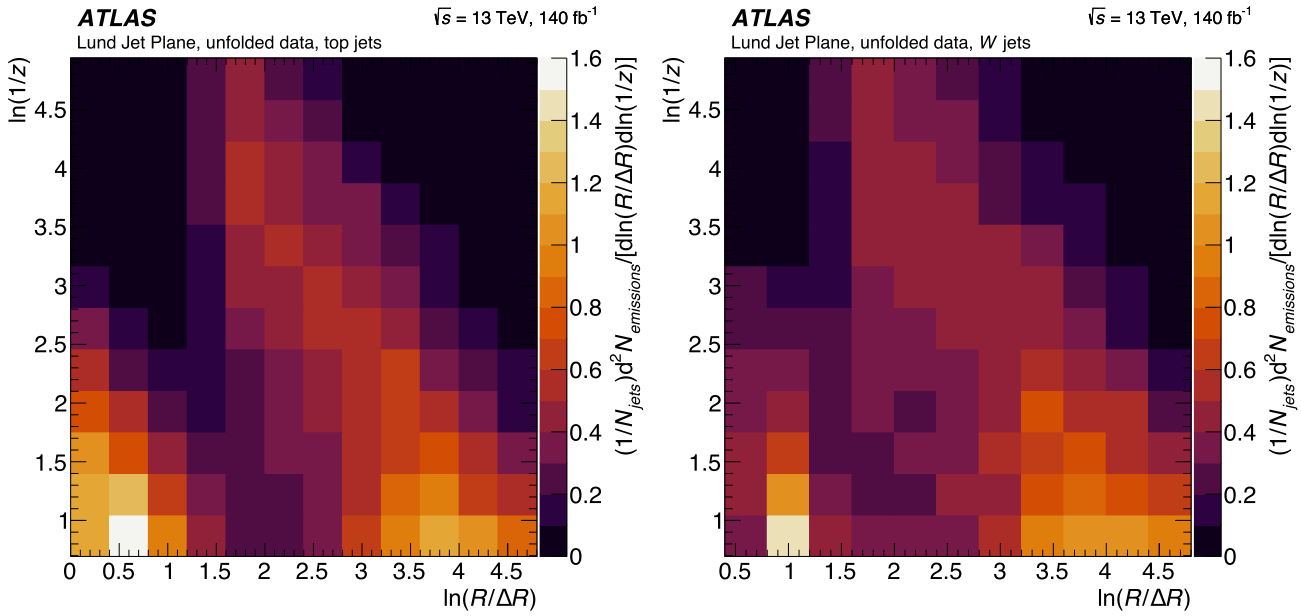

(a) (b)

Fig. 10 Measured LJP for the **a** top jet and **b** W jet selections

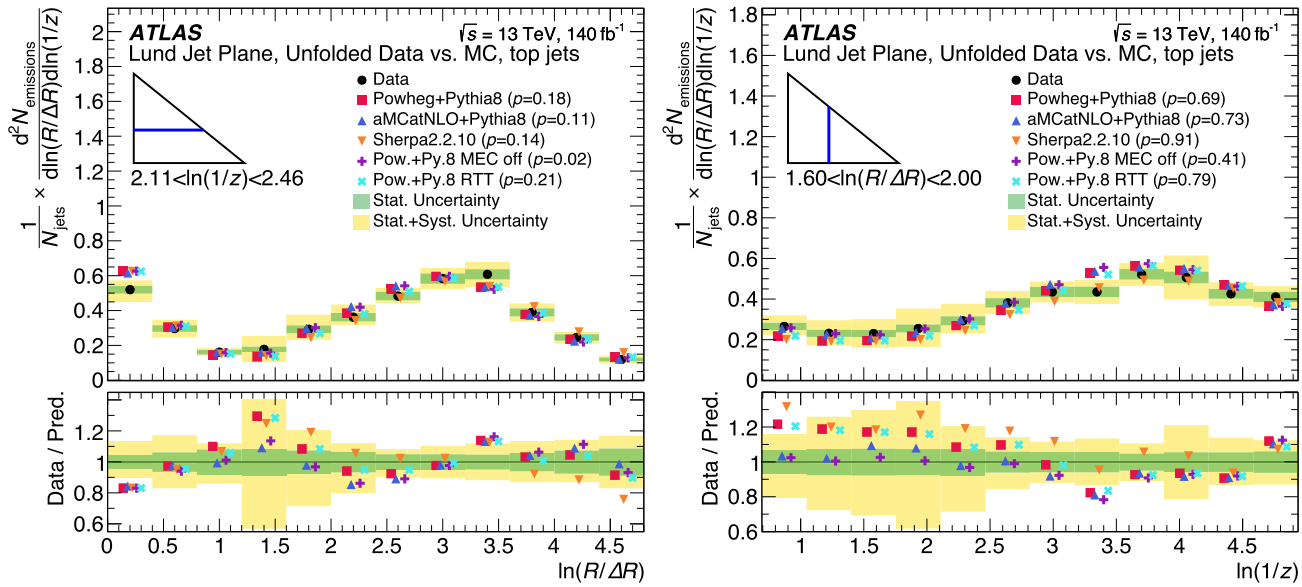

(a) (b)

Fig. 11 Slices through the measured top jet LJP, as a function of **a** $\ln(R/\Delta R)$ and **b** $\ln(1/z)$. The data are compared with several predictions, differing from the nominal POWHEG+PYTHIA 8 predictions in both the hard scatter and showering generator setting. The bottom pad reports the ratio of the data to the different predictions, with both the total and statistical uncertainty of the measured LJP shown as a coloured band. Local p values for the bins in the slice are shown for each prediction. The number of degrees of freedom in the p value calculation is equal to the number of bins in the slice

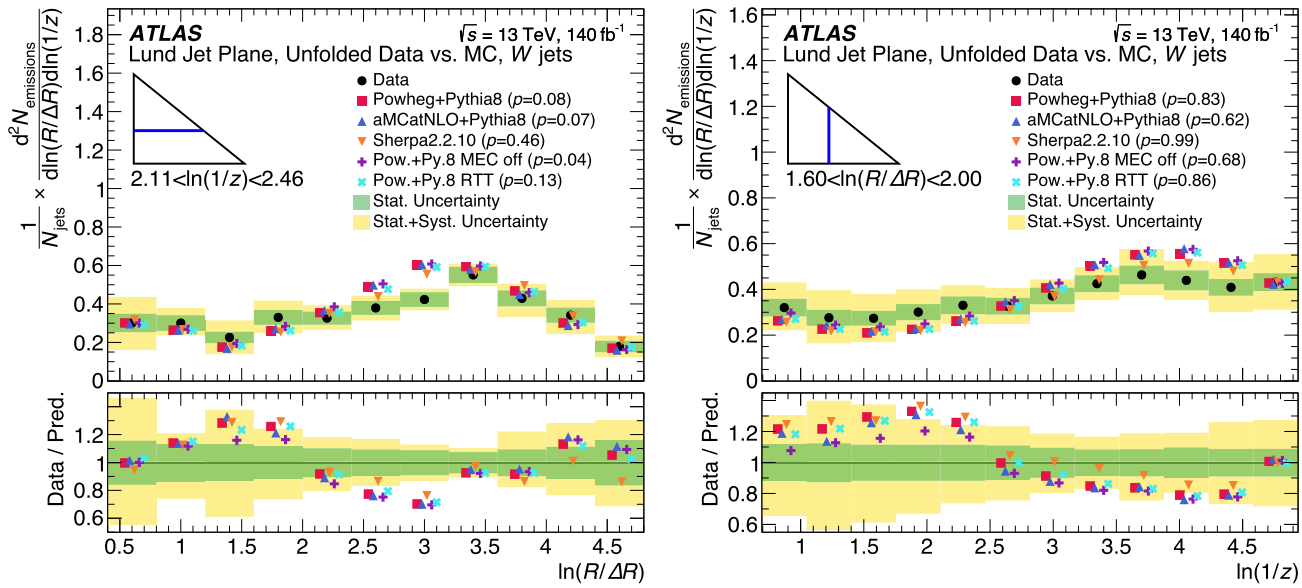

(a) (b)

Fig. 12 Slices through the measured W jet LJP, as a function of **a** $\ln(R/\Delta R)$ and **b** $\ln(1/z)$. The data are compared with several predictions, differing from the nominal POWHEG+PYTHIA 8 predictions in both the hard scatter and showering generator setting. The bottom pad reports the ratio of the data to the different predictions, with both the total and statistical uncertainty of the measured LJP shown as a coloured band. Local p values for the bins in the slice are shown for each prediction. The number of degrees of freedom in the p value calculation is equal to the number of bins in the slice

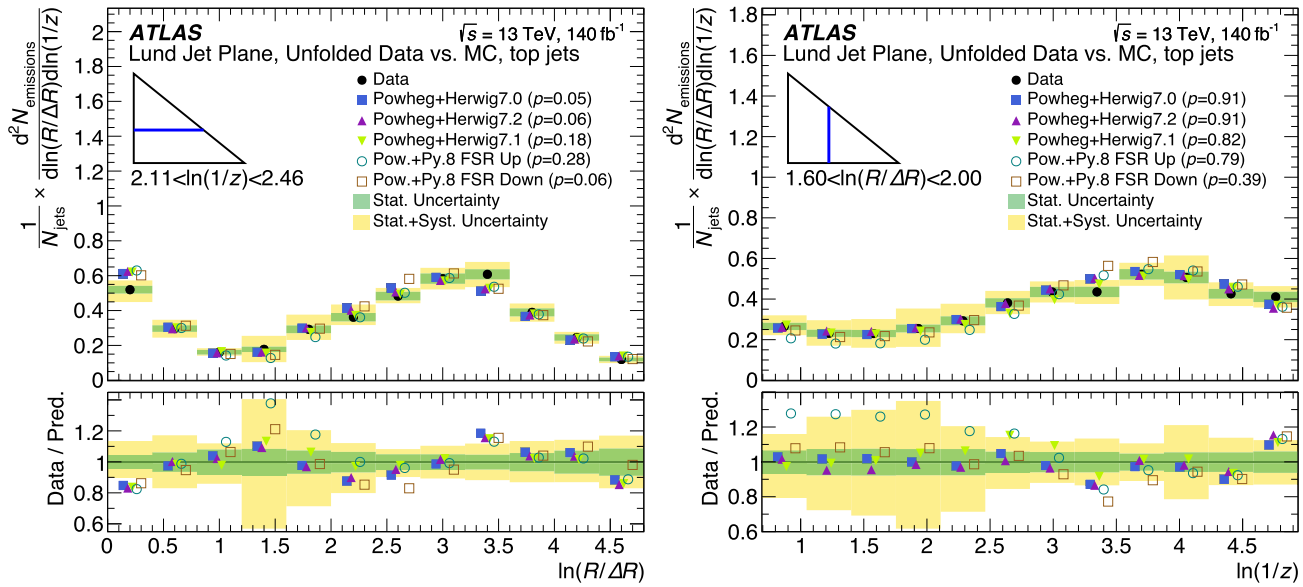

(a) (b)

Fig. 13 Slices through the measured top jet LJP, as a function of **a** $\ln(R/\Delta R)$ and **b** $\ln(1/z)$. The data are compared with several predictions, differing from the nominal POWHEG+PYTHIA 8 predictions in both the hard scatter and showering generator setting. The bottom pad reports the ratio of the data to the different predictions, with both the total and statistical uncertainty of the measured LJP shown as a coloured band. Local p values for the bins in the slice are shown for each prediction. The number of degrees of freedom in the p value calculation is equal to the number of bins in the slice

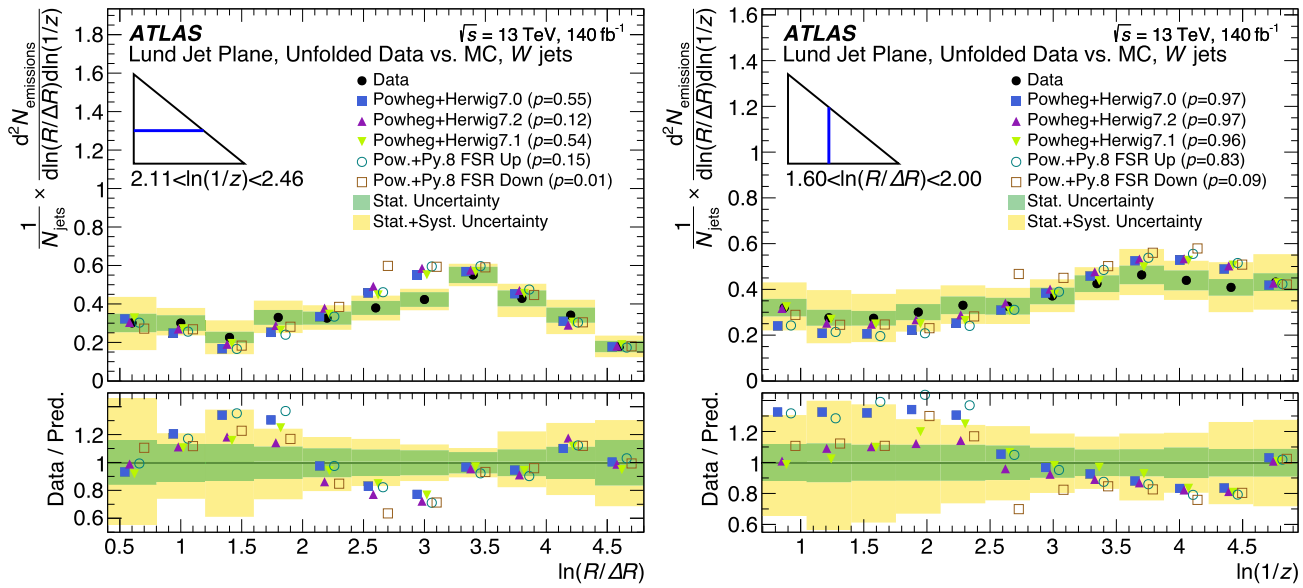

(a) (b)

Fig. 14 Slices through the measured W jet LJP, as a function of **a** $\ln(R/\Delta R)$ and **b** $\ln(1/z)$. The data are compared with several predictions, differing from the nominal POWHEG+PYTHIA 8 predictions in both the hard scatter and showering generator setting. The bottom pad reports the ratio of the data to the different predictions, with both the total and statistical uncertainty of the measured LJP shown as a coloured band. Local p values for the bins in the slice are shown for each prediction. The number of degrees of freedom in the p value calculation is equal to the number of bins in the slice

Table 2 Values of χ^2 and corresponding p values for the top jets, calculated for the full LJP and the various $t\bar{t}$ Monte Carlo samples

Sample name	χ^2	χ^2/NDF (NDF = 132)	p value (%)
Powheg + Pythia 8	149	1.13	15
aMCatNLO + Pythia 8	149	1.13	14
Sherpa 2.2.10	139	1.05	33
Powheg + Herwig 7.0	169	1.28	2
Powheg + Herwig 7.2	165	1.25	3
Powheg + Herwig 7.1	150	1.14	14
Powheg + Pythia 8 MEC Off	176	1.34	1
Powheg + Pythia 8 RTT	145	1.10	20
Powheg + Pythia 8 FSR Up	148	1.12	17
Powheg + Pythia 8 FSR Down	162	1.23	4

Table 3 Values of χ^2 for the W jets, calculated for the full LJP and the various $t\bar{t}$ Monte Carlo samples. The corresponding p values are all smaller than 1%

Sample name	χ^2	χ^2/NDF (NDF = 121)
Powheg + Pythia 8	233	1.92
aMCatNLO + Pythia 8	204	1.69
Sherpa 2.2.10	168	1.39
Powheg + Herwig 7.0	170	1.41
Powheg + Herwig 7.2	168	1.39
Powheg + Herwig 7.1	177	1.46
Powheg + Pythia 8 MEC Off	240	1.99
Powheg + Pythia 8 RTT	227	1.88
Powheg + Pythia 8 FSR Up	230	1.90
Powheg + Pythia 8 FSR Down	213	1.76

Comparisons with various generator set-ups are performed in central slices through the plane in Figs. 11 and 12. MC event generator predictions using different matrix-element, parton-shower and hadronisation models are investigated. In Figs. 13 and 14 the measurement is compared with three versions of the HERWIG 7 PS and hadronisation generator as well as with the PYTHIA 8 generator with various amounts of FSR. These slices cover the most densely populated region of the LJP, including the regions with the smallest total uncertainty, while also showing the transitions between regions dominated by ME-matching, parton-shower and hadronisation effects. Differences between predictions and the data are found to lie within the estimated uncertainties in large sections of the spectra. Sizeable differences are found in the central region of the plane, particularly in the W jet selection, as can be seen in the slices shown in Figs. 12a and 14a where all predictions are found to lie outside the uncertainty band in the two bins covering $2.4 < \ln(R/\Delta R) < 3.2$. As statistical sources contribute more than 50% of the total uncertainty in many bins (45% of bins in the slice shown in Figs. 12a, 14a), the precision of the measurement could be expected to improve significantly if repeated with a larger dataset.

The level of agreement between the predictions and the data in the slices shown in Figs. 11, 12, 13 and 14 is quantified by evaluating a local p value using the method outlined above and considering only the bins within the slice. In both selections, agreement with the various predictions is better for slices along the $\ln(1/z)$ direction. It should be noted that the average uncertainty is larger for these slices than for the $\ln(R/\Delta R)$ slices. Along the $\ln(R/\Delta R)$ direction in the top jets, the p values for the slice shown range from 2 to 28%. For the W jets in the same slice, they range from 1 to 55%. Only the lowest of these p values, $< 5\%$ for POWHEG+PYTHIA 8 (FSR Down), implies disagreement with the data. Along the $\ln(1/z)$ direction, p values in the range 39–91% are observed for the top jets. For the W jets, p values are in the range 62–99% for all predictions except the POWHEG+PYTHIA 8 (FSR Down) sample, which yields a somewhat lower p value of 9%. This is likely due to the large differences between this prediction and the measurement around $\ln(1/z) \approx 2.7$ and $\ln(1/z) \approx 4.2$.

A global picture of how well the various generators agree with the measurement is given by the figures shown in Tables 2 and 3, which report the χ^2 values and corresponding p values for the whole plane. In the top jet selection, disagreement with the measurement is observed for POWHEG+PYTHIA 8 (MEC Off) and POWHEG+PYTHIA 8 (FSR Down) as well as POWHEG+HERWIG 7.0 and POWHEG+HERWIG 7.2 with p values $< 5\%$. The lowest p value, at 1%, is obtained for the POWHEG+PYTHIA 8 (MEC Off) sample. SHERPA 2.2.10 shows the highest degree of agreement with the data at a p value of 33%. For the W jets, disagreement is observed between all the tested predictions and the measurement, as the p values are less than 1%. The greatest disagreement is again observed for POWHEG+PYTHIA 8 (MEC Off).

Local p values are evaluated for nine subregions of the LJPs. These as well as the boundaries of the subregions are shown in Fig. 15. The values are calculated from the χ^2 and NDF corresponding to the number of bins in each subregion. In the top jets, p values $\leq 10\%$ are observed for SHERPA 2.2.10, POWHEG+PYTHIA 8 (FSR Down) and POWHEG+PYTHIA 8 (FSR Up) in one subregion each. In the W jets, POWHEG+PYTHIA 8 (FSR Down) yields p values $\leq 10\%$ in three subregions and POWHEG+PYTHIA 8 (MEC Off) in one. Due to large bin-to-bin correlations across the whole plane, including bins with large data–MC differences, the global p values in Table 2 are generally much smaller than the smallest local p values, which only consider correlations within the respective subregions.

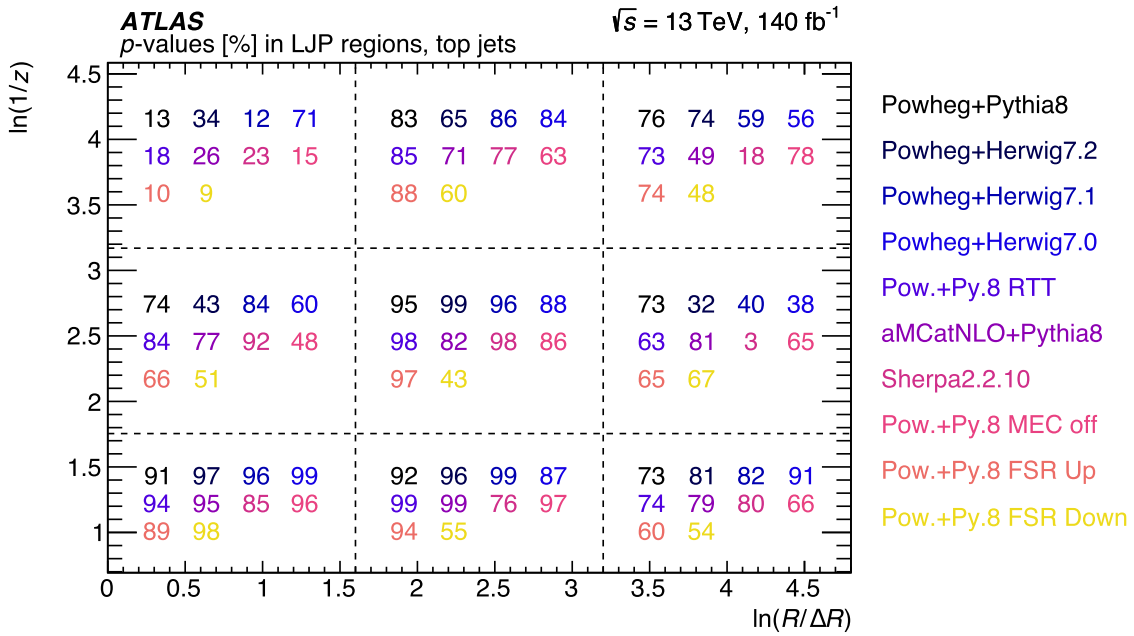

(a)

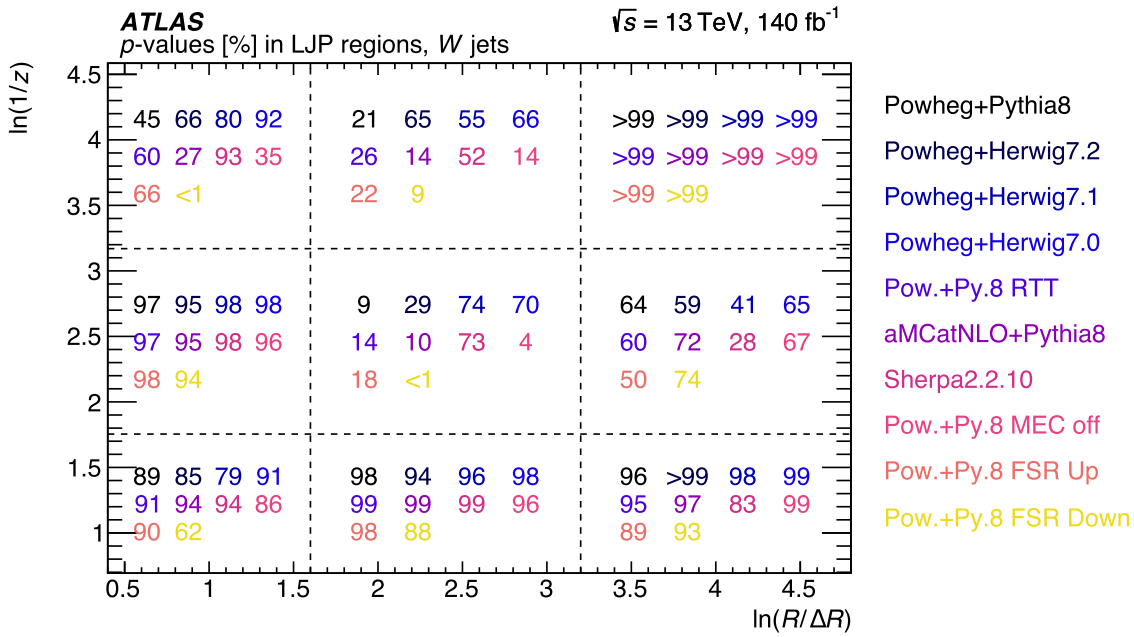

(b)

Fig. 15 The p values for the MC predictions in different regions of the LJP in the **a** top jet and **b** W jet selections. The number of degrees of freedom used in calculating the p values is equal to the number of bins in each region

In the lower-left corner of the plane, at wide angles and large momentum fractions, no p value below 50% is observed for either the top jets or the W jets, showing no disagreement between the data and the predictions. The p values for the top jets range from 85 to 99%. In the W jets, p values of 85–94% are observed for all predictions except POWHEG+PYTHIA 8 (FSR Down), which gives a p value of 62%.

In the subregion at the centre of the plane, p values $< 50\%$ are observed for only one MC prediction in the top jets, namely POWHEG+PYTHIA 8 (FSR Down) at 43%. For the W jets, POWHEG+PYTHIA 8 (FSR Down) and POWHEG+PYTHIA

8 (MEC Off) disagree with the measurement with p values of $< 1\%$ and 4% respectively, while POWHEG+PYTHIA 8 and AMC@NLO+PYTHIA 8 score slightly better at 9%, respectively 10%.

Low p values are also observed for the W jets in the centre-top subregion at $\ln(1/z) > 3.2$, the lowest being a p value of 9% from POWHEG+PYTHIA 8 (FSR Down). All but four generators yield p values of 26% or less, the exceptions being SHERPA 2.2.10 and the three versions of HERWIG, all with p values $> 52\%$.

In the subregion at narrow angles and medium momentum fractions ($3.2 < \ln(R/\Delta R) < 4.8$, $1.7 < \ln(1/z) < 3.2$) in the top jets, a p value of 3% indicates disagreement between SHERPA 2.2.10 and the data. Among the generators, SHERPA 2.2.10 also yields the lowest p value, at 18%, in the higher $\ln(1/z)$ subregion ($3.2 < \ln(1/z) < 4.6$). In the W jets, the lowest degree of agreement is observed for SHERPA 2.2.10 in the former of the two regions, but at a considerably higher p value of 28%. This tendency towards local disagreement with the data may indicate mismodelling of narrow-angle emissions by the SHERPA 2.2.10 parton-shower generator.

In the subregion at wide angles and small momentum fractions ($\ln(R/\Delta R) < 1.6$, $\ln(1/z) > 3.2$) in the top jets, all MC predictions except POWHEG+HERWIG 7.0 give p values $\leq 50\%$, although only POWHEG+PYTHIA 8 (FSR Down) and (FSR Up) are $\leq 10\%$ and none are $< 5\%$. This is the subregion in which contributions from the underlying event are most likely to enter, provided that these were not already removed by the trimming algorithm. For the W jets in the said subregion, POWHEG+PYTHIA 8 (FSR Down) disagrees with the measurement at a p value $< 1\%$, while POWHEG+PYTHIA 8, AMC@NLO+PYTHIA 8 and POWHEG+PYTHIA 8 (MEC Off) yield p values $\leq 50\%$.

10 Conclusion

The primary Lund jet plane density has been measured in large hadronic jets initiated by the decays of top quarks or W bosons in 140 fb^{-1} of 13 TeV pp collision data collected with the ATLAS detector at the LHC. The jets were selected from events matching the topology of $t\bar{t}$ pair production in which one of the (anti-)top candidates decays fully hadronically while the other produces a lepton, a neutrino and a b-tagged jet. Jets containing the full decay products of either a top quark or its daughter W boson were studied separately by refining the selections on the large jets. This is the first measurement of the LJP for jets produced in the decays of boosted heavy particles, and it is the first LJP measurement by ATLAS to use $R = 1.0$ jets. The measurement builds on and complements previous analyses by ATLAS and other LHC experiments, including measurements of the LJP for small-radius jets initiated by light quarks or gluons, as well as many measurements of related jet-substructure observables in jets initiated by top quarks or W bosons.

The LJP is measured at the level of stable particles after removing the effects of limited detector resolution and reconstruction efficiency. The statistical procedure for the removal of detector effects makes use of Monte Carlo event generator predictions. The total uncertainty in the measured observable is dominated by systematic uncertainties due to modelling of the $t\bar{t}$ signal across most of the measured phase space. In the centre of the Lund jet plane, where it is most densely populated (around $0.5 < \ln(R/\Delta R) < 3.5$, $\ln(1/z) < 3.5$), the size of the uncertainty is in the range 15–40% for both the top and W jets. The modelling uncertainty is dominated by components related to the choice of parton-shower and hadronisation model, and value of α_s^{FSR}. The measured LJP has a structure distinctly different from the LJP for jets initiated by light quarks or gluons. Two densely populated regions are visible: one mainly related to the decays of the top quarks and W bosons into highly boosted quarks, and the other corresponding to subsequent emissions of softer QCD radiation.

The measurement is compared with a wide range of predictions using different Monte Carlo generator settings. Alternative MC generator samples were considered for the $t\bar{t}$ production at NLO in QCD and for the parton shower, while the remaining samples were obtained using alternative configurations of the nominal POWHEG+PYTHIA 8 set-up. A quantitative comparison was performed both in the whole LJP and in multiple subregions of it. For the W jets, no generator agrees with the measurement across the whole LJP, although there is better agreement in the subregions. In the top jets, the highest level of agreement is observed for the SHERPA 2.2.10 prediction, with a p value of 33%. Disagreement with the data is observed for POWHEG+HERWIG 7.0, POWHEG+HERWIG 7.2, POWHEG+PYTHIA 8 (MEC Off) and POWHEG+PYTHIA 8 (FSR Down), with p values $< 5\%$. The extent to which the various generators agree with the measurement was found to be highly dependent on the LJP coordinate ranges considered, as local p values close to 1, and more rarely $< 10\%$, are found when restricting the tests to one of nine subregions of the plane. The lack of overall compatibility between the measurement and the MC predictions, particularly in the W jets, can be compared with results of previous measurements of the LJP in dijet events [13,15], where differences of more than four times the total uncertainty were observed across many bins making small statistical contributions to the uncertainty.

The results show that many aspects of hadronic top quark or W boson decays, including parton-shower and hadronisation effects, can be investigated by measuring a single two-dimensional jet-substructure observable. The results could be useful for improving the tuning of MC $t\bar{t}$ event generators by targeting the parameters controlling sources of radiation that are poorly modelled in the LJP. They will also be a valu-

able resource for the ongoing development of new, highly performant top and W jet taggers that make use of the LJP or related jet-substructure observables.

Acknowledgements We thank CERN for the very successful operation of the LHC and its injectors, as well as the support staff at CERN and at our institutions worldwide without whom ATLAS could not be operated efficiently. The crucial computing support from all WLCG partners is acknowledged gratefully, in particular from CERN, the ATLAS Tier-1 facilities at TRIUMF/SFU (Canada), NDGF (Denmark, Norway, Sweden), CC-IN2P3 (France), KIT/GridKA (Germany), INFN-CNAF (Italy), NL-T1 (Netherlands), PIC (Spain), RAL (UK) and BNL (USA), the Tier-2 facilities worldwide and large non-WLCG resource providers. Major contributors of computing resources are listed in Ref. [104]. We gratefully acknowledge the support of ANPCyT, Argentina; YerPhI, Armenia; ARC, Australia; BMWFW and FWF, Austria; ANAS, Azerbaijan; CNPq and FAPESP, Brazil; NSERC, NRC and CFI, Canada; CERN; ANID, Chile; CAS, MOST and NSFC, China; Minciencias, Colombia; MEYS CR, Czech Republic; DNRF and DNSRC, Denmark; IN2P3-CNRS and CEA-DRF/IRFU, France; SRNSFG, Georgia; BMBF, HGF and MPG, Germany; GSRI, Greece; RGC and Hong Kong SAR, China; ISF and Benoziyo Center, Israel; INFN, Italy; MEXT and JSPS, Japan; CNRST, Morocco; NWO, Netherlands; RCN, Norway; MNiSW, Poland; FCT, Portugal; MNE/IFA, Romania; MESTD, Serbia; MSSR, Slovakia; ARIS and MVZI, Slovenia; DSI/NRF, South Africa; MICIU/AEI, Spain; SRC and Wallenberg Foundation, Sweden; SERI, SNSF and Cantons of Bern and Geneva, Switzerland; NSTC, Taipei; TENMAK, Türkiye; STFC/UKRI, United Kingdom; DOE and NSF, USA. Individual groups and members have received support from BCKDF, CANARIE, CRC and DRAC, Canada; PRIMUS 21/SCI/017, CERN-CZ and FORTE, Czech Republic; COST, ERC, ERDF, Horizon 2020, ICSC-NextGenerationEU and Marie Skłodowska-Curie Actions, European Union; Investissements d'Avenir Labex, Investissements d'Avenir Idex and ANR, France; DFG and AvH Foundation, Germany; Herakleitos, Thales and Aristeia programmes co-financed by EU-ESF and the Greek NSRF, Greece; BSF-NSF and MINERVA, Israel; Norwegian Financial Mechanism 2014-2021, Norway; NCN and NAWA, Poland; La Caixa Banking Foundation, CERCA Programme Generalitat de Catalunya and PROMETEO and GenT Programmes Generalitat Valenciana, Spain; Göran Gustafssons Stiftelse, Sweden; The Royal Society and Leverhulme Trust, United Kingdom. In addition, individual members wish to acknowledge support from CERN: European Organization for Nuclear Research (CERN PJAS); Chile: Agencia Nacional de Investigación y Desarrollo (FONDECYT 1190886, FONDECYT 1210400, FONDECYT 1230812, FONDECYT 1230987); China: Chinese Ministry of Science and Technology (MOST-2023YFA1605700, MOST-2023YFA1609300), National Natural Science Foundation of China (NSFC - 12175119, NSFC 12275265, NSFC-12075060); Czech Republic: Czech Science Foundation (GACR - 24-11373 S), Ministry of Education Youth and Sports (FORTE CZ.02.01.01/00/22_008/0004632), PRIMUS Research Programme (PRIMUS/21/SCI/017); EU: H2020 European Research Council (ERC - 101002463); European Union: European Research Council (ERC - 948254, ERC 101089007), Horizon 2020 Framework Programme (MUCCA - CHIST-ERA-19-XAI-00), European Union, Future Artificial Intelligence Research (FAIR-NextGenerationEU PE00000013), Italian Center for High Performance Computing, Big Data and Quantum Computing (ICSC, NextGenerationEU); France: Agence Nationale de la Recherche (ANR-20-CE31-0013, ANR-21-CE31-0013, ANR-21-CE31-0022, ANR-22-EDIR-0002), Investissements d'Avenir Labex (ANR-11-LABX-0012); Germany: Baden-Württemberg Stiftung (BW Stiftung-Postdoc Eliteprogramme), Deutsche Forschungsgemeinschaft (DFG - 469666862, DFG - CR 312/5-2); Italy: Istituto Nazionale di Fisica Nucleare (ICSC, NextGenerationEU), Ministero dell'Università e della Ricerca (PRIN - 20223N7F8K - PNRR M4.C2.1.1); Japan: Japan Society for the Promotion of Science (JSPS KAKENHI JP21H05085, JSPS KAKENHI JP22H01227, JSPS KAKENHI JP22H04944, JSPS KAKENHI JP22KK0227); Netherlands: Netherlands Organisation for Scientific Research (NWO Veni 2020 - VI.Veni.202.179); Norway: Research Council of Norway (RCN-314472); Poland: Ministry of Science and Higher Education (IDUB AGH, POB8, D4 no 9722), Polish National Agency for Academic Exchange (PPN/PPO/2020/1/00002/U/00001), Polish National Science Centre (NCN 2021/42/E/ST2/00350, NCN OPUS nr 2022/47/B/ST2/03059, NCN UMO-2019/34/E/ST2/00393, NCN & H2020 MSCA 945339, UMO-2020/37/B/ST2/01043, UMO-2021/40/C/ST2/00187, UMO-2022/47/O/ST2/00148, UMO-2023/49/B/ST2/04085); Slovenia: Slovenian Research Agency (ARIS grant J1-3010); Spain: Generalitat Valenciana (Artemisa, FEDER, IDIFEDER/2018/048), Ministry of Science and Innovation (MCIN & NextGenEU PCI2022-135018-2, MICIN & FEDER PID2021-125273NB, RYC2019-028510-I, RYC2020-030254-I, RYC2021-031273-I, RYC2022-038164-I), PROMETEO and GenT Programmes Generalitat Valenciana (CIDEGENT/2019/023, CIDEGENT/2019/027); Sweden: Carl Trygger Foundation (Carl Trygger Foundation CTS 22:2312), Swedish Research Council (Swedish Research Council 2023-04654, VR 2018-00482, VR 2022-03845, VR 2022-04683, VR 2023-03403, VR grant 2021-03651), Knut and Alice Wallenberg Foundation (KAW 2018.0157, KAW 2018.0458, KAW 2019.0447, KAW 2022.0358); Switzerland: Swiss National Science Foundation (SNSF - PCEFP2_194658); United Kingdom: Leverhulme Trust (Leverhulme Trust RPG-2020-004), Royal Society (NIF-R1-231091); USA: U.S. Department of Energy (ECA DE-AC02-76SF00515), Neubauer Family Foundation.

Data Availability Statement This manuscript has no associated data. [Author's comment: The data displayed in tables and plots for this publication, and a corresponding RIVET routine, will be made available on HEPDATA at https://www.hepdata.net/record/157586. All ATLAS scientific output is published in journals, and preliminary results are made available in Conference Notes. All are openly available, without restriction on use by external parties beyond copyright law and the standard conditions agreed by CERN. Data associated with journal publications are also made available: tables and data from plots (e.g. cross-section values, likelihood profiles, selection efficiencies, cross-section limits, ...) are stored in appropriate repositories such as HEPDATA (http://hepdata.cedar.ac.uk/). ATLAS also strives to make additional material related to the paper available that allows a reinterpretation of the data in the context of new theoretical models. For example, an extended encapsulation of the analysis is often provided for measurements in the framework of RIVET (http://rivet.hepforge.org/). This information is taken from the ATLAS Data Access Policy, which is a public document that can be downloaded from http://opendata.cern.ch/record/413.]

Code Availability Statement The manuscript has no associated code/software. [Author's comment: Code/Software sharing not applicable to this article as no code/software was generated or analysed during the current study.]

Funded by SCOAP[3].

References

1. L. Evans, P. Bryant, LHC Machine. JINST **3**, S08001 (2008). https://doi.org/10.1088/1748-0221/3/08/S08001
2. F.A. Dreyer, G.P. Salam, G. Soyez, The Lund jet plane. JHEP **12**, 064 (2018). https://doi.org/10.1007/JHEP12(2018)064. arXiv:1807.04758 [hep-ph]
3. ATLAS Collaboration, Measurements of differential cross-sections in top-quark pair events with a high transverse momentum top quark and limits on beyond the Standard Model contributions to top-quark pair production with the ATLAS detector at $\sqrt{s} = 13TeV$. JHEP **06**, 063 (2022). https://doi.org/10.1007/JHEP06(2022)063. arXiv:2202.12134 [hep-ex]
4. CMS Collaboration, Measurement of differential $\bar{t}$ production cross sections in the full kinematic range using lepton+jets events from proton-proton collisions at $\sqrt{s} = 13TeV$. Phys. Rev. D **104**, 092013 (2021). https://doi.org/10.1103/PhysRevD.104.092013. arXiv:2108.02803 [hep-ex]
5. ATLAS Collaboration, Measurement of jet-substructure observables in top quark, W boson and light jet production in proton–proton collisions at $\sqrt{s} = 13TeV$ with the ATLAS detector. JHEP **08**, 033 (2019). https://doi.org/10.1007/JHEP08(2019)033. arXiv:1903.02942 [hep-ex]
6. ATLAS Collaboration, Measurement of jet substructure in boosted $t\bar{t}$ events with the ATLAS detector using 140, fb^{-1} of $13TeV$ pp collisions. Phys. Rev. D **109**, 112016 (2024). https://doi.org/10.1103/PhysRevD.109.112016. arXiv:2312.03797 [hep-ex]
7. CMS Collaboration, Measurement of jet substructure observables in $t\bar{t}$ events from proton–proton collisions at $\sqrt{s} = 13$TeV. Phys. Rev. D **98**, 092014 (2018). https://doi.org/10.1103/PhysRevD.98.092014. arXiv:1808.07340 [hep-ex]
8. S.D. Ellis, D.E. Soper, Successive combination jet algorithm for hadron collisions. Phys. Rev. D **48**, 3160 (1993). https://doi.org/10.1103/physrevd.48.3160. arXiv:hep-ph/9305266
9. M. Cacciari, G.P. Salam, G. Soyez, The anti-k_t jet clustering algorithm. JHEP **04**, 063 (2008). https://doi.org/10.1088/1126-6708/2008/04/063. arXiv:0802.1189 [hep-ph]
10. Y.L. Dokshitzer, G.D. Leder, S. Moretti, B.R. Webber, Better jet clustering algorithms. JHEP **8**, 001 (1997). https://doi.org/10.1088/1126-6708/1997/08/001. arXiv:hep-ph/9707323 [hep-ph]
11. G. Sterman et al., Handbook of perturbative QCD. Rev. Mod. Phys. **67**, 157 (1995). https://doi.org/10.1103/RevModPhys.67.157
12. B. Andersson, G. Gustafson, L. Lönnblad, U. Pettersson, Coherence effects in deep inelastic scattering. Z. Phys. C **43**, 625 (1989). https://doi.org/10.1007/BF01550942
13. ATLAS Collaboration, Measurement of the Lund jet plane using charged particles in $13TeV$ proton–proton collisions with the ATLAS detector. Phys. Rev. Lett. **124**, 222002 (2020). https://doi.org/10.1103/PhysRevLett.124.222002. arXiv:2004.03540 [hep-ex]
14. A. Lifson, G.P. Salam, G. Soyez, Calculating the primary Lund Jet Plane density. JHEP **10**, 170 (2020). https://doi.org/10.1007/jhep10(2020)170. arXiv:2007.06578
15. CMS Collaboration, Measurement of the primary Lund jet plane density in proton–proton collisions at $\sqrt{s} = 13TeV$. JHEP **5**, 116 (2024). https://doi.org/10.1007/JHEP05(2024)116. arXiv:2312.16343 [hep-ex]
16. ATLAS Collaboration, Measurements of Lund subjet multiplicities in $13TeV$ proton–proton collisions with the ATLAS detector (2024). arXiv:2402.13052 [hep-ex]
17. Yu.L. Dokshitzer, V.A. Khoze, S.I. Troian, On specific QCD properties of heavy quark fragmentation ('dead cone'). J. Phys. G **17**, 1602 (1991). https://doi.org/10.1088/0954-3899/17/10/023
18. ALICE Collaboration, Direct observation of the dead-cone effect in quantum chromodynamics. Nature **605**, 440 (2022). https://doi.org/10.1038/s41586-022-04572-w. arXiv:2106.05713 [nucl-ex]
19. C.M.S. Collaboration, Identification of heavy, energetic, hadronically decaying particles using machine-learning techniques. JINST **15**, P06005 (2020). https://doi.org/10.1088/1748-0221/15/06/P06005. arXiv:2004.08262 [hep-ex]
20. ATLAS Collaboration, Performance of top-quark and W-boson tagging with ATLAS in Run 2 of the LHC. Eur. Phys. J. C **79**, 375 (2019). https://doi.org/10.1140/epjc/s10052-019-6847-8. arXiv:1808.07858 [hep-ex]
21. G. Kasieczka et al., The machine learning landscape of top taggers. SciPost Phys. **7**, 014 (2019). https://doi.org/10.21468/SciPostPhys.7.1.014. arXiv:1902.09914 [hep-ex]
22. F.A. Dreyer, G. Soyez, A. Takacs, Quarks and gluons in the Lund plane. JHEP **08**, 177 (2022). https://doi.org/10.1007/jhep08(2022)177. arXiv:2112.09140 [hep-ph]
23. F.A. Dreyer, H. Qu, Jet tagging in the Lund plane with graph networks. JHEP **03**, 52 (2021). https://doi.org/10.1007/jhep03(2021)052. arXiv:2012.08526 [hep-ph]
24. CMS Collaboration, Lund plane reweighting for jet substructure correction, CMS-DP-2023-046 (2023). https://cds.cern.ch/record/2866330
25. ATLAS Collaboration, The ATLAS experiment at the CERN large hadron collider. JINST **3**, S08003 (2008). https://doi.org/10.1088/1748-0221/3/08/S08003
26. ATLAS Collaboration, Software and computing for Run 3 of the ATLAS experiment at the LHC (2024). arXiv:2404.06335 [hep-ex]
27. ATLAS Collaboration, ATLAS data quality operations and performance for 2015–2018 data-taking. JINST **15**, P04003 (2020). https://doi.org/10.1088/1748-0221/15/04/P04003. arXiv:1911.04632 [physics.ins-det]
28. ATLAS Collaboration, Luminosity determination in pp collisions at $\sqrt{s} = 13TeV$ using the ATLAS detector at the LHC. Eur. Phys. J. C **83**, 982 (2023). https://doi.org/10.1140/epjc/s10052-023-11747-w. arXiv:2212.09379 [hep-ex]
29. G. Avoni et al., The new LUCID-2 detector for luminosity measurement and monitoring in ATLAS. JINST **13**, P07017 (2018). https://doi.org/10.1088/1748-0221/13/07/P07017
30. ATLAS Collaboration, Performance of the ATLAS trigger system in 2015. Eur. Phys. J. C **77**(2017), 317 (2015). https://doi.org/10.1140/epjc/s10052-017-4852-3. arXiv:1611.09661 [hep-ex]
31. ATLAS Collaboration, Performance of electron and photon triggers in ATLAS during LHC Run 2. Eur. Phys. J. C **80**, 47 (2020). https://doi.org/10.1140/epjc/s10052-019-7500-2. arXiv:1909.00761 [hep-ex]
32. ATLAS Collaboration, Performance of the ATLAS muon triggers in Run 2. JINST **15**, P09015 (2020). https://doi.org/10.1088/1748-0221/15/09/p09015. arXiv:2004.13447 [physics.ins-det]
33. ATLAS Collaboration, The ATLAS simulation infrastructure, Eur. Phys. J. C **70**, 823 (2010). https://doi.org/10.1140/epjc/s10052-010-1429-9. arXiv:1005.4568 [physics.ins-det]
34. S. Agostinelli et al., Geant4: a simulation toolkit. Nucl. Instrum. Methods A **506**, 250 (2003). https://doi.org/10.1016/S0168-9002(03)01368-8
35. D.J. Lange, The EvtGen particle decay simulation package. Nucl. Instrum. Methods A **462**, 152 (2001). https://doi.org/10.1016/S0168-9002(01)00089-4

36. T. Sjöstrand, S. Mrenna, P. Skands, A brief introduction to PYTHIA 8.1. Comput. Phys. Commun. **178**, 852 (2008). https://doi.org/10.1016/j.cpc.2008.01.036. arXiv:0710.3820 [hep-ph]
37. ATLAS Collaboration, The Pythia 8 A3 tune description of ATLAS minimum bias and inelastic measurements incorporating the Donnachie–Landshoff diffractive model, ATL-PHYS-PUB-2016-017 (2016) https://cds.cern.ch/record/2206965
38. S. Frixione, G. Ridolfi, P. Nason, A positive-weight next-to-leading-order Monte Carlo for heavy flavour hadroproduction. JHEP **09**, 126 (2007). https://doi.org/10.1088/1126-6708/2007/09/126. arXiv:0707.3088 [hep-ph]
39. P. Nason, A new method for combining NLO QCD with shower Monte Carlo algorithms. JHEP **11**, 040 (2004). https://doi.org/10.1088/1126-6708/2004/11/040. arXiv:hep-ph/0409146
40. S. Frixione, P. Nason, C. Oleari, Matching NLO QCD computations with parton shower simulations: the POWHEG method. JHEP **11**, 070 (2007). https://doi.org/10.1088/1126-6708/2007/11/070. arXiv:0709.2092 [hep-ph]
41. S. Alioli, P. Nason, C. Oleari, E. Re, A general framework for implementing NLO calculations in shower Monte Carlo programs: the POWHEG BOX. JHEP **06**, 043 (2010). https://doi.org/10.1007/JHEP06(2010)043. arXiv:1002.2581 [hep-ph]
42. NNPDF Collaboration, Parton distributions for the LHC run II. JHEP **04**, 040 (2015). https://doi.org/10.1007/JHEP04(2015)040. arXiv:1410.8849 [hep-ph]
43. ATLAS Collaboration, Studies on top-quark Monte Carlo modelling for Top2016, ATL-PHYS-PUB-2016-020 (2016). https://cds.cern.ch/record/2216168
44. ATLAS Collaboration, Studies on the improvement of the matching uncertainty definition in top-quark processes simulated with Powheg+Pythia8, ATL-PHYS-PUB-2023-029 (2013). https://cds.cern.ch/record/2872787
45. T. Sjöstrand et al., An introduction to PYTHIA 8.2. Comput. Phys. Commun. **191**, 159 (2015). https://doi.org/10.1016/j.cpc.2015.01.024. arXiv:1410.3012 [hep-ph]
46. ATLAS Collaboration, ATLAS Pythia 8 tunes to $7TeV$ data, ATL-PHYS-PUB-2014-021 (2014) https://cds.cern.ch/record/1966419
47. NNPDF Collaboration, Parton distributions with LHC data. Nucl. Phys. B **867**, 244 (2013). https://doi.org/10.1016/j.nuclphysb.2012.10.003. arXiv:1207.1303 [hep-ph]
48. ATLAS Collaboration, Improvements in $t\bar{t}$ modelling using NLO+PS Monte Carlo generators for Run 2, ATL-PHYS-PUB-2018-009 (2018). https://cds.cern.ch/record/2630327
49. S. Frixione, S. Amoroso, S. Mrenna, Matrix element corrections in the Pythia8 parton shower in the context of matched simulations at next-to-leading order. Eur. Phys. J. C **83**, 970 (2023). arXiv:2308.06389 [hep-ph]
50. H. Brooks, P. Skands, Coherent showers in decays of colored resonances. Phys. Rev. D **100**, 076006 (2019). https://doi.org/10.1103/PhysRevD.100.076006. arXiv:1907.08980 [hep-ph]
51. S. Höche, S. Mrenna, S. Payne, C.T. Preuss, P. Skands, A study of QCD radiation in VBF Higgs production with Vincia and Pythia. SciPost Phys. **12**, 010 (2022). https://doi.org/10.21468/SciPostPhys.12.1.010. arXiv:2106.10987 [hep-ph]
52. J. Bellm et al., Herwig 7.2 release note. Eur. Phys. J. C **80**, 452 (2020). https://doi.org/10.1140/epjc/s10052-020-8011-x. arXiv:1912.06509 [hep-ph]
53. L.A. Harland-Lang, A.D. Martin, P. Motylinski, R.S. Thorne, Parton distributions in the LHC era: MMHT 2014 PDFs. Eur. Phys. J. C **75**, 204 (2015). https://doi.org/10.1140/epjc/s10052-015-3397-6. arXiv:1412.3989 [hep-ph]
54. J. Bellm et al., Herwig 7.0/Herwig++ 3.0 release note. Eur. Phys. J. C **76**, 196 (2016). https://doi.org/10.1140/epjc/s10052-016-4018-8. arXiv:1512.01178 [hep-ph]
55. J. Bellm et al., Herwig 7.1 Release Note (2017). arXiv:1705.06919 [hep-ph]
56. J. Alwall et al., The automated computation of tree-level and next-to-leading order differential cross sections, and their matching to parton shower simulations. JHEP **07**, 079 (2014). https://doi.org/10.1007/JHEP07(2014)079. arXiv:1405.0301 [hep-ph]
57. E. Bothmann et al., Event generation with Sherpa 2.2. SciPost Phys. **7**, 034 (2019). https://doi.org/10.21468/SciPostPhys.7.3.034. arXiv:1905.09127 [hep-ph]
58. T. Gleisberg, S. Höche, Comix, a new matrix element generator. JHEP **12**, 039 (2008). https://doi.org/10.1088/1126-6708/2008/12/039. arXiv:0808.3674 [hep-ph]
59. F. Buccioni et al., OpenLoops 2. Eur. Phys. J. C **79**, 866 (2019). https://doi.org/10.1140/epjc/s10052-019-7306-2. arXiv:1907.13071 [hep-ph]
60. F. Cascioli, P. Maierhöfer, S. Pozzorini, Scattering amplitudes with open loops. Phys. Rev. Lett. **108**, 111601 (2012). https://doi.org/10.1103/PhysRevLett.108.111601. arXiv:1111.5206 [hep-ph]
61. A. Denner, S. Dittmaier, L. Hofer, Collier: a fortran-based complex one-loop library in extended regularizations. Comput. Phys. Commun. **212**, 220 (2017). https://doi.org/10.1016/j.cpc.2016.10.013. arXiv:1604.06792 [hep-ph]
62. S. Schumann, F. Krauss, A parton shower algorithm based on Catani-Seymour dipole factorisation. JHEP **03**, 038 (2008). https://doi.org/10.1088/1126-6708/2008/03/038. arXiv:0709.1027 [hep-ph]
63. S. Frixione, E. Laenen, P. Motylinski, B.R. Webber, Angular correlations of lepton pairs from vector boson and top quark decays in Monte Carlo simulations. JHEP **04**, 081 (2007). https://doi.org/10.1088/1126-6708/2007/04/081. arXiv:hep-ph/0702198
64. M. Beneke, P. Falgari, S. Klein, C. Schwinn, Hadronic top-quark pair production with NNLL threshold resummation. Nucl. Phys. B **855**, 695 (2012). https://doi.org/10.1016/j.nuclphysb.2011.10.021. arXiv:1109.1536 [hep-ph]
65. M. Cacciari, M. Czakon, M. Mangano, A. Mitov, P. Nason, Top-pair production at hadron colliders with next-to-next-to-leading logarithmic soft-gluon resummation. Phys. Lett. B **710**, 612 (2012). https://doi.org/10.1016/j.physletb.2012.03.013. arXiv:1111.5869 [hep-ph]
66. P. Bärnreuther, M. Czakon, A. Mitov, Percent-level-precision physics at the tevatron: next-to-next-to-leading order QCD corrections to $q\bar{q} \to t\bar{t} + X$. Phys. Rev. Lett. **109**, 132001 (2012). https://doi.org/10.1103/PhysRevLett.109.132001. arXiv:1204.5201 [hep-ph]
67. M. Czakon, A. Mitov, NNLO corrections to top-pair production at hadron colliders: the all-fermionic scattering channels. JHEP **12**, 054 (2012). https://doi.org/10.1007/JHEP12(2012)054. arXiv:1207.0236 [hep-ph]
68. M. Czakon, A. Mitov, NNLO corrections to top pair production at hadron colliders: the quark-gluon reaction. JHEP **01**, 080 (2013). https://doi.org/10.1007/JHEP01(2013)080. arXiv:1210.6832 [hep-ph]
69. M. Czakon, P. Fiedler, A. Mitov, Total top-quark pair-production cross section at hadron colliders through $\mathcal{O}(\alpha_S^4)$. Phys. Rev. Lett. **110**, 252004 (2013). https://doi.org/10.1103/PhysRevLett.110.252004. arXiv:1303.6254 [hep-ph]
70. M. Czakon, A. Mitov, Top++: a program for the calculation of the top-pair cross-section at hadron colliders. Comput. Phys. Commun. **185**, 2930 (2014). https://doi.org/10.1016/j.cpc.2014.06.021. arXiv:1112.5675 [hep-ph]
71. S. Frixione, E. Laenen, P. Motylinski, C. White, B.R. Webber, Single-top hadroproduction in association with a W boson. JHEP **07**, 029 (2008). https://doi.org/10.1088/1126-6708/2008/07/029. arXiv:0805.3067 [hep-ph]

72. C. Anastasiou, L. Dixon, K. Melnikov, F. Petriello, High-precision QCD at hadron colliders: electroweak gauge boson rapidity distributions at next-to-next-to leading order. Phys. Rev. D **69**, 094008 (2004). https://doi.org/10.1103/PhysRevD.69.094008. arXiv:hep-ph/0312266
73. ATLAS Collaboration, Early inner detector tracking performance in the 2015 data at $\sqrt{s} = 13\ TeV$, ATL-PHYS-PUB-2015-051 (2015) https://cds.cern.ch/record/2110140
74. M. Cacciari, G.P. Salam, G. Soyez, FastJet user manual. Eur. Phys. J. C **72**, 1896 (2012). https://doi.org/10.1140/epjc/s10052-012-1896-2. arXiv:1111.6097 [hep-ph]
75. ATLAS Collaboration, Topological cell clustering in the ATLAS calorimeters and its performance in LHC Run 1. Eur. Phys. J. C **77**, 490 (2017). https://doi.org/10.1140/epjc/s10052-017-5004-5. arXiv:1603.02934 [hep-ex]
76. D. Krohn, J. Thaler, L.-T. Wang, Jet trimming. JHEP **02**, 084 (2010). https://doi.org/10.1007/JHEP02(2010)084. arXiv:0912.1342 [hep-ph]
77. ATLAS Collaboration, In situ calibration of large-radius jet energy and mass in $13TeV$ proton–proton collisions with the ATLAS detector. Eur. Phys. J. C **79**, 135 (2019). https://doi.org/10.1140/epjc/s10052-019-6632-8. arXiv:1807.09477 [hep-ex]
78. ATLAS Collaboration, Jet reconstruction and performance using particle flow with the ATLAS Detector. Eur. Phys. J. C **77**, 466 (2017). https://doi.org/10.1140/epjc/s10052-017-5031-2. arXiv:1703.10485 [hep-ex]
79. ATLAS Collaboration, Performance of pile-up mitigation techniques for jets in pp collisions at $\sqrt{s} = 8TeV$ using the ATLAS detector. Eur. Phys. J. C **76** 581 (2016). https://doi.org/10.1140/epjc/s10052-016-4395-z. arXiv:1510.03823 [hep-ex]
80. ATLAS Collaboration, ATLAS flavour-tagging algorithms for the LHC Run 2 pp collision dataset. Eur. Phys. J. C **83**, 681 (2023). https://doi.org/10.1140/epjc/s10052-023-11699-1. arXiv:2211.16345 [physics.data-an]
81. ATLAS Collaboration, Jet energy scale and resolution measured in proton–proton collisions at $\sqrt{s} = 13TeV$ with the ATLAS detector. Eur. Phys. J. C **81**, 689 (2021). https://doi.org/10.1140/epjc/s10052-021-09402-3. arXiv:2007.02645 [hep-ex]
82. ATLAS Collaboration, Electron and photon performance measurements with the ATLAS detector using the 2015–2017 LHC proton–proton collision data. JINST **14**, P12006 (2019). https://doi.org/10.1088/1748-0221/14/12/P12006. arXiv:1908.00005 [hep-ex]
83. ATLAS Collaboration, Electron reconstruction and identification in the ATLAS experiment using the 2015 and 2016 LHC proton–proton collision data at $\sqrt{s} = 13TeV$. Eur. Phys. J. C **79**, 639 (2019). https://doi.org/10.1140/epjc/s10052-019-7140-6. arXiv:1902.04655 [physics.ins-det]
84. ATLAS Collaboration, Muon reconstruction and identification efficiency in ATLAS using the full Run 2 pp collision data set at $\sqrt{s} = 13TeV$. Eur. Phys. J. C **81**, 578 (2021). https://doi.org/10.1140/epjc/s10052-021-09233-2. arXiv:2012.00578 [hep-ex]
85. ATLAS Collaboration, The performance of missing transverse momentum reconstruction and its significance with the ATLAS detector using $140\,fb^{-1}$ of $\sqrt{s} = 13TeV$ pp collisions (2024). arXiv:2402.05858 [hep-ex]
86. ATLAS Collaboration, Tools for estimating fake/non-prompt lepton backgrounds with the ATLAS detector at the LHC. JINST **18**, T11004 (2022). https://doi.org/10.1088/1748-0221/18/11/T11004. arXiv:2211.16178 [hep-ex]
87. ATLAS Collaboration, Differential $t\bar{t}$ cross-section measurements using boosted top quarks in the all-hadronic final state with 139 fb^{-1} of ATLAS data. JHEP **04**, 080 (2023). https://doi.org/10.1007/JHEP04(2023)080. arXiv:2205.02817 [hep-ex]
88. CMS Collaboration, Measurement of differential $t\bar{t}$ production cross sections using top quarks at large transverse momenta in pp collisions at $\sqrt{s} = 13TeV$. Phys. Rev. D **103**, 052008 (2021). https://doi.org/10.1103/PhysRevD.103.052008. arXiv:2008.07860 [hep-ex]
89. M. Cacciari, G.P. Salam, G. Soyez, The catchment area of jets. JHEP **04**, 005 (2008). https://doi.org/10.1088/1126-6708/2008/04/005. arXiv:0802.1188 [hep-ph]
90. G. D'Agostini, A multidimensional unfolding method based on Bayes' theorem. Nucl. Instrum. Methods A **362**, 487 (1995). https://doi.org/10.1016/0168-9002(95)00274-X
91. ATLAS Collaboration, Measurement of the ATLAS Detector Jet Mass Response using Forward Folding with 80, fb^{-1} of $\sqrt{s} = 13TeV$ pp data, ATLAS-CONF-2020-022 (2020). https://cds.cern.ch/record/2724442
92. ATLAS Collaboration, ATLAS b-jet identification performance and efficiency measurement with $t\bar{t}$ events in pp collisions at $\sqrt{s} = 13TeV$. Eur. Phys. J. C **79**, 970 (2019). https://doi.org/10.1140/epjc/s10052-019-7450-8. arXiv:1907.05120 [hep-ex]
93. ATLAS Collaboration, Measurement of the c-jet mistagging efficiency in $t\bar{t}$ events using pp collision data at $\sqrt{s} = 13TeV$ collected with the ATLAS detector. Eur. Phys. J. C **82**, 95 (2022). https://doi.org/10.1140/epjc/s10052-021-09843-w. arXiv:2109.10627 [hep-ex]
94. ATLAS Collaboration, Calibration of the light-flavour jet mistagging efficiency of the b-tagging algorithms with Z+jets events using $139\,fb^{-1}$ of ATLAS proton–proton collision data at $\sqrt{s} = 13TeV$. Eur. Phys. J. C **83**, 728 (2023). https://doi.org/10.1140/epjc/s10052-023-11736-z. arXiv:2301.06319 [hep-ex]
95. ATLAS Collaboration, Performance of missing transverse momentum reconstruction with the ATLAS detector using proton–proton collisions at $\sqrt{s} = 13TeV$. Eur. Phys. J. C **78**, 903 (2018). https://doi.org/10.1140/epjc/s10052-018-6288-9. arXiv:1802.08168 [hep-ex]
96. ATLAS Collaboration, Studies of the muon momentum calibration and performance of the ATLAS detector with pp collisions at $\sqrt{s} = 13TeV$. Eur. Phys. J. C **83**, 686 (2023). https://doi.org/10.1140/epjc/s10052-023-11584-x. arXiv:2212.07338 [hep-ex]
97. ATLAS Collaboration, Performance of the ATLAS track reconstruction algorithms in dense environments in LHC Run 2. Eur. Phys. J. C **77**, 673 (2017). https://doi.org/10.1140/epjc/s10052-017-5225-7. arXiv:1704.07983 [hep-ex]
98. J. Butterworth et al., PDF4LHC recommendations for LHC Run II. J. Phys. G **43**, 023001 (2016). https://doi.org/10.1088/0954-3899/43/2/023001. arXiv:1510.03865 [hep-ph]
99. N. Kidonakis, Next-to-next-to-leading logarithm resummation for s-channel single top quark production. Phys. Rev. D **81**, 054028 (2010). https://doi.org/10.1103/PhysRevD.81.054028. arXiv:1001.5034 [hep-ph]
100. N. Kidonakis, Next-to-next-to-next-to-leading-order soft-gluon corrections in hard-scattering processes near threshold. Phys. Rev. D **73**, 034001 (2006). https://doi.org/10.1103/PhysRevD.73.034001. arXiv:hep-ph/0509079
101. D. de Florian et al., Handbook of LHC Higgs cross sections: 4. Deciphering the nature of the higgs sector (2017). https://doi.org/10.23731/CYRM-2017-002. arXiv:1610.07922 [hep-ph]
102. B. Malaescu, An iterative, dynamically stabilized method of data unfolding (2009). arXiv:0907.3791 [physics.data-an]
103. B. Efron, Bootstrap methods: another look at the jackknife. Ann. Stat. **7**, 1 (1979). https://doi.org/10.1214/aos/1176344552
104. ATLAS Collaboration, ATLAS Computing Acknowledgements, ATL-SOFT-PUB-2023-001 (2023). https://cds.cern.ch/record/2869272

ATLAS Collaboration*

G. Aad[103], E. Aakvaag[16], B. Abbott[121], S. Abdelhameed[117a], K. Abeling[55], N. J. Abicht[49], S. H. Abidi[29], M. Aboelela[44], A. Aboulhorma[35e], H. Abramowicz[153], H. Abreu[152], Y. Abulaiti[118], B. S. Acharya[69a,69b,l], A. Ackermann[63a], C. Adam Bourdarios[4], L. Adamczyk[86a], S. V. Addepalli[26], M. J. Addison[102], J. Adelman[116], A. Adiguzel[21c], T. Adye[135], A. A. Affolder[137], Y. Afik[39], M. N. Agaras[13], J. Agarwala[73a,73b], A. Aggarwal[101], C. Agheorghiesei[27c], A. Ahmad[36], F. Ahmadov[38,z], W. S. Ahmed[105], S. Ahuja[96], X. Ai[62e], G. Aielli[76a,76b], A. Aikot[164], M. Ait Tamlihat[35e], B. Aitbenchikh[35a], M. Akbiyik[101], T. P. A. Åkesson[99], A. V. Akimov[37], D. Akiyama[169], N. N. Akolkar[24], S. Aktas[21a], K. Al Khoury[41], G. L. Alberghi[23b], J. Albert[166], P. Albicocco[53], G. L. Albouy[60], S. Alderweireldt[52], Z. L. Alegria[122], M. Aleksa[36], I. N. Aleksandrov[38], C. Alexa[27b], T. Alexopoulos[10], F. Alfonsi[23b], M. Algren[56], M. Alhroob[168], B. Ali[133], H. M. J. Ali[92], S. Ali[31], S. W. Alibocus[93], M. Aliev[33c], G. Alimonti[71a], W. Alkakhi[55], C. Allaire[66], B. M. M. Allbrooke[148], J. F. Allen[52], C. A. Allendes Flores[138f], P. P. Allport[20], A. Aloisio[72a,72b], F. Alonso[91], C. Alpigiani[140], Z. M. K. Alsolami[92], M. Alvarez Estevez[100], A. Alvarez Fernandez[101], M. Alves Cardoso[56], M. G. Alviggi[72a,72b], M. Aly[102], Y. Amaral Coutinho[83b], A. Ambler[105], C. Amelung[36], M. Amerl[102], C. G. Ames[110], D. Amidei[107], K. J. Amirie[156], S. P. Amor Dos Santos[131a], K. R. Amos[164], S. An[84], V. Ananiev[126], C. Anastopoulos[141], T. Andeen[11], J. K. Anders[36], S. Y. Andrean[47a,47b], A. Andreazza[71a,71b], S. Angelidakis[9], A. Angerami[41,ab], A. V. Anisenkov[37], A. Annovi[74a], C. Antel[56], E. Antipov[147], M. Antonelli[53], F. Anulli[75a], M. Aoki[84], T. Aoki[155], M. A. Aparo[148], L. Aperio Bella[48], C. Appelt[18], A. Apyan[26], S. J. Arbiol Val[87], C. Arcangeletti[53], A. T. H. Arce[51], E. Arena[93], J-F. Arguin[109], S. Argyropoulos[54], J.-H. Arling[48], O. Arnaez[4], H. Arnold[147], G. Artoni[75a,75b], H. Asada[112], K. Asai[119], S. Asai[155], N. A. Asbah[36], R. A. Ashby Pickering[168], K. Assamagan[29], R. Astalos[28a], K. S. V. Astrand[99], S. Atashi[160], R. J. Atkin[33a], M. Atkinson[163], H. Atmani[35f], P. A. Atmasiddha[129], K. Augsten[133], S. Auricchio[72a,72b], A. D. Auriol[20], V. A. Austrup[102], G. Avolio[36], K. Axiotis[56], G. Azuelos[109,af], D. Babal[28b], H. Bachacou[136], K. Bachas[154,p], A. Bachiu[34], F. Backman[47a,47b], A. Badea[39], T. M. Baer[107], P. Bagnaia[75a,75b], M. Bahmani[18], D. Bahner[54], K. Bai[124], J. T. Baines[135], L. Baines[95], O. K. Baker[173], E. Bakos[15], D. Bakshi Gupta[8], V. Balakrishnan[121], R. Balasubramanian[115], E. M. Baldin[37], P. Balek[86a], E. Ballabene[23a,23b], F. Balli[136], L. M. Baltes[63a], W. K. Balunas[32], J. Balz[101], I. Bamwidhi[117b], E. Banas[87], M. Bandieramonte[130], A. Bandyopadhyay[24], S. Bansal[24], L. Barak[153], M. Barakat[48], E. L. Barberio[106], D. Barberis[57a,57b], M. Barbero[103], M. Z. Barel[115], K. N. Barends[33a], T. Barillari[111], M-S. Barisits[36], T. Barklow[145], P. Baron[123], D. A. Baron Moreno[102], A. Baroncelli[62a], G. Barone[29], A. J. Barr[127], J. D. Barr[97], F. Barreiro[100], J. Barreiro Guimarães da Costa[14a], U. Barron[153], M. G. Barros Teixeira[131a], S. Barsov[37], F. Bartels[63a], R. Bartoldus[145], A. E. Barton[92], P. Bartos[28a], A. Basan[101], M. Baselga[49], A. Bassalat[66,b], M. J. Basso[157a], R. Bate[165], R. L. Bates[59], S. Batlamous[100], B. Batool[143], M. Battaglia[137], D. Battulga[18], M. Bauce[75a,75b], M. Bauer[36], P. Bauer[24], L. T. Bazzano Hurrell[30], J. B. Beacham[51], T. Beau[128], J. Y. Beaucamp[91], P. H. Beauchemin[159], P. Bechtle[24], H. P. Beck[19,o], K. Becker[168], A. J. Beddall[82], V. A. Bednyakov[38], C. P. Bee[147], L. J. Beemster[15], T. A. Beermann[36], M. Begalli[83d], M. Begel[29], A. Behera[147], J. K. Behr[48], J. F. Beirer[36], F. Beisiegel[24], M. Belfkir[117b], G. Bella[153], L. Bellagamba[23b], A. Bellerive[34], P. Bellos[20], K. Beloborodov[37], D. Benchekroun[35a], F. Bendebba[35a], Y. Benhammou[153], K. C. Benkendorfer[61], L. Beresford[48], M. Beretta[53], E. Bergeaas Kuutmann[162], N. Berger[4], B. Bergmann[133], J. Beringer[17a], G. Bernardi[5], C. Bernius[145], F. U. Bernlochner[24], F. Bernon[36,103], A. Berrocal Guardia[13], T. Berry[96], P. Berta[134], A. Berthold[50], S. Bethke[111], A. Betti[75a,75b], A. J. Bevan[95], N. K. Bhalla[54], S. Bhatta[147], D. S. Bhattacharya[167], P. Bhattarai[145], K. D. Bhide[54], V. S. Bhopatkar[122], R. M. Bianchi[130], G. Bianco[23a,23b], O. Biebel[110], R. Bielski[124], M. Biglietti[77a], C. S. Billingsley[44], M. Bindi[55], A. Bingul[21b], C. Bini[75a,75b], A. Biondini[93], G. A. Bird[32], M. Birman[170], M. Biros[134], S. Biryukov[148], T. Bisanz[49], E. Bisceglie[43a,43b], J. P. Biswal[135], D. Biswas[143], I. Bloch[48], A. Blue[59], U. Blumenschein[95], J. Blumenthal[101], V. S. Bobrovnikov[37], M. Boehler[54], B. Boehm[167], D. Bogavac[36], A. G. Bogdanchikov[37], C. Bohm[47a], V. Boisvert[96], P. Bokan[36], T. Bold[86a], M. Bomben[5], M. Bona[95], M. Boonekamp[136], C. D. Booth[96], A. G. Borbély[59], I. S. Bordulev[37], H. M. Borecka-Bielska[109], G. Borissov[92], D. Bortoletto[127], D. Boscherini[23b], M. Bosman[13], J. D. Bossio Sola[36], K. Bouaouda[35a], N. Bouchhar[164], L. Boudet[4], J. Boudreau[130], E. V. Bouhova-Thacker[92], D. Boumediene[40], R. Bouquet[57a,57b], A. Boveia[120], J. Boyd[36], D. Boye[29], I. R. Boyko[38], L. Bozianu[56], J. Bracinik[20], N. Brahimi[4], G. Brandt[172], O. Brandt[32], F. Braren[48], B. Brau[104], J. E. Brau[124], R. Brener[170], L. Brenner[115],

R. Brenner[162], S. Bressler[170], D. Britton[59], D. Britzger[111], I. Brock[24], R. Brock[108], G. Brooijmans[41], E. Brost[29], L. M. Brown[166], L. E. Bruce[61], T. L. Bruckler[127], P. A. Bruckman de Renstrom[87], B. Brüers[48], A. Bruni[23b], G. Bruni[23b], M. Bruschi[23b], N. Bruscino[75a,75b], T. Buanes[16], Q. Buat[140], D. Buchin[111], A. G. Buckley[59], O. Bulekov[37], B. A. Bullard[145], S. Burdin[93], C. D. Burgard[49], A. M. Burger[36], B. Burghgrave[8], O. Burlayenko[54], J. T. P. Burr[32], J. C. Burzynski[144], E. L. Busch[41], V. Büscher[101], P. J. Bussey[59], J. M. Butler[25], C. M. Buttar[59], J. M. Butterworth[97], W. Buttinger[135], C. J. Buxo Vazquez[108], A. R. Buzykaev[37], S. Cabrera Urbán[164], L. Cadamuro[66], D. Caforio[58], H. Cai[130], Y. Cai[14a,14e], Y. Cai[14c], V. M. M. Cairo[36], O. Cakir[3a], N. Calace[36], P. Calafiura[17a], G. Calderini[128], P. Calfayan[68], G. Callea[59], L. P. Caloba[83b], D. Calvet[40], S. Calvet[40], M. Calvetti[74a,74b], R. Camacho Toro[128], S. Camarda[36], D. Camarero Munoz[26], P. Camarri[76a,76b], M. T. Camerlingo[72a,72b], D. Cameron[36], C. Camincher[166], M. Campanelli[97], A. Camplani[42], V. Canale[72a,72b], A. C. Canbay[3a], E. Canonero[96], J. Cantero[164], Y. Cao[163], F. Capocasa[26], M. Capua[43a,43b], A. Carbone[71a,71b], R. Cardarelli[76a], J. C. J. Cardenas[8], G. Carducci[43a,43b], T. Carli[36], G. Carlino[72a], J. I. Carlotto[13], B. T. Carlson[130,q], E. M. Carlson[157a,166], J. Carmignani[93], L. Carminati[71a,71b], A. Carnelli[136], M. Carnesale[75a,75b], S. Caron[114], E. Carquin[138f], S. Carrá[71a], G. Carratta[23a,23b], A. M. Carroll[124], T. M. Carter[52], M. P. Casado[13,i], M. Caspar[48], F. L. Castillo[4], L. Castillo Garcia[13], V. Castillo Gimenez[164], N. F. Castro[131a,131e], A. Catinaccio[36], J. R. Catmore[126], T. Cavaliere[4], V. Cavaliere[29], N. Cavalli[23a,23b], Y. C. Cekmecelioglu[48], E. Celebi[21a], S. Cella[36], F. Celli[127], M. S. Centonze[70a,70b], V. Cepaitis[56], K. Cerny[123], A. S. Cerqueira[83a], A. Cerri[148], L. Cerrito[76a,76b], F. Cerutti[17a], B. Cervato[143], A. Cervelli[23b], G. Cesarini[53], S. A. Cetin[82], D. Chakraborty[116], J. Chan[17a], W. Y. Chan[155], J. D. Chapman[32], E. Chapon[136], B. Chargeishvili[151b], D. G. Charlton[20], M. Chatterjee[19], C. Chauhan[134], Y. Che[14c], S. Chekanov[6], S. V. Chekulaev[157a], G. A. Chelkov[38,a], A. Chen[107], B. Chen[153], B. Chen[166], H. Chen[14c], H. Chen[29], J. Chen[62c], J. Chen[144], M. Chen[127], S. Chen[155], S. J. Chen[14c], X. Chen[62c,136], X. Chen[14b,ae], Y. Chen[62a], C. L. Cheng[171], H. C. Cheng[64a], S. Cheong[145], A. Cheplakov[38], E. Cheremushkina[48], E. Cherepanova[115], R. Cherkaoui El Moursli[35e], E. Cheu[7], K. Cheung[65], L. Chevalier[136], V. Chiarella[53], G. Chiarelli[74a], N. Chiedde[103], G. Chiodini[70a], A. S. Chisholm[20], A. Chitan[27b], M. Chitishvili[164], M. V. Chizhov[38,r], K. Choi[11], Y. Chou[140], E. Y. S. Chow[114], K. L. Chu[170], M. C. Chu[64a], X. Chu[14a,14e], J. Chudoba[132], J. J. Chwastowski[87], D. Cieri[111], K. M. Ciesla[86a], V. Cindro[94], A. Ciocio[17a], F. Cirotto[72a,72b], Z. H. Citron[170], M. Citterio[71a], D. A. Ciubotaru[27b], A. Clark[56], P. J. Clark[52], C. Clarry[156], J. M. Clavijo Columbie[48], S. E. Clawson[48], C. Clement[47a,47b], J. Clercx[48], Y. Coadou[103], M. Cobal[69a,69c], A. Coccaro[57b], R. F. Coelho Barrue[131a], R. Coelho Lopes De Sa[104], S. Coelli[71a], B. Cole[41], J. Collot[60], P. Conde Muiño[131a,131g], M. P. Connell[33c], S. H. Connell[33c], E. I. Conroy[127], F. Conventi[72a,ag], H. G. Cooke[20], A. M. Cooper-Sarkar[127], F. A. Corchia[23a,23b], A. Cordeiro Oudot Choi[128], L. D. Corpe[40], M. Corradi[75a,75b], F. Corriveau[105,x], A. Cortes-Gonzalez[18], M. J. Costa[164], F. Costanza[4], D. Costanzo[141], B. M. Cote[120], J. Couthures[4], G. Cowan[96], K. Cranmer[171], D. Cremonini[23a,23b], S. Crépé-Renaudin[60], F. Crescioli[128], M. Cristinziani[143], M. Cristoforetti[78a,78b], V. Croft[115], J. E. Crosby[122], G. Crosetti[43a,43b], A. Cueto[100], Z. Cui[7], W. R. Cunningham[59], F. Curcio[164], J. R. Curran[52], P. Czodrowski[36], M. M. Czurylo[36], M. J. Da Cunha Sargedas De Sousa[57a,57b], J. V. Da Fonseca Pinto[83b], C. Da Via[102], W. Dabrowski[86a], T. Dado[49], S. Dahbi[150], T. Dai[107], D. Dal Santo[19], C. Dallapiccola[104], M. Dam[42], G. D'amen[29], V. D'Amico[110], J. Damp[101], J. R. Dandoy[34], D. Dannheim[36], M. Danninger[144], V. Dao[147], G. Darbo[57b], S. J. Das[29,ah], F. Dattola[48], S. D'Auria[71a,71b], A. D'Avanzo[72a,72b], C. David[33a], T. Davidek[134], I. Dawson[95], H. A. Day-hall[133], K. De[8], R. De Asmundis[72a], N. De Biase[48], S. De Castro[23a,23b], N. De Groot[114], P. de Jong[115], H. De la Torre[116], A. De Maria[14c], A. De Salvo[75a], U. De Sanctis[76a,76b], F. De Santis[70a,70b], A. De Santo[148], J. B. De Vivie De Regie[60], D. V. Dedovich[38], J. Degens[93], A. M. Deiana[44], F. Del Corso[23a,23b], J. Del Peso[100], F. Del Rio[63a], L. Delagrange[128], F. Deliot[136], C. M. Delitzsch[49], M. Della Pietra[72a,72b], D. Della Volpe[56], A. Dell'Acqua[36], L. Dell'Asta[71a,71b], M. Delmastro[4], P. A. Delsart[60], S. Demers[173], M. Demichev[38], S. P. Denisov[37], L. D'Eramo[40], D. Derendarz[87], F. Derue[128], P. Dervan[93], K. Desch[24], C. Deutsch[24], F. A. Di Bello[57a,57b], A. Di Ciaccio[76a,76b], L. Di Ciaccio[4], A. Di Domenico[75a,75b], C. Di Donato[72a,72b], A. Di Girolamo[36], G. Di Gregorio[36], A. Di Luca[78a,78b], B. Di Micco[77a,77b], R. Di Nardo[77a,77b], M. Diamantopoulou[34], F. A. Dias[115], T. Dias Do Vale[144], M. A. Diaz[138a,138b], F. G. Diaz Capriles[24], M. Didenko[164], E. B. Diehl[107], S. Díez Cornell[48], C. Diez Pardos[143], C. Dimitriadi[24,162], A. Dimitrievska[20], J. Dingfelder[24], I-M. Dinu[27b], S. J. Dittmeier[63b], F. Dittus[36], M. Divisek[134], F. Djama[103], T. Djobava[151b], C. Doglioni[99,102], A. Dohnalova[28a], J. Dolejsi[134], Z. Dolezal[134], K. Domijan[86a], K. M. Dona[39], M. Donadelli[83d], B. Dong[108], J. Donini[40], A. D'Onofrio[72a,72b],

M. D'Onofrio[93], J. Dopke[135], A. Doria[72a], N. Dos Santos Fernandes[131a], P. Dougan[102], M. T. Dova[91], A. T. Doyle[59], M. A. Draguet[127], E. Dreyer[170], I. Drivas-koulouris[10], M. Drnevich[118], M. Drozdova[56], D. Du[62a], T. A. du Pree[115], F. Dubinin[37], M. Dubovsky[28a], E. Duchovni[170], G. Duckeck[110], O. A. Ducu[27b], D. Duda[52], A. Dudarev[36], E. R. Duden[26], M. D'uffizi[102], L. Duflot[66], M. Dührssen[36], I. Duminica[27g], A. E. Dumitriu[27b], M. Dunford[63a], S. Dungs[49], K. Dunne[47a,47b], A. Duperrin[103], H. Duran Yildiz[3a], M. Düren[58], A. Durglishvili[151b], B. L. Dwyer[116], G. I. Dyckes[17a], M. Dyndal[86a], B. S. Dziedzic[36], Z. O. Earnshaw[148], G. H. Eberwein[127], B. Eckerova[28a], S. Eggebrecht[55], E. Egidio Purcino De Souza[128], L. F. Ehrke[56], G. Eigen[16], K. Einsweiler[17a], T. Ekelof[162], P. A. Ekman[99], S. El Farkh[35b], Y. El Ghazali[35b], H. El Jarrari[36], A. El Moussaouy[35a], V. Ellajosyula[162], M. Ellert[162], F. Ellinghaus[172], N. Ellis[36], J. Elmsheuser[29], M. Elsawy[117a], M. Elsing[36], D. Emeliyanov[135], Y. Enari[155], I. Ene[17a], S. Epari[13], P. A. Erland[87], M. Errenst[172], M. Escalier[66], C. Escobar[164], E. Etzion[153], G. Evans[131a,131b], H. Evans[68], L. S. Evans[96], A. Ezhilov[37], S. Ezzarqtouni[35a], F. Fabbri[23a,23b], L. Fabbri[23a,23b], G. Facini[97], V. Fadeyev[137], R. M. Fakhrutdinov[37], D. Fakoudis[101], S. Falciano[75a], L. F. Falda Ulhoa Coelho[36], F. Fallavollita[111], J. Faltova[134], C. Fan[163], Y. Fan[14a], Y. Fang[14a,14e], M. Fanti[71a,71b], M. Faraj[69a,69b], Z. Farazpay[98], A. Farbin[8], A. Farilla[77a], T. Farooque[108], S. M. Farrington[52], F. Fassi[35e], D. Fassouliotis[9], M. Faucci Giannelli[76a,76b], W. J. Fawcett[32], L. Fayard[66], P. Federic[134], P. Federicova[132], O. L. Fedin[37,a], M. Feickert[171], L. Feligioni[103], D. E. Fellers[124], C. Feng[62b], M. Feng[14b], Z. Feng[115], M. J. Fenton[160], L. Ferencz[48], R. A. M. Ferguson[92], S. I. Fernandez Luengo[138f], P. Fernandez Martinez[13], M. J. V. Fernoux[103], J. Ferrando[92], A. Ferrari[162], P. Ferrari[114,115], R. Ferrari[73a], D. Ferrere[56], C. Ferretti[107], F. Fiedler[101], P. Fiedler[133], A. Filipčič[94], E. K. Filmer[1], F. Filthaut[114], M. C. N. Fiolhais[131a,131c,c], L. Fiorini[164], W. C. Fisher[108], T. Fitschen[102], P. M. Fitzhugh[136], I. Fleck[143], P. Fleischmann[107], T. Flick[172], M. Flores[33d,ac], L. R. Flores Castillo[64a], L. Flores Sanz De Acedo[36], F. M. Follega[78a,78b], N. Fomin[16], J. H. Foo[156], A. Formica[136], A. C. Forti[102], E. Fortin[36], A. W. Fortman[17a], M. G. Foti[17a], L. Fountas[9,j], D. Fournier[66], H. Fox[92], P. Francavilla[74a,74b], S. Francescato[61], S. Franchellucci[56], M. Franchini[23a,23b], S. Franchino[63a], D. Francis[36], L. Franco[114], V. Franco Lima[36], L. Franconi[48], M. Franklin[61], G. Frattari[26], Y. Y. Frid[153], J. Friend[59], N. Fritzsche[50], A. Froch[54], D. Froidevaux[36], J. A. Frost[127], Y. Fu[62a], S. Fuenzalida Garrido[138f], M. Fujimoto[103], K. Y. Fung[64a], E. Furtado De Simas Filho[83e], M. Furukawa[155], J. Fuster[164], A. Gabrielli[23a,23b], A. Gabrielli[156], P. Gadow[36], G. Gagliardi[57a,57b], L. G. Gagnon[17a], S. Gaid[161], S. Galantzan[153], E. J. Gallas[127], B. J. Gallop[135], K. K. Gan[120], S. Ganguly[155], Y. Gao[52], F. M. Garay Walls[138a,138b], B. Garcia[29], C. García[164], A. Garcia Alonso[115], A. G. Garcia Caffaro[173], J. E. García Navarro[164], M. Garcia-Sciveres[17a], G. L. Gardner[129], R. W. Gardner[39], N. Garelli[159], D. Garg[80], R. B. Garg[145], J. M. Gargan[52], C. A. Garner[156], C. M. Garvey[33a], V. K. Gassmann[159], G. Gaudio[73a], V. Gautam[13], P. Gauzzi[75a,75b], I. L. Gavrilenko[37], A. Gavrilyuk[37], C. Gay[165], G. Gaycken[48], E. N. Gazis[10], A. A. Geanta[27b], C. M. Gee[137], A. Gekow[120], C. Gemme[57b], M. H. Genest[60], A. D. Gentry[113], S. George[96], W. F. George[20], T. Geralis[46], P. Gessinger-Befurt[36], M. E. Geyik[172], M. Ghani[168], K. Ghorbanian[95], A. Ghosal[143], A. Ghosh[160], A. Ghosh[7], B. Giacobbe[23b], S. Giagu[75a,75b], T. Giani[115], P. Giannetti[74a], A. Giannini[62a], S. M. Gibson[96], M. Gignac[137], D. T. Gil[86b], A. K. Gilbert[86a], B. J. Gilbert[41], D. Gillberg[34], G. Gilles[115], L. Ginabat[128], D. M. Gingrich[2,af], M. P. Giordani[69a,69c], P. F. Giraud[136], G. Giugliarelli[69a,69c], D. Giugni[71a], F. Giuli[36], I. Gkialas[9,j], L. K. Gladilin[37], C. Glasman[100], G. R. Gledhill[124], G. Glemža[48], M. Glisic[124], I. Gnesi[43b,f], Y. Go[29], M. Goblirsch-Kolb[36], B. Gocke[49], D. Godin[109], B. Gokturk[21a], S. Goldfarb[106], T. Golling[56], M. G. D. Gololo[33g], D. Golubkov[37], J. P. Gombas[108], A. Gomes[131a,131b], G. Gomes Da Silva[143], A. J. Gomez Delegido[164], R. Gonçalo[131a], L. Gonella[20], A. Gongadze[151c], F. Gonnella[20], J. L. Gonski[145], R. Y. González Andana[52], S. González de la Hoz[164], R. Gonzalez Lopez[93], C. Gonzalez Renteria[17a], M. V. Gonzalez Rodrigues[48], R. Gonzalez Suarez[162], S. Gonzalez-Sevilla[56], L. Goossens[36], B. Gorini[36], E. Gorini[70a,70b], A. Gorišek[94], T. C. Gosart[129], A. T. Goshaw[51], M. I. Gostkin[38], S. Goswami[122], C. A. Gottardo[36], S. A. Gotz[110], M. Gouighri[35b], V. Goumarre[48], A. G. Goussiou[140], N. Govender[33c], I. Grabowska-Bold[86a], K. Graham[34], E. Gramstad[126], S. Grancagnolo[70a,70b], C. M. Grant[1,136], P. M. Gravila[27f], F. G. Gravili[70a,70b], H. M. Gray[17a], M. Greco[70a,70b], C. Grefe[24], A. S. Grefsrud[16], I. M. Gregor[48], K. T. Greif[160], P. Grenier[145], S. G. Grewe[111], A. A. Grillo[137], K. Grimm[31], S. Grinstein[13,t], J.-F. Grivaz[66], E. Gross[170], J. Grosse-Knetter[55], J. C. Grundy[127], L. Guan[107], J. G. R. Guerrero Rojas[164], G. Guerrieri[69a,69c], R. Gugel[101], J. A. M. Guhit[107], A. Guida[18], E. Guilloton[168], S. Guindon[36], F. Guo[14a,14e], J. Guo[62c], L. Guo[48], Y. Guo[107], R. Gupta[130], S. Gurbuz[24], S. S. Gurdasani[54], G. Gustavino[36], M. Guth[56], P. Gutierrez[121], L. F. Gutierrez Zagazeta[129], M. Gutsche[50], C. Gutschow[97], C. Gwenlan[127], C. B. Gwilliam[93],

E. S. Haaland[126], A. Haas[118], M. Habedank[48], C. Haber[17a], H. K. Hadavand[8], A. Hadef[50], S. Hadzic[111], A. I. Hagan[92], J. J. Hahn[143], E. H. Haines[97], M. Haleem[167], J. Haley[122], J. J. Hall[141], G. D. Hallewell[103], L. Halser[19], K. Hamano[166], M. Hamer[24], G. N. Hamity[52], E. J. Hampshire[96], J. Han[62b], K. Han[62a], L. Han[14c], L. Han[62a], S. Han[17a], Y. F. Han[156], K. Hanagaki[84], M. Hance[137], D. A. Hangal[41], H. Hanif[144], M. D. Hank[129], J. B. Hansen[42], P. H. Hansen[42], K. Hara[158], D. Harada[56], T. Harenberg[172], S. Harkusha[37], M. L. Harris[104], Y. T. Harris[127], J. Harrison[13], N. M. Harrison[120], P. F. Harrison[168], N. M. Hartman[111], N. M. Hartmann[110], R. Z. Hasan[96,135], Y. Hasegawa[142], S. Hassan[16], R. Hauser[108], C. M. Hawkes[20], R. J. Hawkings[36], Y. Hayashi[155], S. Hayashida[112], D. Hayden[108], C. Hayes[107], R. L. Hayes[115], C. P. Hays[127], J. M. Hays[95], H. S. Hayward[93], F. He[62a], M. He[14a,14e], Y. He[139], Y. He[48], Y. He[97], N. B. Heatley[95], V. Hedberg[99], A. L. Heggelund[126], N. D. Hehir[95,*], C. Heidegger[54], K. K. Heidegger[54], J. Heilman[34], S. Heim[48], T. Heim[17a], J. G. Heinlein[129], J. J. Heinrich[124], L. Heinrich[111,ad], J. Hejbal[132], A. Held[171], S. Hellesund[16], C. M. Helling[165], S. Hellman[47a,47b], R. C. W. Henderson[92], L. Henkelmann[32], A. M. Henriques Correia[36], H. Herde[99], Y. Hernández Jiménez[147], L. M. Herrmann[24], T. Herrmann[50], G. Herten[54], R. Hertenberger[110], L. Hervas[36], M. E. Hesping[101], N. P. Hessey[157a], M. Hidaoui[35b], E. Hill[156], S. J. Hillier[20], J. R. Hinds[108], F. Hinterkeuser[24], M. Hirose[125], S. Hirose[158], D. Hirschbuehl[172], T. G. Hitchings[102], B. Hiti[94], J. Hobbs[147], R. Hobincu[27e], N. Hod[170], M. C. Hodgkinson[141], B. H. Hodkinson[127], A. Hoecker[36], D. D. Hofer[107], J. Hofer[48], T. Holm[24], M. Holzbock[111], L. B. A. H. Hommels[32], B. P. Honan[102], J. J. Hong[68], J. Hong[62c], T. M. Hong[130], B. H. Hooberman[163], W. H. Hopkins[6], M. C. Hoppesch[163], Y. Horii[112], S. Hou[150], A. S. Howard[94], J. Howarth[59], J. Hoya[6], M. Hrabovsky[123], A. Hrynevich[48], T. Hryn'ova[4], P. J. Hsu[65], S.-C. Hsu[140], T. Hsu[66], M. Hu[17a], Q. Hu[62a], S. Huang[64b], X. Huang[14a,14e], Y. Huang[141], Y. Huang[101], Y. Huang[14a], Z. Huang[102], Z. Hubacek[133], M. Huebner[24], F. Huegging[24], T. B. Huffman[127], C. A. Hugli[48], M. Huhtinen[36], S. K. Huiberts[16], R. Hulsken[105], N. Huseynov[12], J. Huston[108], J. Huth[61], R. Hyneman[145], G. Iacobucci[56], G. Iakovidis[29], L. Iconomidou-Fayard[66], J. P. Iddon[36], P. Iengo[72a,72b], R. Iguchi[155], T. Iizawa[127], Y. Ikegami[84], N. Ilic[156], H. Imam[35a], M. Ince Lezki[56], T. Ingebretsen Carlson[47a,47b], G. Introzzi[73a,73b], M. Iodice[77a], V. Ippolito[75a,75b], R. K. Irwin[93], M. Ishino[155], W. Islam[171], C. Issever[18,48], S. Istin[21a,aj], H. Ito[169], R. Iuppa[78a,78b], A. Ivina[170], J. M. Izen[45], V. Izzo[72a], P. Jacka[132], P. Jackson[1], C. S. Jagfeld[110], G. Jain[157a], P. Jain[48], K. Jakobs[54], T. Jakoubek[170], J. Jamieson[59], M. Javurkova[104], L. Jeanty[124], J. Jejelava[151a,aa], P. Jenni[54,g], C. E. Jessiman[34], C. Jia[62b], J. Jia[147], X. Jia[61], X. Jia[14a,14e], Z. Jia[14c], C. Jiang[52], S. Jiggins[48], J. Jimenez Pena[13], S. Jin[14c], A. Jinaru[27b], O. Jinnouchi[139], P. Johansson[141], K. A. Johns[7], J. W. Johnson[137], D. M. Jones[148], E. Jones[48], P. Jones[32], R. W. L. Jones[92], T. J. Jones[93], H. L. Joos[36,55], R. Joshi[120], J. Jovicevic[15], X. Ju[17a], J. J. Junggeburth[104], T. Junkermann[63a], A. Juste Rozas[13,t], M. K. Juzek[87], S. Kabana[138e], A. Kaczmarska[87], M. Kado[111], H. Kagan[120], M. Kagan[145], A. Kahn[129], C. Kahra[101], T. Kaji[155], E. Kajomovitz[152], N. Kakati[170], I. Kalaitzidou[54], C. W. Kalderon[29], N. J. Kang[137], D. Kar[33g], K. Karava[127], M. J. Kareem[157b], E. Karentzos[54], O. Karkout[115], S. N. Karpov[38], Z. M. Karpova[38], V. Kartvelishvili[92], A. N. Karyukhin[37], E. Kasimi[154], J. Katzy[48], S. Kaur[34], K. Kawade[142], M. P. Kawale[121], C. Kawamoto[88], T. Kawamoto[62a], E. F. Kay[36], F. I. Kaya[159], S. Kazakos[108], V. F. Kazanin[37], Y. Ke[147], J. M. Keaveney[33a], R. Keeler[166], G. V. Kehris[61], J. S. Keller[34], A. S. Kelly[97], J. J. Kempster[148], P. D. Kennedy[101], O. Kepka[132], B. P. Kerridge[135], S. Kersten[172], B. P. Kerševan[94], L. Keszeghova[28a], S. Ketabchi Haghighat[156], R. A. Khan[130], A. Khanov[122], A. G. Kharlamov[37], T. Kharlamova[37], E. E. Khoda[140], M. Kholodenko[37], T. J. Khoo[18], G. Khoriauli[167], J. Khubua[151b,*], Y. A. R. Khwaira[128], B. Kibirige[33g], D. W. Kim[47a,47b], Y. K. Kim[39], N. Kimura[97], M. K. Kingston[55], A. Kirchhoff[55], C. Kirfel[24], F. Kirfel[24], J. Kirk[135], A. E. Kiryunin[111], C. Kitsaki[10], O. Kivernyk[24], M. Klassen[159], C. Klein[34], L. Klein[167], M. H. Klein[44], S. B. Klein[56], U. Klein[93], P. Klimek[36], A. Klimentov[29], T. Klioutchnikova[36], P. Kluit[115], S. Kluth[111], E. Kneringer[79], T. M. Knight[156], A. Knue[49], R. Kobayashi[88], D. Kobylianskii[170], S. F. Koch[127], M. Kocian[145], P. Kodyš[134], D. M. Koeck[124], P. T. Koenig[24], T. Koffas[34], O. Kolay[50], I. Koletsou[4], T. Komarek[123], K. Köneke[54], A. X. Y. Kong[1], T. Kono[119], N. Konstantinidis[97], P. Kontaxakis[56], B. Konya[99], R. Kopeliansky[41], S. Koperny[86a], K. Korcyl[87], K. Kordas[154,e], A. Korn[97], S. Korn[55], I. Korolkov[13], N. Korotkova[37], B. Kortman[115], O. Kortner[111], S. Kortner[111], W. H. Kostecka[116], V. V. Kostyukhin[143], A. Kotsokechagia[136], A. Kotwal[51], A. Koulouris[36], A. Kourkoumeli-Charalampidi[73a,73b], C. Kourkoumelis[9], E. Kourlitis[111,ad], O. Kovanda[124], R. Kowalewski[166], W. Kozanecki[136], A. S. Kozhin[37], V. A. Kramarenko[37], G. Kramberger[94], P. Kramer[101], M. W. Krasny[128], A. Krasznahorkay[36], J. W. Kraus[172], J. A. Kremer[48], T. Kresse[50], J. Kretzschmar[93], K. Kreul[18], P. Krieger[156], S. Krishnamurthy[104], M. Krivos[134],

K. Krizka[20], K. Kroeninger[49], H. Kroha[111], J. Kroll[132], J. Kroll[129], K. S. Krowpman[108], U. Kruchonak[38], H. Krüger[24], N. Krumnack[81], M. C. Kruse[51], O. Kuchinskaia[37], S. Kuday[3a], S. Kuehn[36], R. Kuesters[54], T. Kuhl[48], V. Kukhtin[38], Y. Kulchitsky[37,a], S. Kuleshov[138b,138d], M. Kumar[33g], N. Kumari[48], P. Kumari[157b], A. Kupco[132], T. Kupfer[49], A. Kupich[37], O. Kuprash[54], H. Kurashige[85], L. L. Kurchaninov[157a], O. Kurdysh[66], Y. A. Kurochkin[37], A. Kurova[37], M. Kuze[139], A. K. Kvam[104], J. Kvita[123], T. Kwan[105], N. G. Kyriacou[107], L. A. O. Laatu[103], C. Lacasta[164], F. Lacava[75a,75b], H. Lacker[18], D. Lacour[128], N. N. Lad[97], E. Ladygin[38], A. Lafarge[40], B. Laforge[128], T. Lagouri[173], F. Z. Lahbabi[35a], S. Lai[55], J. E. Lambert[166], S. Lammers[68], W. Lampl[7], C. Lampoudis[154,e], G. Lamprinoudis[101], A. N. Lancaster[116], E. Lançon[29], U. Landgraf[54], M. P. J. Landon[95], V. S. Lang[54], O. K. B. Langrekken[126], A. J. Lankford[160], F. Lanni[36], K. Lantzsch[24], A. Lanza[73a], J. F. Laporte[136], T. Lari[71a], F. Lasagni Manghi[23b], M. Lassnig[36], V. Latonova[132], A. Laudrain[101], A. Laurier[152], S. D. Lawlor[141], Z. Lawrence[102], R. Lazaridou[168], M. Lazzaroni[71a,71b], B. Le[102], E. M. Le Boulicaut[51], L. T. Le Pottier[17a], B. Leban[23a,23b], A. Lebedev[81], M. LeBlanc[102], F. Ledroit-Guillon[60], S. C. Lee[150], S. Lee[47a,47b], T. F. Lee[93], L. L. Leeuw[33c], H. P. Lefebvre[96], M. Lefebvre[166], C. Leggett[17a], G. Lehmann Miotto[36], M. Leigh[56], W. A. Leight[104], W. Leinonen[114], A. Leisos[154,s], M. A. L. Leite[83c], C. E. Leitgeb[18], R. Leitner[134], K. J. C. Leney[44], T. Lenz[24], S. Leone[74a], C. Leonidopoulos[52], A. Leopold[146], C. Leroy[109], R. Les[108], C. G. Lester[32], M. Levchenko[37], J. Levêque[4], L. J. Levinson[170], G. Levrini[23a,23b], M. P. Lewicki[87], C. Lewis[140], D. J. Lewis[4], A. Li[5], B. Li[62b], C. Li[62a], C.-Q. Li[111], H. Li[62a], H. Li[62b], H. Li[14c], H. Li[14b], H. Li[62b], J. Li[62c], K. Li[140], L. Li[62c], M. Li[14a,14e], S. Li[14a,14e], S. Li[62d,62c,d], T. Li[5], X. Li[105], Z. Li[127], Z. Li[155], Z. Li[14a,14e], S. Liang[14a,14e], Z. Liang[14a], M. Liberatore[136], B. Liberti[76a], K. Lie[64c], J. Lieber Marin[83e], H. Lien[68], H. Lin[107], K. Lin[108], R. E. Lindley[7], J. H. Lindon[2], E. Lipeles[129], A. Lipniacka[16], A. Lister[165], J. D. Little[68], B. Liu[14a], B. X. Liu[14d], D. Liu[62c,62d], E. H. L. Liu[20], J. B. Liu[62a], J. K. K. Liu[32], K. Liu[62d], K. Liu[62c,62d], M. Liu[62a], M. Y. Liu[62a], P. Liu[14a], Q. Liu[62c,62d,140], X. Liu[62a], X. Liu[62b], Y. Liu[14d,14e], Y. L. Liu[62b], Y. W. Liu[62a], J. Llorente Merino[144], S. L. Lloyd[95], E. M. Lobodzinska[48], P. Loch[7], T. Lohse[18], K. Lohwasser[141], E. Loiacono[48], M. Lokajicek[132,*], J. D. Lomas[20], J. D. Long[163], I. Longarini[160], R. Longo[163], I. Lopez Paz[67], A. Lopez Solis[48], N. Lorenzo Martinez[4], A. M. Lory[110], M. Losada[117a], G. Löschcke Centeno[148], O. Loseva[37], X. Lou[47a,47b], X. Lou[14a,14e], A. Lounis[66], P. A. Love[92], G. Lu[14a,14e], M. Lu[66], S. Lu[129], Y. J. Lu[65], H. J. Lubatti[140], C. Luci[75a,75b], F. L. Lucio Alves[14c], F. Luehring[68], I. Luise[147], O. Lukianchuk[66], O. Lundberg[146], B. Lund-Jensen[146,*], N. A. Luongo[6], M. S. Lutz[36], A. B. Lux[25], D. Lynn[29], R. Lysak[132], E. Lytken[99], V. Lyubushkin[38], T. Lyubushkina[38], M. M. Lyukova[147], M. Firdaus M. Soberi[52], H. Ma[29], K. Ma[62a], L. L. Ma[62b], W. Ma[62a], Y. Ma[122], J. C. MacDonald[101], P. C. Machado De Abreu Farias[83e], R. Madar[40], T. Madula[97], J. Maeda[85], T. Maeno[29], H. Maguire[141], V. Maiboroda[136], A. Maio[131a,131b,131d], K. Maj[86a], O. Majersky[48], S. Majewski[124], N. Makovec[66], V. Maksimovic[15], B. Malaescu[128], Pa. Malecki[87], V. P. Maleev[37], F. Malek[60,n], M. Mali[94], D. Malito[96], U. Mallik[80,*], S. Maltezos[10], S. Malyukov[38], J. Mamuzic[13], G. Mancini[53], M. N. Mancini[26], G. Manco[73a,73b], J. P. Mandalia[95], I. Mandić[94], L. Manhaes de Andrade Filho[83a], I. M. Maniatis[170], J. Manjarres Ramos[90], D. C. Mankad[170], A. Mann[110], S. Manzoni[36], L. Mao[62c], X. Mapekula[33c], A. Marantis[154,s], G. Marchiori[5], M. Marcisovsky[132], C. Marcon[71a], M. Marinescu[20], S. Marium[48], M. Marjanovic[121], A. Markhoos[54], M. Markovitch[66], E. J. Marshall[92], Z. Marshall[17a], S. Marti-Garcia[164], J. Martin[97], T. A. Martin[135], V. J. Martin[52], B. Martin dit Latour[16], L. Martinelli[75a,75b], M. Martinez[13,t], P. Martinez Agullo[164], V. I. Martinez Outschoorn[104], P. Martinez Suarez[13], S. Martin-Haugh[135], G. Martinovicova[134], V. S. Martoiu[27b], A. C. Martyniuk[97], A. Marzin[36], D. Mascione[78a,78b], L. Masetti[101], T. Mashimo[155], J. Masik[102], A. L. Maslennikov[37], P. Massarotti[72a,72b], P. Mastrandrea[74a,74b], A. Mastroberardino[43a,43b], T. Masubuchi[155], T. Mathisen[162], J. Matousek[134], N. Matsuzawa[155], J. Maurer[27b], A. J. Maury[66], B. Maček[94], D. A. Maximov[37], A. E. May[102], R. Mazini[150], I. Maznas[116], M. Mazza[108], S. M. Mazza[137], E. Mazzeo[71a,71b], C. Mc Ginn[29], J. P. Mc Gowan[166], S. P. Mc Kee[107], C. C. McCracken[165], E. F. McDonald[106], A. E. McDougall[115], J. A. Mcfayden[148], R. P. McGovern[129], R. P. Mckenzie[33g], T. C. Mclachlan[48], D. J. Mclaughlin[97], S. J. McMahon[135], C. M. Mcpartland[93], R. A. McPherson[166,x], S. Mehlhase[110], A. Mehta[93], D. Melini[164], B. R. Mellado Garcia[33g], A. H. Melo[55], F. Meloni[48], A. M. Mendes Jacques Da Costa[102], H. Y. Meng[156], L. Meng[92], S. Menke[111], M. Mentink[36], E. Meoni[43a,43b], G. Mercado[116], S. Merianos[154], C. Merlassino[69a,69c], L. Merola[72a,72b], C. Meroni[71a,71b], J. Metcalfe[6], A. S. Mete[6], E. Meuser[101], C. Meyer[68], J-P. Meyer[136], R. P. Middleton[135], L. Mijović[52], G. Mikenberg[170], M. Mikestikova[132], M. Mikuž[94], H. Mildner[101], A. Milic[36], D. W. Miller[39], E. H. Miller[145],

L. S. Miller[34], A. Milov[170], D. A. Milstead[47a,47b], T. Min[14c], A. A. Minaenko[37], I. A. Minashvili[151b], L. Mince[59], A. I. Mincer[118], B. Mindur[86a], M. Mineev[38], Y. Mino[88], L. M. Mir[13], M. Miralles Lopez[59], M. Mironova[17a], A. Mishima[155], M. C. Missio[114], A. Mitra[168], V. A. Mitsou[164], Y. Mitsumori[112], O. Miu[156], P. S. Miyagawa[95], T. Mkrtchyan[63a], M. Mlinarevic[97], T. Mlinarevic[97], M. Mlynarikova[36], S. Mobius[19], P. Mogg[110], M. H. Mohamed Farook[113], A. F. Mohammed[14a,14e], S. Mohapatra[41], G. Mokgatitswane[33g], L. Moleri[170], B. Mondal[143], S. Mondal[133], K. Mönig[48], E. Monnier[103], L. Monsonis Romero[164], J. Montejo Berlingen[13], M. Montella[120], F. Montereali[77a,77b], F. Monticelli[91], S. Monzani[69a,69c], N. Morange[66], A. L. Moreira De Carvalho[48], M. Moreno Llácer[164], C. Moreno Martinez[56], P. Morettini[57b], S. Morgenstern[36], M. Morii[61], M. Morinaga[155], F. Morodei[75a,75b], L. Morvaj[36], P. Moschovakos[36], B. Moser[36], M. Mosidze[151b], T. Moskalets[44], P. Moskvitina[114], J. Moss[31,k], P. Moszkowicz[86a], A. Moussa[35d], E. J. W. Moyse[104], O. Mtintsilana[33g], S. Muanza[103], J. Mueller[130], D. Muenstermann[92], R. Müller[19], G. A. Mullier[162], A. J. Mullin[32], J. J. Mullin[129], D. P. Mungo[156], D. Munoz Perez[164], F. J. Munoz Sanchez[102], M. Murin[102], W. J. Murray[135,168], M. Muškinja[94], C. Mwewa[29], A. G. Myagkov[37,a], A. J. Myers[8], G. Myers[107], M. Myska[133], B. P. Nachman[17a], O. Nackenhorst[49], K. Nagai[127], K. Nagano[84], J. L. Nagle[29,ah], E. Nagy[103], A. M. Nairz[36], Y. Nakahama[84], K. Nakamura[84], K. Nakkalil[5], H. Nanjo[125], E. A. Narayanan[113], I. Naryshkin[37], L. Nasella[71a,71b], M. Naseri[34], S. Nasri[117b], C. Nass[24], G. Navarro[22a], J. Navarro-Gonzalez[164], R. Nayak[153], A. Nayaz[18], P. Y. Nechaeva[37], S. Nechaeva[23a,23b], F. Nechansky[48], L. Nedic[127], T. J. Neep[20], A. Negri[73a,73b], M. Negrini[23b], C. Nellist[115], C. Nelson[105], K. Nelson[107], S. Nemecek[132], M. Nessi[36,h], M. S. Neubauer[163], F. Neuhaus[101], J. Neundorf[48], P. R. Newman[20], C. W. Ng[130], Y. W. Y. Ng[48], B. Ngair[117a], H. D. N. Nguyen[109], R. B. Nickerson[127], R. Nicolaidou[136], J. Nielsen[137], M. Niemeyer[55], J. Niermann[55], N. Nikiforou[36], V. Nikolaenko[37,a], I. Nikolic-Audit[128], K. Nikolopoulos[20], P. Nilsson[29], I. Ninca[48], G. Ninio[153], A. Nisati[75a], N. Nishu[2], R. Nisius[111], J-E. Nitschke[50], E. K. Nkadimeng[33g], T. Nobe[155], T. Nommensen[149], M. B. Norfolk[141], B. J. Norman[34], M. Noury[35a], J. Novak[94], T. Novak[94], L. Novotny[133], R. Novotny[113], L. Nozka[123], K. Ntekas[160], N. M. J. Nunes De Moura Junior[83b], J. Ocariz[128], A. Ochi[85], I. Ochoa[131a], S. Oerdek[48,u], J. T. Offermann[39], A. Ogrodnik[134], A. Oh[102], C. C. Ohm[146], H. Oide[84], R. Oishi[155], M. L. Ojeda[48], Y. Okumura[155], L. F. Oleiro Seabra[131a], S. A. Olivares Pino[138d], G. Oliveira Correa[13], D. Oliveira Damazio[29], D. Oliveira Goncalves[83a], J. L. Oliver[160], Ö. O. Öncel[54], A. P. O'Neill[19], A. Onofre[131a,131e], P. U. E. Onyisi[11], M. J. Oreglia[39], G. E. Orellana[91], D. Orestano[77a,77b], N. Orlando[13], R. S. Orr[156], L. M. Osojnak[129], R. Ospanov[62a], G. Otero y Garzon[30], H. Otono[89], P. S. Ott[63a], G. J. Ottino[17a], M. Ouchrif[35d], F. Ould-Saada[126], T. Ovsiannikova[140], M. Owen[59], R. E. Owen[135], V. E. Ozcan[21a], F. Ozturk[87], N. Ozturk[8], S. Ozturk[82], H. A. Pacey[127], A. Pacheco Pages[13], C. Padilla Aranda[13], G. Padovano[75a,75b], S. Pagan Griso[17a], G. Palacino[68], A. Palazzo[70a,70b], J. Pampel[24], J. Pan[173], T. Pan[64a], D. K. Panchal[11], C. E. Pandini[115], J. G. Panduro Vazquez[135], H. D. Pandya[1], H. Pang[14b], P. Pani[48], G. Panizzo[69a,69c], L. Panwar[128], L. Paolozzi[56], S. Parajuli[163], A. Paramonov[6], C. Paraskevopoulos[53], D. Paredes Hernandez[64b], A. Pareti[73a,73b], K. R. Park[41], T. H. Park[156], M. A. Parker[32], F. Parodi[57a,57b], E. W. Parrish[116], V. A. Parrish[52], J. A. Parsons[41], U. Parzefall[54], B. Pascual Dias[109], L. Pascual Dominguez[100], E. Pasqualucci[75a], S. Passaggio[57b], F. Pastore[96], P. Patel[87], U. M. Patel[51], J. R. Pater[102], T. Pauly[36], C. I. Pazos[159], J. Pearkes[145], M. Pedersen[126], R. Pedro[131a], S. V. Peleganchuk[37], O. Penc[36], E. A. Pender[52], G. D. Penn[173], K. E. Penski[110], M. Penzin[37], B. S. Peralva[83d], A. P. Pereira Peixoto[140], L. Pereira Sanchez[145], D. V. Perepelitsa[29,ah], E. Perez Codina[157a], M. Perganti[10], H. Pernegger[36], S. Perrella[75a,75b], O. Perrin[40], K. Peters[48], R. F. Y. Peters[102], B. A. Petersen[36], T. C. Petersen[42], E. Petit[103], V. Petousis[133], C. Petridou[154,e], T. Petru[134], A. Petrukhin[143], M. Pettee[17a], A. Petukhov[37], K. Petukhova[134], R. Pezoa[138f], L. Pezzotti[36], G. Pezzullo[173], T. M. Pham[171], T. Pham[106], P. W. Phillips[135], G. Piacquadio[147], E. Pianori[17a], F. Piazza[124], R. Piegaia[30], D. Pietreanu[27b], A. D. Pilkington[102], M. Pinamonti[69a,69c], J. L. Pinfold[2], B. C. Pinheiro Pereira[131a], A. E. Pinto Pinoargote[136], L. Pintucci[69a,69c], K. M. Piper[148], A. Pirttikoski[56], D. A. Pizzi[34], L. Pizzimento[64b], A. Pizzini[115], M.-A. Pleier[29], V. Pleskot[134], E. Plotnikova[38], G. Poddar[95], R. Poettgen[99], L. Poggioli[128], I. Pokharel[55], S. Polacek[134], G. Polesello[73a], A. Poley[144,157a], A. Polini[23b], C. S. Pollard[168], Z. B. Pollock[120], E. Pompa Pacchi[75a,75b], N. I. Pond[97], D. Ponomarenko[114], L. Pontecorvo[36], S. Popa[27a], G. A. Popeneciu[27d], A. Poreba[36], D. M. Portillo Quintero[157a], S. Pospisil[133], M. A. Postill[141], P. Postolache[27c], K. Potamianos[168], P. A. Potepa[86a], I. N. Potrap[38], C. J. Potter[32], H. Potti[1], J. Poveda[164], M. E. Pozo Astigarraga[36], A. Prades Ibanez[164], J. Pretel[54], D. Price[102], M. Primavera[70a], M. A. Principe Martin[100], R. Privara[123],

T. Procter[59], M. L. Proffitt[140], N. Proklova[129], K. Prokofiev[64c], G. Proto[111], J. Proudfoot[6], M. Przybycien[86a], W. W. Przygoda[86b], A. Psallidas[46], J. E. Puddefoot[141], D. Pudzha[37], D. Pyatiizbyantseva[37], J. Qian[107], D. Qichen[102], Y. Qin[13], T. Qiu[52], A. Quadt[55], M. Queitsch-Maitland[102], G. Quetant[56], R. P. Quinn[165], G. Rabanal Bolanos[61], D. Rafanoharana[54], F. Raffaeli[76a,76b], F. Ragusa[71a,71b], J. L. Rainbolt[39], J. A. Raine[56], S. Rajagopalan[29], E. Ramakoti[37], I. A. Ramirez-Berend[34], K. Ran[48,14e], N. P. Rapheeha[33g], H. Rasheed[27b], V. Raskina[128], D. F. Rassloff[63a], A. Rastogi[17a], S. Rave[101], S. Ravera[57a,57b], B. Ravina[55], I. Ravinovich[170], M. Raymond[36], A. L. Read[126], N. P. Readioff[141], D. M. Rebuzzi[73a,73b], G. Redlinger[29], A. S. Reed[111], K. Reeves[26], J. A. Reidelsturz[172], D. Reikher[153], A. Rej[49], C. Rembser[36], M. Renda[27b], M. B. Rendel[111], F. Renner[48], A. G. Rennie[160], A. L. Rescia[48], S. Resconi[71a], M. Ressegotti[57a,57b], S. Rettie[36], J. G. Reyes Rivera[108], E. Reynolds[17a], O. L. Rezanova[37], P. Reznicek[134], H. Riani[35d], N. Ribaric[92], E. Ricci[78a,78b], R. Richter[111], S. Richter[47a,47b], E. Richter-Was[86b], M. Ridel[128], S. Ridouani[35d], P. Rieck[118], P. Riedler[36], E. M. Riefel[47a,47b], J. O. Rieger[115], M. Rijssenbeek[147], M. Rimoldi[36], L. Rinaldi[23a,23b], T. T. Rinn[29], M. P. Rinnagel[110], G. Ripellino[162], I. Riu[13], J. C. Rivera Vergara[166], F. Rizatdinova[122], E. Rizvi[95], B. R. Roberts[17a], S. H. Robertson[105,x], D. Robinson[32], C. M. Robles Gajardo[138f], M. Robles Manzano[101], A. Robson[59], A. Rocchi[76a,76b], C. Roda[74a,74b], S. Rodriguez Bosca[36], Y. Rodriguez Garcia[22a], A. Rodriguez Rodriguez[54], A. M. Rodríguez Vera[116], S. Roe[36], J. T. Roemer[160], A. R. Roepe-Gier[137], J. Roggel[172], O. Røhne[126], R. A. Rojas[104], C. P. A. Roland[128], J. Roloff[29], A. Romaniouk[37], E. Romano[73a,73b], M. Romano[23b], A. C. Romero Hernandez[163], N. Rompotis[93], L. Roos[128], S. Rosati[75a], B. J. Rosser[39], E. Rossi[127], E. Rossi[72a,72b], L. P. Rossi[61], L. Rossini[54], R. Rosten[120], M. Rotaru[27b], B. Rottler[54], C. Rougier[90], D. Rousseau[66], D. Rousso[48], A. Roy[163], S. Roy-Garand[156], A. Rozanov[103], Z. M. A. Rozario[59], Y. Rozen[152], A. Rubio Jimenez[164], A. J. Ruby[93], V. H. Ruelas Rivera[18], T. A. Ruggeri[1], A. Ruggiero[127], A. Ruiz-Martinez[164], A. Rummler[36], Z. Rurikova[54], N. A. Rusakovich[38], H. L. Russell[166], G. Russo[75a,75b], J. P. Rutherfoord[7], S. Rutherford Colmenares[32], M. Rybar[134], E. B. Rye[126], A. Ryzhov[44], J. A. Sabater Iglesias[56], P. Sabatini[164], H.F-W. Sadrozinski[137], F. Safai Tehrani[75a], B. Safarzadeh Samani[135], S. Saha[1], M. Sahinsoy[111], A. Saibel[164], M. Saimpert[136], M. Saito[155], T. Saito[155], A. Sala[71a,71b], D. Salamani[36], A. Salnikov[145], J. Salt[164], A. Salvador Salas[153], D. Salvatore[43a,43b], F. Salvatore[148], A. Salzburger[36], D. Sammel[54], E. Sampson[92], D. Sampsonidis[154,e], D. Sampsonidou[124], J. Sánchez[164], V. Sanchez Sebastian[164], H. Sandaker[126], C. O. Sander[48], J. A. Sandesara[104], M. Sandhoff[172], C. Sandoval[22b], L. Sanfilippo[63a], D. P. C. Sankey[135], T. Sano[88], A. Sansoni[53], L. Santi[36,75b], C. Santoni[40], H. Santos[131a,131b], A. Santra[170], E. Sanzani[23a,23b], K. A. Saoucha[161], J. G. Saraiva[131a,131d], J. Sardain[7], O. Sasaki[84], K. Sato[158], C. Sauer[63b], E. Sauvan[4], P. Savard[156,af], R. Sawada[155], C. Sawyer[135], L. Sawyer[98], C. Sbarra[23b], A. Sbrizzi[23a,23b], T. Scanlon[97], J. Schaarschmidt[140], U. Schäfer[101], A. C. Schaffer[44,66], D. Schaile[110], R. D. Schamberger[147], C. Scharf[18], M. M. Schefer[19], V. A. Schegelsky[37], D. Scheirich[134], M. Schernau[160], C. Scheulen[55], C. Schiavi[57a,57b], M. Schioppa[43a,43b], B. Schlag[145], K. E. Schleicher[54], S. Schlenker[36], J. Schmeing[172], M. A. Schmidt[172], K. Schmieden[101], C. Schmitt[101], N. Schmitt[101], S. Schmitt[48], L. Schoeffel[136], A. Schoening[63b], P. G. Scholer[34], E. Schopf[127], M. Schott[24], J. Schovancova[36], S. Schramm[56], T. Schroer[56], H-C. Schultz-Coulon[63a], M. Schumacher[54], B. A. Schumm[137], Ph. Schune[136], A. J. Schuy[140], H. R. Schwartz[137], A. Schwartzman[145], T. A. Schwarz[107], Ph. Schwemling[136], R. Schwienhorst[108], A. Sciandra[29], G. Sciolla[26], F. Scuri[74a], C. D. Sebastiani[93], K. Sedlaczek[116], S. C. Seidel[113], A. Seiden[137], B. D. Seidlitz[41], C. Seitz[48], J. M. Seixas[83b], G. Sekhniaidze[72a], L. Selem[60], N. Semprini-Cesari[23a,23b], D. Sengupta[56], V. Senthilkumar[164], L. Serin[66], M. Sessa[76a,76b], H. Severini[121], F. Sforza[57a,57b], A. Sfyrla[56], Q. Sha[14a], E. Shabalina[55], A. H. Shah[32], R. Shaheen[146], J. D. Shahinian[129], D. Shaked Renous[170], L. Y. Shan[14a], M. Shapiro[17a], A. Sharma[36], A. S. Sharma[165], P. Sharma[80], P. B. Shatalov[37], K. Shaw[148], S. M. Shaw[102], Q. Shen[5,62c], D. J. Sheppard[144], P. Sherwood[97], L. Shi[97], X. Shi[14a], C. O. Shimmin[173], J. D. Shinner[96], I. P. J. Shipsey[127,*], S. Shirabe[89], M. Shiyakova[38,v], M. J. Shochet[39], J. Shojaii[106], D. R. Shope[126], B. Shrestha[121], S. Shrestha[120,ai], M. J. Shroff[166], P. Sicho[132], A. M. Sickles[163], E. Sideras Haddad[33g], A. C. Sidley[115], A. Sidoti[23b], F. Siegert[50], Dj. Sijacki[15], F. Sili[91], J. M. Silva[52], M. V. Silva Oliveira[29], S. B. Silverstein[47a], S. Simion[66], R. Simoniello[36], E. L. Simpson[102], H. Simpson[148], L. R. Simpson[107], N. D. Simpson[99], S. Simsek[82], S. Sindhu[55], P. Sinervo[156], S. Singh[156], S. Sinha[48], S. Sinha[102], M. Sioli[23a,23b], I. Siral[36], E. Sitnikova[48], J. Sjölin[47a,47b], A. Skaf[55], E. Skorda[20], P. Skubic[121], M. Slawinska[87], V. Smakhtin[170], B. H. Smart[135], S. Yu. Smirnov[37], Y. Smirnov[37], L. N. Smirnova[37,a], O. Smirnova[99], A. C. Smith[41], D. R. Smith[160], E. A. Smith[39], H. A. Smith[127], J. L. Smith[102], R. Smith[145], M. Smizanska[92], K. Smolek[133], A. A. Snesarev[37], S. R. Snider[156],

H. L. Snoek[115], S. Snyder[29], R. Sobie[166,x], A. Soffer[153], C. A. Solans Sanchez[36], E.Yu. Soldatov[37], U. Soldevila[164], A. A. Solodkov[37], S. Solomon[26], A. Soloshenko[38], K. Solovieva[54], O. V. Solovyanov[40], P. Sommer[36], A. Sonay[13], W. Y. Song[157b], A. Sopczak[133], A. L. Sopio[97], F. Sopkova[28b], J. D. Sorenson[113], I. R. Sotarriva Alvarez[139], V. Sothilingam[63a], O. J. Soto Sandoval[138b,138c], S. Sottocornola[68], R. Soualah[161], Z. Soumaimi[35e], D. South[48], N. Soybelman[170], S. Spagnolo[70a,70b], M. Spalla[111], D. Sperlich[54], G. Spigo[36], S. Spinali[92], D. P. Spiteri[59], M. Spousta[134], E. J. Staats[34], R. Stamen[63a], A. Stampekis[20], M. Standke[24], E. Stanecka[87], W. Stanek-Maslouska[48], M. V. Stange[50], B. Stanislaus[17a], M. M. Stanitzki[48], B. Stapf[48], E. A. Starchenko[37], G. H. Stark[137], J. Stark[90], P. Staroba[132], P. Starovoitov[63a], S. Stärz[105], R. Staszewski[87], G. Stavropoulos[46], J. Steentoft[162], P. Steinberg[29], B. Stelzer[144,157a], H. J. Stelzer[130], O. Stelzer-Chilton[157a], H. Stenzel[58], T. J. Stevenson[148], G. A. Stewart[36], J. R. Stewart[122], M. C. Stockton[36], G. Stoicea[27b], M. Stolarski[131a], S. Stonjek[111], A. Straessner[50], J. Strandberg[146], S. Strandberg[47a,47b], M. Stratmann[172], M. Strauss[121], T. Strebler[103], P. Strizenec[28b], R. Ströhmer[167], D. M. Strom[124], R. Stroynowski[44], A. Strubig[47a,47b], S. A. Stucci[29], B. Stugu[16], J. Stupak[121], N. A. Styles[48], D. Su[145], S. Su[62a], W. Su[62d], X. Su[62a], D. Suchy[28a], K. Sugizaki[155], V. V. Sulin[37], M. J. Sullivan[93], D. M. S. Sultan[127], L. Sultanaliyeva[37], S. Sultansoy[3b], T. Sumida[88], S. Sun[171], O. Sunneborn Gudnadottir[162], N. Sur[103], M. R. Sutton[148], H. Suzuki[158], M. Svatos[132], M. Swiatlowski[157a], T. Swirski[167], I. Sykora[28a], M. Sykora[134], T. Sykora[134], D. Ta[101], K. Tackmann[48,u], A. Taffard[160], R. Tafirout[157a], J. S. Tafoya Vargas[66], Y. Takubo[84], M. Talby[103], A. A. Talyshev[37], K. C. Tam[64b], N. M. Tamir[153], A. Tanaka[155], J. Tanaka[155], R. Tanaka[66], M. Tanasini[147], Z. Tao[165], S. Tapia Araya[138f], S. Tapprogge[101], A. Tarek Abouelfadl Mohamed[108], S. Tarem[152], K. Tariq[14a], G. Tarna[27b], G. F. Tartarelli[71a], M. J. Tartarin[90], P. Tas[134], M. Tasevsky[132], E. Tassi[43a,43b], A. C. Tate[163], G. Tateno[155], Y. Tayalati[35e,w], G. N. Taylor[106], W. Taylor[157b], R. Teixeira De Lima[145], P. Teixeira-Dias[96], J. J. Teoh[156], K. Terashi[155], J. Terron[100], S. Terzo[13], M. Testa[53], R. J. Teuscher[156,x], A. Thaler[79], O. Theiner[56], N. Themistokleous[52], T. Theveneaux-Pelzer[103], O. Thielmann[172], D. W. Thomas[96], J. P. Thomas[20], E. A. Thompson[17a], P. D. Thompson[20], E. Thomson[129], R. E. Thornberry[44], C. Tian[62a], Y. Tian[55], V. Tikhomirov[37,a], Yu.A. Tikhonov[37], S. Timoshenko[37], D. Timoshyn[134], E. X. L. Ting[1], P. Tipton[173], A. Tishelman-Charny[29], S. H. Tlou[33g], K. Todome[139], S. Todorova-Nova[134], S. Todt[50], L. Toffolin[69a,69c], M. Togawa[84], J. Tojo[89], S. Tokár[28a], K. Tokushuku[84], O. Toldaiev[68], R. Tombs[32], M. Tomoto[84,112], L. Tompkins[145,m], K. W. Topolnicki[86b], E. Torrence[124], H. Torres[90], E. Torró Pastor[164], M. Toscani[30], C. Tosciri[39], M. Tost[11], D. R. Tovey[141], I. S. Trandafir[27b], T. Trefzger[167], A. Tricoli[29], I. M. Trigger[157a], S. Trincaz-Duvoid[128], D. A. Trischuk[26], B. Trocmé[60], L. Truong[33c], M. Trzebinski[87], A. Trzupek[87], F. Tsai[147], M. Tsai[107], A. Tsiamis[154,e], P. V. Tsiareshka[37], S. Tsigaridas[157a], A. Tsirigotis[154,s], V. Tsiskaridze[156], E. G. Tskhadadze[151a], M. Tsopoulou[154], Y. Tsujikawa[88], I. I. Tsukerman[37], V. Tsulaia[17a], S. Tsuno[84], K. Tsuri[119], D. Tsybychev[147], Y. Tu[64b], A. Tudorache[27b], V. Tudorache[27b], A. N. Tuna[61], S. Turchikhin[57a,57b], I. Turk Cakir[3a], R. Turra[71a], T. Turtuvshin[38,y], P. M. Tuts[41], S. Tzamarias[154,e], E. Tzovara[101], F. Ukegawa[158], P. A. Ulloa Poblete[138b,138c], E. N. Umaka[29], G. Unal[36], A. Undrus[29], G. Unel[160], J. Urban[28b], P. Urrejola[138a], G. Usai[8], R. Ushioda[139], M. Usman[109], Z. Uysal[82], V. Vacek[133], B. Vachon[105], T. Vafeiadis[36], A. Vaitkus[97], C. Valderanis[110], E. Valdes Santurio[47a,47b], M. Valente[157a], S. Valentinetti[23a,23b], A. Valero[164], E. Valiente Moreno[164], A. Vallier[90], J. A. Valls Ferrer[164], D. R. Van Arneman[115], T. R. Van Daalen[140], A. Van Der Graaf[49], P. Van Gemmeren[6], M. Van Rijnbach[36], S. Van Stroud[97], I. Van Vulpen[115], P. Vana[134], M. Vanadia[76a,76b], W. Vandelli[36], E. R. Vandewall[122], D. Vannicola[153], L. Vannoli[53], R. Vari[75a], E. W. Varnes[7], C. Varni[17b], T. Varol[150], D. Varouchas[66], L. Varriale[164], K. E. Varvell[149], M. E. Vasile[27b], L. Vaslin[84], G. A. Vasquez[166], A. Vasyukov[38], R. Vavricka[101], T. Vazquez Schroeder[36], J. Veatch[31], V. Vecchio[102], M. J. Veen[104], I. Veliscek[29], L. M. Veloce[156], F. Veloso[131a,131c], S. Veneziano[75a], A. Ventura[70a,70b], S. Ventura Gonzalez[136], A. Verbytskyi[111], M. Verducci[74a,74b], C. Vergis[95], M. Verissimo De Araujo[83b], W. Verkerke[115], J. C. Vermeulen[115], C. Vernieri[145], M. Vessella[104], M. C. Vetterli[144,af], A. Vgenopoulos[154,e], N. Viaux Maira[138f], T. Vickey[141], O. E. Vickey Boeriu[141], G. H. A. Viehhauser[127], L. Vigani[63b], M. Villa[23a,23b], M. Villaplana Perez[164], E. M. Villhauer[52], E. Vilucchi[53], M. G. Vincter[34], A. Visibile[115], C. Vittori[36], I. Vivarelli[23a,23b], E. Voevodina[111], F. Vogel[110], J. C. Voigt[50], P. Vokac[133], Yu. Volkotrub[86b], J. Von Ahnen[48], E. Von Toerne[24], B. Vormwald[36], V. Vorobel[134], K. Vorobev[37], M. Vos[164], K. Voss[143], M. Vozak[115], L. Vozdecky[121], N. Vranjes[15], M. Vranjes Milosavljevic[15], M. Vreeswijk[115], N. K. Vu[62c,62d], R. Vuillermet[36], O. Vujinovic[101], I. Vukotic[39], S. Wada[158], C. Wagner[104], J. M. Wagner[17a], W. Wagner[172], S. Wahdan[172], H. Wahlberg[91], M. Wakida[112], J. Walder[135], R. Walker[110], W. Walkowiak[143], A. Wall[129], E. J. Wallin[99], T. Wamorkar[6], A. Z. Wang[137],

C. Wang[101], C. Wang[11], H. Wang[17a], J. Wang[64c], R. Wang[61], R. Wang[6], S. M. Wang[150], S. Wang[62b], S. Wang[14a], T. Wang[62a], W. T. Wang[80], W. Wang[14a], X. Wang[14c], X. Wang[163], X. Wang[62c], Y. Wang[62d], Y. Wang[14c], Z. Wang[107], Z. Wang[51,62c,62d], Z. Wang[107], A. Warburton[105], R. J. Ward[20], N. Warrack[59], S. Waterhouse[96], A. T. Watson[20], H. Watson[59], M. F. Watson[20], E. Watton[59,135], G. Watts[140], B. M. Waugh[97], J. M. Webb[54], C. Weber[29], H. A. Weber[18], M. S. Weber[19], S. M. Weber[63a], C. Wei[62a], Y. Wei[54], A. R. Weidberg[127], E. J. Weik[118], J. Weingarten[49], C. Weiser[54], C. J. Wells[48], T. Wenaus[29], B. Wendland[49], T. Wengler[36], N. S. Wenke[111], N. Wermes[24], M. Wessels[63a], A. M. Wharton[92], A. S. White[61], A. White[8], M. J. White[1], D. Whiteson[160], L. Wickremasinghe[125], W. Wiedenmann[171], M. Wielers[135], C. Wiglesworth[42], D. J. Wilbern[121], H. G. Wilkens[36], J. J. H. Wilkinson[32], D. M. Williams[41], H. H. Williams[129], S. Williams[32], S. Willocq[104], B. J. Wilson[102], P. J. Windischhofer[39], F. I. Winkel[30], F. Winklmeier[124], B. T. Winter[54], J. K. Winter[102], M. Wittgen[145], M. Wobisch[98], T. Wojtkowski[60], Z. Wolffs[115], J. Wollrath[160], M. W. Wolter[87], H. Wolters[131a,131c], M. C. Wong[137], E. L. Woodward[41], S. D. Worm[48], B. K. Wosiek[87], K. W. Woźniak[87], S. Wozniewski[55], K. Wraight[59], C. Wu[20], M. Wu[14d], M. Wu[114], S. L. Wu[171], X. Wu[56], Y. Wu[62a], Z. Wu[4], J. Wuerzinger[111,ad], T. R. Wyatt[102], B. M. Wynne[52], S. Xella[42], L. Xia[14c], M. Xia[14b], J. Xiang[64c], M. Xie[62a], S. Xin[14a,14e], A. Xiong[124], J. Xiong[17a], D. Xu[14a], H. Xu[62a], L. Xu[62a], R. Xu[129], T. Xu[107], Y. Xu[14b], Z. Xu[52], Z. Xu[14c], B. Yabsley[149], S. Yacoob[33a], Y. Yamaguchi[139], E. Yamashita[155], H. Yamauchi[158], T. Yamazaki[17a], Y. Yamazaki[85], J. Yan[62c], S. Yan[59], Z. Yan[104], H. J. Yang[62c,62d], H. T. Yang[62a], S. Yang[62a], T. Yang[64c], X. Yang[36], X. Yang[14a], Y. Yang[44], Y. Yang[62a], Z. Yang[62a], W-M. Yao[17a], H. Ye[14c], H. Ye[55], J. Ye[14a], S. Ye[29], X. Ye[62a], Y. Yeh[97], I. Yeletskikh[38], B. Yeo[17b], M. R. Yexley[97], T. P. Yildirim[127], P. Yin[41], K. Yorita[169], S. Younas[27b], C. J. S. Young[36], C. Young[145], C. Yu[14a,14e], Y. Yu[62a], M. Yuan[107], R. Yuan[62c,62d], L. Yue[97], M. Zaazoua[62a], B. Zabinski[87], E. Zaid[52], Z. K. Zak[87], T. Zakareishvili[164], N. Zakharchuk[34], S. Zambito[56], J. A. Zamora Saa[138b,138d], J. Zang[155], D. Zanzi[54], O. Zaplatilek[133], C. Zeitnitz[172], H. Zeng[14a], J. C. Zeng[163], D. T. Zenger Jr[26], O. Zenin[37], T. Ženiš[28a], S. Zenz[95], S. Zerradi[35a], D. Zerwas[66], M. Zhai[14a,14e], D. F. Zhang[141], J. Zhang[62b], J. Zhang[6], K. Zhang[14a,14e], L. Zhang[62a], L. Zhang[14c], P. Zhang[14a,14e], R. Zhang[171], S. Zhang[107], S. Zhang[90], T. Zhang[155], X. Zhang[62c], X. Zhang[62b], Y. Zhang[62c], Y. Zhang[97], Y. Zhang[14c], Z. Zhang[17a], Z. Zhang[62b], Z. Zhang[66], H. Zhao[140], T. Zhao[62b], Y. Zhao[137], Z. Zhao[62a], Z. Zhao[62a], A. Zhemchugov[38], J. Zheng[14c], K. Zheng[163], X. Zheng[62a], Z. Zheng[145], D. Zhong[163], B. Zhou[107], H. Zhou[7], N. Zhou[62c], Y. Zhou[14b], Y. Zhou[14c], Y. Zhou[7], C. G. Zhu[62b], J. Zhu[107], X. Zhu[62d], Y. Zhu[62c], Y. Zhu[62a], X. Zhuang[14a], K. Zhukov[37], N. I. Zimine[38], J. Zinsser[63b], M. Ziolkowski[143], L. Živković[15], A. Zoccoli[23a,23b], K. Zoch[61], T. G. Zorbas[141], O. Zormpa[46], W. Zou[41], L. Zwalinski[36]

[1] Department of Physics, University of Adelaide, Adelaide, Australia
[2] Department of Physics, University of Alberta, Edmonton, AB, Canada
[3] [(a)]Department of Physics, Ankara University, Ankara, Turkey; [(b)]Division of Physics, TOBB University of Economics and Technology, Ankara, Turkey
[4] LAPP, Université Savoie Mont Blanc, CNRS/IN2P3, Annecy, France
[5] APC, Université Paris Cité, CNRS/IN2P3, Paris, France
[6] High Energy Physics Division, Argonne National Laboratory, Argonne, IL, USA
[7] Department of Physics, University of Arizona, Tucson, AZ, USA
[8] Department of Physics, University of Texas at Arlington, Arlington, TX, USA
[9] Physics Department, National and Kapodistrian University of Athens, Athens, Greece
[10] Physics Department, National Technical University of Athens, Zografou, Greece
[11] Department of Physics, University of Texas at Austin, Austin, TX, USA
[12] Institute of Physics, Azerbaijan Academy of Sciences, Baku, Azerbaijan
[13] Institut de Física d'Altes Energies (IFAE), Barcelona Institute of Science and Technology, Barcelona, Spain
[14] [(a)]Institute of High Energy Physics, Chinese Academy of Sciences, Beijing, China; [(b)]Physics Department, Tsinghua University, Beijing, China; [(c)]Department of Physics, Nanjing University, Nanjing, China; [(d)]School of Science, Shenzhen Campus of Sun Yat-sen University, Guangzhou, China; [(e)]University of Chinese Academy of Science (UCAS), Beijing, China
[15] Institute of Physics, University of Belgrade, Belgrade, Serbia
[16] Department for Physics and Technology, University of Bergen, Bergen, Norway

[17] [(a)]Physics Division, Lawrence Berkeley National Laboratory, Berkeley, CA, USA; [(b)]University of California, Berkeley, CA, USA
[18] Institut für Physik, Humboldt Universität zu Berlin, Berlin, Germany
[19] Albert Einstein Center for Fundamental Physics and Laboratory for High Energy Physics, University of Bern, Bern, Switzerland
[20] School of Physics and Astronomy, University of Birmingham, Birmingham, UK
[21] [(a)]Department of Physics, Bogazici University, Istanbul, Turkey; [(b)]Department of Physics Engineering, Gaziantep University, Gaziantep, Turkey; [(c)]Department of Physics, Istanbul University, Istanbul, Turkey
[22] [(a)]Facultad de Ciencias y Centro de Investigaciónes, Universidad Antonio Nariño, Bogotá, Colombia; [(b)]Departamento de Física, Universidad Nacional de Colombia, Bogotá, Colombia
[23] [(a)]Dipartimento di Fisica e Astronomia A. Righi, Universitá di Bologna, Bologna, Italy; [(b)]INFN Sezione di Bologna, Bologna, Italy
[24] Physikalisches Institut, Universität Bonn, Bonn, Germany
[25] Department of Physics, Boston University, Boston, MA, USA
[26] Department of Physics, Brandeis University, Waltham, MA, USA
[27] [(a)]Transilvania University of Brasov, Brasov, Romania; [(b)]Horia Hulubei National Institute of Physics and Nuclear Engineering, Bucharest, Romania; [(c)]Department of Physics, Alexandru Ioan Cuza University of Iasi, Iasi, Romania; [(d)]Physics Department, National Institute for Research and Development of Isotopic and Molecular Technologies, Cluj-Napoca, Romania; [(e)]National University of Science and Technology Politechnica, Bucharest, Romania; [(f)]West University in Timisoara, Timisoara, Romania; [(g)]Faculty of Physics, University of Bucharest, Bucharest, Romania
[28] [(a)]Faculty of Mathematics, Physics and Informatics, Comenius University, Bratislava, Slovakia; [(b)]Department of Subnuclear Physics, Institute of Experimental Physics of the Slovak Academy of Sciences, Kosice, Slovak Republic
[29] Physics Department, Brookhaven National Laboratory, Upton, NY, USA
[30] Departamento de Física, y CONICET, Instituto de Física de Buenos Aires (IFIBA), Universidad de Buenos Aires, Facultad de Ciencias Exactas y Naturales, Buenos Aires, Argentina
[31] California State University, Long Beach, CA, USA
[32] Cavendish Laboratory, University of Cambridge, Cambridge, UK
[33] [(a)]Department of Physics, University of Cape Town, Cape Town, South Africa; [(b)]iThemba Labs, Western Cape, Cape Town, South Africa; [(c)]Department of Mechanical Engineering Science, University of Johannesburg, Johannesburg, South Africa; [(d)]National Institute of Physics, University of the Philippines Diliman, Quezon City, Philippines; [(e)]Department of Physics, University of South Africa, Pretoria, South Africa; [(f)]University of Zululand, KwaDlangezwa, South Africa; [(g)]School of Physics, University of the Witwatersrand, Johannesburg, South Africa
[34] Department of Physics, Carleton University, Ottawa, ON, Canada
[35] [(a)]Faculté des Sciences Ain Chock, Université Hassan II de Casablanca, Casablanca, Morocco; [(b)]Faculté des Sciences, Université Ibn-Tofail, Kenitra, Morocco; [(c)]Faculté des Sciences Semlalia, Université Cadi Ayyad, LPHEA-Marrakech, Marrakech, Morocco; [(d)]LPMR, Faculté des Sciences, Université Mohamed Premier, Oujda, Morocco; [(e)]Faculté des sciences, Université Mohammed V, Rabat, Morocco; [(f)]Institute of Applied Physics, Mohammed VI Polytechnic University, Ben Guerir, Morocco
[36] CERN, Geneva, Switzerland
[37] Affiliated with an institute covered by a cooperation agreement with CERN, Geneva, Switzerland
[38] Affiliated with an international laboratory covered by a cooperation agreement with CERN, Geneva, Switzerland
[39] Enrico Fermi Institute, University of Chicago, Chicago, IL, USA
[40] LPC, Université Clermont Auvergne, CNRS/IN2P3, Clermont-Ferrand, France
[41] Nevis Laboratory, Columbia University, Irvington, NY, USA
[42] Niels Bohr Institute, University of Copenhagen, Copenhagen, Denmark
[43] [(a)]Dipartimento di Fisica, Università della Calabria, Rende, Italy; [(b)]INFN Gruppo Collegato di Cosenza, Laboratori Nazionali di Frascati, Frascati, Italy
[44] Physics Department, Southern Methodist University, Dallas, TX, USA
[45] Physics Department, University of Texas at Dallas, Richardson, TX, USA
[46] National Centre for Scientific Research "Demokritos", Agia Paraskevi, Greece
[47] [(a)]Department of Physics, Stockholm University, Stockholm, Sweden; [(b)]Oskar Klein Centre, Stockholm, Sweden
[48] Deutsches Elektronen-Synchrotron DESY, Hamburg and Zeuthen, Germany

[49] Fakultät Physik , Technische Universität Dortmund, Dortmund, Germany
[50] Institut für Kern- und Teilchenphysik, Technische Universität Dresden, Dresden, Germany
[51] Department of Physics, Duke University, Durham, NC, USA
[52] SUPA-School of Physics and Astronomy, University of Edinburgh, Edinburgh, UK
[53] INFN e Laboratori Nazionali di Frascati, Frascati, Italy
[54] Physikalisches Institut, Albert-Ludwigs-Universität Freiburg, Freiburg, Germany
[55] II. Physikalisches Institut, Georg-August-Universität Göttingen, Göttingen, Germany
[56] Département de Physique Nucléaire et Corpusculaire, Université de Genève, Geneve, Switzerland
[57] [(a)]Dipartimento di Fisica, Università di Genova, Genoa, Italy; [(b)]INFN Sezione di Genova, Genoa, Italy
[58] II. Physikalisches Institut, Justus-Liebig-Universität Giessen, Giessen, Germany
[59] SUPA-School of Physics and Astronomy, University of Glasgow, Glasgow, UK
[60] LPSC, Université Grenoble Alpes, CNRS/IN2P3, Grenoble INP, Grenoble, France
[61] Laboratory for Particle Physics and Cosmology, Harvard University, Cambridge, MA, USA
[62] [(a)]Department of Modern Physics and State Key Laboratory of Particle Detection and Electronics, University of Science and Technology of China, Hefei, China; [(b)]Institute of Frontier and Interdisciplinary Science and Key Laboratory of Particle Physics and Particle Irradiation (MOE), Shandong University, Qingdao, China; [(c)]School of Physics and Astronomy, Shanghai Jiao Tong University, Key Laboratory for Particle Astrophysics and Cosmology (MOE), SKLPPC, Shanghai, China; [(d)]Tsung-Dao Lee Institute, Shanghai, China; [(e)]School of Physics, Zhengzhou University, Zhengzhou, China
[63] [(a)]Kirchhoff-Institut für Physik, Ruprecht-Karls-Universität Heidelberg, Heidelberg, Germany; [(b)]Physikalisches Institut, Ruprecht-Karls-Universität Heidelberg, Heidelberg, Germany
[64] [(a)]Department of Physics, Chinese University of Hong Kong, Shatin, N.T., Hong Kong, China; [(b)]Department of Physics, University of Hong Kong, Hong Kong, China; [(c)]Department of Physics and Institute for Advanced Study, Hong Kong University of Science and Technology, Clear Water Bay, Kowloon, Hong Kong, China
[65] Department of Physics, National Tsing Hua University, Hsinchu, Taiwan
[66] IJCLab, Université Paris-Saclay, CNRS/IN2P3, 91405 Orsay, France
[67] Centro Nacional de Microelectrónica (IMB-CNM-CSIC), Barcelona, Spain
[68] Department of Physics, Indiana University, Bloomington, IN, USA
[69] [(a)]INFN Gruppo Collegato di Udine, Sezione di Trieste, Udine, Italy; [(b)]ICTP, Trieste, Italy; [(c)]Dipartimento Politecnico di Ingegneria e Architettura, Università di Udine, Udine, Italy
[70] [(a)]INFN Sezione di Lecce, Lecce, Italy; [(b)]Dipartimento di Matematica e Fisica, Università del Salento, Lecce, Italy
[71] [(a)]INFN Sezione di Milano, Milan, Italy; [(b)]Dipartimento di Fisica, Università di Milano, Milan, Italy
[72] [(a)]INFN Sezione di Napoli, Naples, Italy; [(b)]Dipartimento di Fisica, Università di Napoli, Naples, Italy
[73] [(a)]INFN Sezione di Pavia, Pavia, Italy; [(b)]Dipartimento di Fisica, Università di Pavia, Pavia, Italy
[74] [(a)]INFN Sezione di Pisa, Pisa, Italy; [(b)]Dipartimento di Fisica E. Fermi, Università di Pisa, Pisa, Italy
[75] [(a)]INFN Sezione di Roma, Rome, Italy; [(b)]Dipartimento di Fisica, Sapienza Università di Roma, Rome, Italy
[76] [(a)]INFN Sezione di Roma Tor Vergata, Rome, Italy; [(b)]Dipartimento di Fisica, Università di Roma Tor Vergata, Rome, Italy
[77] [(a)]INFN Sezione di Roma Tre, Rome, Italy; [(b)]Dipartimento di Matematica e Fisica, Università Roma Tre, Rome, Italy
[78] [(a)]INFN-TIFPA, Trento, Italy; [(b)]Università degli Studi di Trento, Trento, Italy
[79] Universität Innsbruck, Department of Astro and Particle Physics, Innsbruck, Austria
[80] University of Iowa, Iowa City, IA, USA
[81] Department of Physics and Astronomy, Iowa State University, Ames, IA, USA
[82] Istinye University, Sariyer, Istanbul, Turkey
[83] [(a)]Departamento de Engenharia Elétrica, Universidade Federal de Juiz de Fora (UFJF), Juiz de Fora, Brazil; [(b)]Universidade Federal do Rio De Janeiro COPPE/EE/IF, Rio de Janeiro, Brazil; [(c)]Instituto de Física, Universidade de São Paulo, São Paulo, Brazil; [(d)]Rio de Janeiro State University, Rio de Janeiro, Brazil; [(e)]Federal University of Bahia, Bahia, Brazil
[84] KEK, High Energy Accelerator Research Organization, Tsukuba, Japan
[85] Graduate School of Science, Kobe University, Kobe, Japan
[86] [(a)]AGH University of Krakow, Faculty of Physics and Applied Computer Science, Kraków, Poland; [(b)]Marian Smoluchowski Institute of Physics, Jagiellonian University, Kraków, Poland
[87] Institute of Nuclear Physics Polish Academy of Sciences, Kraków, Poland

[88] Faculty of Science, Kyoto University, Kyoto, Japan
[89] Research Center for Advanced Particle Physics and Department of Physics, Kyushu University, Fukuoka , Japan
[90] L2IT, Université de Toulouse, CNRS/IN2P3, UPS, Toulouse, France
[91] Instituto de Física La Plata, Universidad Nacional de La Plata and CONICET, La Plata, Argentina
[92] Physics Department, Lancaster University, Lancaster, UK
[93] Oliver Lodge Laboratory, University of Liverpool, Liverpool, UK
[94] Department of Experimental Particle Physics, Jožef Stefan Institute and Department of Physics, University of Ljubljana, Ljubljana, Slovenia
[95] School of Physics and Astronomy, Queen Mary University of London, London, UK
[96] Department of Physics, Royal Holloway University of London, Egham, UK
[97] Department of Physics and Astronomy, University College London, London, UK
[98] Louisiana Tech University, Ruston, LA, USA
[99] Fysiska institutionen, Lunds universitet, Lund, Sweden
[100] Departamento de Física Teorica C-15 and CIAFF, Universidad Autónoma de Madrid, Madrid, Spain
[101] Institut für Physik, Universität Mainz, Mainz, Germany
[102] School of Physics and Astronomy, University of Manchester, Manchester, UK
[103] CPPM, Aix-Marseille Université, CNRS/IN2P3, Marseille, France
[104] Department of Physics, University of Massachusetts, Amherst, MA, USA
[105] Department of Physics, McGill University, Montreal, QC, Canada
[106] School of Physics, University of Melbourne, Melbourne, VIC, Australia
[107] Department of Physics, University of Michigan, Ann Arbor, MI, USA
[108] Department of Physics and Astronomy, Michigan State University, East Lansing, MI, USA
[109] Group of Particle Physics, University of Montreal, Montreal, QC, Canada
[110] Fakultät für Physik, Ludwig-Maximilians-Universität München, Munich, Germany
[111] Max-Planck-Institut für Physik (Werner-Heisenberg-Institut), Munich, Germany
[112] Graduate School of Science and Kobayashi-Maskawa Institute, Nagoya University, Nagoya, Japan
[113] Department of Physics and Astronomy, University of New Mexico, Albuquerque, NM, USA
[114] Institute for Mathematics, Astrophysics and Particle Physics, Radboud University/Nikhef, Nijmegen, The Netherlands
[115] Nikhef National Institute for Subatomic Physics and University of Amsterdam, Amsterdam, The Netherlands
[116] Department of Physics, Northern Illinois University, DeKalb, IL, USA
[117] [(a)]New York University Abu Dhabi, Abu Dhabi, United Arab Emirates; [(b)]United Arab Emirates University, Al Ain, United Arab Emirates
[118] Department of Physics, New York University, New York, NY, USA
[119] Ochanomizu University, Otsuka, Bunkyo-ku, Tokyo, Japan
[120] Ohio State University, Columbus, OH, USA
[121] Homer L. Dodge Department of Physics and Astronomy, University of Oklahoma, Norman, OK, USA
[122] Department of Physics, Oklahoma State University, Stillwater, OK, USA
[123] Palacký University, Joint Laboratory of Optics, Olomouc, Czech Republic
[124] Institute for Fundamental Science, University of Oregon, Eugene, OR, USA
[125] Graduate School of Science, Osaka University, Osaka, Japan
[126] Department of Physics, University of Oslo, Oslo, Norway
[127] Department of Physics, Oxford University, Oxford, UK
[128] LPNHE, Sorbonne Université, Université Paris Cité, CNRS/IN2P3, Paris, France
[129] Department of Physics, University of Pennsylvania, Philadelphia, PA, USA
[130] Department of Physics and Astronomy, University of Pittsburgh, Pittsburgh, PA, USA
[131] [(a)]Laboratório de Instrumentação e Física Experimental de Partículas - LIP, Lisbon, Portugal; [(b)]Departamento de Física, Faculdade de Ciências, Universidade de Lisboa, Lisbon, Portugal; [(c)]Departamento de Física, Universidade de Coimbra, Coimbra, Portugal; [(d)]Centro de Física Nuclear da Universidade de Lisboa, Lisbon, Portugal; [(e)]Departamento de Física, Universidade do Minho, Braga, Portugal; [(f)]Departamento de Física Teórica y del Cosmos, Universidad de Granada, Granada, Spain; [(g)]Departamento de Física, Instituto Superior Técnico, Universidade de Lisboa, Lisbon, Portugal
[132] Institute of Physics of the Czech Academy of Sciences, Prague, Czech Republic
[133] Czech Technical University in Prague, Prague, Czech Republic
[134] Charles University, Faculty of Mathematics and Physics, Prague, Czech Republic

[135] Particle Physics Department, Rutherford Appleton Laboratory, Didcot, UK
[136] IRFU, CEA, Université Paris-Saclay, Gif-sur-Yvette, France
[137] Santa Cruz Institute for Particle Physics, University of California Santa Cruz, Santa Cruz, CA, USA
[138] [(a)]Departamento de Física, Pontificia Universidad Católica de Chile, Santiago, Chile; [(b)]Millennium Institute for Subatomic physics at high energy frontier (SAPHIR), Santiago, Chile; [(c)]Instituto de Investigación Multidisciplinario en Ciencia y Tecnología y Departamento de Física, Universidad de La Serena, La Serena, Chile; [(d)]Department of Physics, Universidad Andres Bello, Santiago, Chile; [(e)]Instituto de Alta Investigación, Universidad de Tarapacá, Arica, Chile; [(f)]Departamento de Física, Universidad Técnica Federico Santa María, Valparaiso, Chile
[139] Department of Physics, Institute of Science, Tokyo, Japan
[140] Department of Physics, University of Washington, Seattle, WA, USA
[141] Department of Physics and Astronomy, University of Sheffield, Sheffield, UK
[142] Department of Physics, Shinshu University, Nagano, Japan
[143] Department Physik, Universität Siegen, Siegen, Germany
[144] Department of Physics, Simon Fraser University, Burnaby, BC, Canada
[145] SLAC National Accelerator Laboratory, Stanford, CA, USA
[146] Department of Physics, Royal Institute of Technology, Stockholm, Sweden
[147] Departments of Physics and Astronomy, Stony Brook University, Stony Brook, NY, USA
[148] Department of Physics and Astronomy, University of Sussex, Brighton, UK
[149] School of Physics, University of Sydney, Sydney, Australia
[150] Institute of Physics, Academia Sinica, Taipei, Taiwan
[151] [(a)]E. Andronikashvili Institute of Physics, Iv. Javakhishvili Tbilisi State University, Tbilisi, Georgia; [(b)]High Energy Physics Institute, Tbilisi State University, Tbilisi, Georgia; [(c)]University of Georgia, Tbilisi, Georgia
[152] Department of Physics, Technion, Israel Institute of Technology, Haifa, Israel
[153] Raymond and Beverly Sackler School of Physics and Astronomy, Tel Aviv University, Tel Aviv, Israel
[154] Department of Physics, Aristotle University of Thessaloniki, Thessaloniki, Greece
[155] International Center for Elementary Particle Physics and Department of Physics, University of Tokyo, Tokyo, Japan
[156] Department of Physics, University of Toronto, Toronto, ON, Canada
[157] [(a)]TRIUMF, Vancouver, BC, Canada; [(b)]Department of Physics and Astronomy, York University, Toronto, ON, Canada
[158] Division of Physics and Tomonaga Center for the History of the Universe, Faculty of Pure and Applied Sciences, University of Tsukuba, Tsukuba, Japan
[159] Department of Physics and Astronomy, Tufts University, Medford, MA, USA
[160] Department of Physics and Astronomy, University of California Irvine, Irvine, CA, USA
[161] University of Sharjah, Sharjah, United Arab Emirates
[162] Department of Physics and Astronomy, University of Uppsala, Uppsala, Sweden
[163] Department of Physics, University of Illinois, Urbana, IL, USA
[164] Instituto de Física Corpuscular (IFIC), Centro Mixto Universidad de Valencia-CSIC, Valencia, Spain
[165] Department of Physics, University of British Columbia, Vancouver, BC, Canada
[166] Department of Physics and Astronomy, University of Victoria, Victoria, BC, Canada
[167] Fakultät für Physik und Astronomie, Julius-Maximilians-Universität Würzburg, Würzburg, Germany
[168] Department of Physics, University of Warwick, Coventry, UK
[169] Waseda University, Tokyo, Japan
[170] Department of Particle Physics and Astrophysics, Weizmann Institute of Science, Rehovot, Israel
[171] Department of Physics, University of Wisconsin, Madison, WI, USA
[172] Fakultät für Mathematik und Naturwissenschaften, Fachgruppe Physik, Bergische Universität Wuppertal, Wuppertal, Germany
[173] Department of Physics, Yale University, New Haven, CT, USA

[a] Also Affiliated with an institute covered by a cooperation agreement with CERN, Geneva, Switzerland
[b] Also at An-Najah National University, Nablus, Palestine
[c] Also at Borough of Manhattan Community College, City University of New York, New York, NY, USA
[d] Also at Center for High Energy Physics, Peking University, China
[e] Also at Center for Interdisciplinary Research and Innovation (CIRI-AUTH), Thessaloniki, Greece

[f] Also at Centro Studi e Ricerche Enrico Fermi, Rome, Italy
[g] Also at CERN, Geneva, Switzerland
[h] Also at Département de Physique Nucléaire et Corpusculaire, Université de Genève, Geneve, Switzerland
[i] Also at Departament de Fisica de la Universitat Autonoma de Barcelona, Barcelona, Spain
[j] Also at Department of Financial and Management Engineering, University of the Aegean, Chios, Greece
[k] Also at Department of Physics, California State University, Sacramento, USA
[l] Also at Department of Physics, King's College London, London, UK
[m] Also at Department of Physics, Stanford University, Stanford, CA, USA
[n] Also at Department of Physics, Stellenbosch University, South Africa
[o] Also at Department of Physics, University of Fribourg, Fribourg, Switzerland
[p] Also at Department of Physics, University of Thessaly, Greece
[q] Also at Department of Physics, Westmont College, Santa Barbara, USA
[r] Also at Faculty of Physics, Sofia University, 'St. Kliment Ohridski', Sofia, Bulgaria
[s] Also at Hellenic Open University, Patras, Greece
[t] Also at Institucio Catalana de Recerca i Estudis Avancats, ICREA, Barcelona, Spain
[u] Also at Institut für Experimentalphysik, Universität Hamburg, Hamburg, Germany
[v] Also at Institute for Nuclear Research and Nuclear Energy (INRNE) of the Bulgarian Academy of Sciences, Sofia, Bulgaria
[w] Also at Institute of Applied Physics, Mohammed VI Polytechnic University, Ben Guerir, Morocco
[x] Also at Institute of Particle Physics (IPP), Montreal, Canada
[y] Also at Institute of Physics and Technology, Mongolian Academy of Sciences, Ulaanbaatar, Mongolia
[z] Also at Institute of Physics, Azerbaijan Academy of Sciences, Baku, Azerbaijan
[aa] Also at Institute of Theoretical Physics, Ilia State University, Tbilisi, Georgia
[ab] Also at Lawrence Livermore National Laboratory, Livermore, USA
[ac] Also at National Institute of Physics, University of the Philippines Diliman (Philippines), Philippines
[ad] Also at Technical University of Munich, Munich, Germany
[ae] Also at The Collaborative Innovation Center of Quantum Matter (CICQM), Beijing, China
[af] Also at TRIUMF, Vancouver, BC, Canada
[ag] Also at Università di Napoli Parthenope, Napoli, Italy
[ah] Also at University of Colorado Boulder, Department of Physics, Colorado, USA
[ai] Also at Washington College, Chestertown, MD, USA
[aj] Also at Yeditepe University, Physics Department, Istanbul, Turkey
[*] Deceased